INSTYTUT PROBLEMÓW JĄDROWYCH
im. ANDRZEJA SOŁTANA
ИНСТИТУТ ЯДЕРНЫХ ПРОБЛЕМ им. А.СОЛТАНА
SOLTAN INSTITUTE FOR NUCLEAR STUDIES

RAPORT SINS-2124 /A

SELECTED TOPICS IN NUCLEAR- AND ASTRO-PHYSICS

OTWOCK-ŚWIERK 1991

SOLTAN INSTITUTE FOR NUCLEAR STUDIES

RAPORT SINS 2124 /A

SELECTED TOPICS IN NUCLEAR- AND ASTRO-PHYSICS

Proceedings of the 22nd Masurian Lakes Summer School

on Nuclear Physics held in Piaski, Poland

August 26 - September 5, 1991

SEMINARS

Edited by

Z. SUJKOWSKI

Soltan Institute for Nuclear Studies

and

G. SZEFLIŃSKA

Institute of Experimental Physics, Warsaw University

OTWOCK-ŚWIERK, NOVEMBER 1991

Selected topics in nuclear- and astro-physics. This books contains the contributed papers presented orally or at the poster session during the XXII Masurian Lakes Summer School on Nuclear Physics /Piaski, Poland, August 26 - September 5, 1991/. The subjects cover the properties of hot and dense matter created in laboratory /the dynamics of the nucleus-nucleus collisions, the structure of hot and spinning nuclei/, the properties of hot and dense stellar matter, the nuclear reactions of astrophysical interest /including the latest developments of the tools such as e.g. the radioactive beams/ and the nucleosynthesis /esp. R-processes/.

Избранные вопросы ядерной физики и астрсфизики. Настоящая книга содержит татьи докладов заслушанных на семинарах или представленных в виде стендовых докладов на XXII Ма - зурской Летней Школе по ядерной физике (Пиаски, Польша, 26 август - 5 сентябрь 1991). Тематика этих работ охватывает широкий круг вопросов связанных: со свойствами горячей и плотной ядерной материи, образованной в лабораторных условиях (динамики ядерных соударений, структура горячих и вращающихся ядер); со свойствами горячей и плотной звездной материи; с ядерными реакциями представляющими научный интерес для астрофизики (реакции с использованием радиоактивных пучков) а также ядерный синтез (в частности R-процессы).

Wybrane zagadnienia fizyki jądrowej i astrofizyki. Książka ta zawiera prace prezentowane na seminariach lub sesji plakatowej podczas XXII Mazurskiej Letniej Szkoły Fizyki Jądrowej /Piaski, Polska, 26 sierpnia - 5 września, 1991/. Zakres tematyczny tych prac obejmuje własności gorącej i gęstej materii wytworzonej w warunkach laboratoryjnych /dynamika zderzeń jądrowych, struktura gorących i wirujących jąder/, własności gorącej i gęstej materii gwiezdnej, reakcje jądrowe o astrofizycznym znaczeniu /w tym reakcje z użyciem radioaktywnych wiązek/ oraz syntezę jądrową /w szczególności procesy R/.

CONTENTS

PREFACE

This book contains the contributed papers presented orally or at the poster session during the XXII MASURIAN LAKES SUMMER SCHOOL ON NUCLEAR PHYSICS (Piaski, Poland, August 26 - September 5, 1991). The invited lectures are published separately (ADAM HILGER , Bristol, England).

The headline of the School, "Selected topics in ...", calls for some comments. The subjects covered can be divided into the following main groups: {i} the properties of hot and dense matter created in the laboratory (the dynamics of the nucleus-nucleus collisions, the structure of hot and spinning nuclei), {ii} the properties of hot and dense stellar matter, {iii} the nuclear reactions of astrophysical interest (including the latest developments of the tools such as e.g. the radioactive beams), and {iv} the nucleosynthesis (esp. the R-process). I hope that the Reader of this book will find here some of the excitement we felt during the School in discovering how closely interrelated these subjects really are.

We have had the good luck of bringing together several leading experts in these fields or sub-fields. Experts, who have taken pains to find a common language, to overcome the easy temptation of talking shop to their peers. It is with a genuine satisfaction that I am presenting this book to the General Reader, confident that it will be of real value to those wanting to find a piece of specialized information as well as to those wishing to expand their ken, to experts as well as to novices.

Those of the old friends of our School who happened to be absent this year might want to know that we have moved from Mikołajki, the site of the preceding sixteen Schools, to Piaski. The new place is less than 20 km away from Mikołajki, at the same chain of lakes. I hope those who did come found the change much to the better. Otherwise the good traditions were preserved; we've welcomed colleagues from 22 countries; twenty crews participated in the regatta (won by Marcin Palacz, Świerk); the string quartet "Camerata" performed for us in the local church; Kenji Katori won the loudest (by far) applauds at the singing contest at the camp-fire; Tomasz Niewodniczański shared with us the secrets and excitement of a manuscript and authograph collector

with his fascinating evening talk on the opening day;...We only wished all of you were there! And I hope you will be there at the next School in 1993 (this is to say that we change to the biannual schedule).

Last but not least, I wish once again to thank all my colleagues of the organizing committee (the "visible" and the anonymous alike), the speakers (counting those who spoke physics inside as well as outside the lecture hall, i.e. everybody), and our sponsors: the "Komitet Badań Naukowych", the Warsaw University and the Soltan Institute for Nuclear Studies.

ZIEMOWIT SUJKOWSKI

Świerk, October 1991

ORGANIZING COMMITTEE

Ziemowid Sujkowski - Chairmam

Danka Chmielewska - Scientific Secretary

Tomasz Czosnyka

Wiktor Kurcewicz

Krzysztof Rusek

Grażyna Szeflińska

List of participants

Józef Andrzejewski	Uniwersytet Łódzki, Łódź, Poland
Ulrich Atzrott,	Universität Tübingen, Tübingen, Germany
Witold Augustyniak	Instytut Problemów Jądrowych, Warsaw, Poland
Jose Bacelar	Kernfysisch Versneller Instituut, Groningen, The Netherlands
Cyrus Baktash	Oak Ridge National Laboratory, Oak Ridge, USA
Andrzej Baran	UMCS, Lublin, Poland
Frank-Dieter Berg	II Physikalisches Institut, Giessen, Germany
Timo Bootsma	Rijksuniversiteit te Utrecht, Utrecht, The Netherlands
Andrzej Bobyk	UMCS, Lublin, Poland
Andrzej Bogusz	UMCS, Lublin, Poland
Günther Borchert	Institut für Kernphysik, Jülich, Germany
Rafał Broda	Instytut Fizyki Jądrowej, Cracow, Poland
Ilona Burzyńska	Warsaw, Poland
Krzysztof Burzyński	Uniwersytet Warszawski, Warsaw, Poland
Danuta Chmielewska	Kernfysisch Versneller Instituut, Groningen, The Netherlands
Hee Dong Choi	University of Birmingham, Birmingham, UK
Britta Clausnitzer	Berlin, Germany
Jonathan Copnell	University of Manchester, Manchester, UK
Serge Czajkowski	IPN, Orsay, France
Jacek Czakański	Uniwersytet Śląski, Katowice, Poland
Tomasz Czosnyka	Uniwersytet Warszawski, Warsaw, Poland
Janusz Dąbrowski	Instytut Problemów Jądrowych, Warsaw, Poland
Patrick Decrock	Instituut voor Kern-en-Stralingsfysika Leuven, Belgium

Katarzyna Delegacz	Instytut Problemów Jądrowych, Warsaw, Poland
Jacek Dobaczewski	Uniwersytet Warszawski, Warsaw, Poland
Maria Dominiak	Uniwersytet Warszawski, Warsaw, Poland
Corinne Donzaud	IPN, Orsay, France
Maria Dworzecka	GMU Fairfax, USA
Dieter Fick	Philipps-Universität, Marburg, Germany
Rosemarie Fick	Marburg, Germany
Leszek Fijałkowski	Uniwersytet Warszawski, Warsaw, Poland
John Barry Fitzgerald	Universität Heidelberg, Heidelberg, Germany
W. Gawlikowicz	Uniwersytet Jagielloński, Cracow, Poland
Leopoldyna Głowacka	Instytut Problemów Jądrowych, Warsaw, Poland
Jerzy Głowacki	Warsaw, Poland
Edmund Gierlik	Uniwersytet Warszawski, Warsaw, Poland
Adriano Gobbi	GSI, Darmstadt, Germany
Gracjana Golakowska	Uniwersytet Warszawski, Warsaw, Poland
Hanna Goldring	Oxford, UK
Gvirol Goldring	Clarendon Laboratory, Oxford, UK
Oleg Goryunov	Institute for Nuclear Research, Kiev, USSR
Andrzej Góźdź	UMCS, Lublin, Poland
Anna Grabowska	Uniwersytet Warszawski, Warsaw, Poland
Dietrich Habs	Universität Heidelberg, Heidelberg, Germany
Małgorzata Haensel	Warsaw, Poland
Paweł Haensel	Centrum Astronomiczne, Warsaw , Poland
Mohsen Harakeh	Vrije Universiteit, Amsterdam, The Netherlands
Pauli Heikkinen	University of Jyvaskyla, Jyvaskyla, Finland
Walter Henning	GSI, Darmstadt, Germany
Gert van't Hof	Vrije Universiteit, Amsterdam, The Netherlands
Jacek Holeczek	Uniwersytet Śląski, Katowice, Poland

Włodzimierz Iskra	Instytut Problemów Jądrowych, Warsaw, Poland
Ryszard Kacprzak	Instytut Problemów Jądrowych, Warsaw, Poland
Rościsław Kaczarowski	Instytut Problemów Jądrowych, Świerk, Poland
Łukasz Kalinowski	Uniwersytet Warszawski, Warsaw, Poland
Kenji Katori	Osaka University, Osaka, Japan
Tomasz Kazimierski	Uniwersytet Warszawski, Warsaw, Poland
Dariusz Kielan	Instytut Problemów Jądrowych, Warsaw, Poland
Marek Kirejczyk	Uniwersytet Warszawski, Warsaw, Poland
Mirosław Kostrubiec	Uniwersytet Śląski, Katowice, Poland
Miłosław Kotyński	Uniwersytet Warszawski, Warsaw, Poland
Beata Kozłowska-Janek	Instytut Problemów Jądrowych, Warsaw, Poland
Tadeusz Kozłowski	Instytut Problemów Jądrowych, Świerk, Poland
Karl-Ludwig Kratz	Johannes-Gutenberg Universität, Mainz, Germany
Gisela Kratz	Mainz, Germany
Gerald Kraus	GSI, Darmstadt, Germany
Harald Krauss	Institut für Kernphysik, Wien, Austria
Walentyna Kruszewska	Instytut Problemów Jądrowych, Świerk, Poland
Ewa Kulczycka	Instytut Problemów Jądrowych, Świerk, Poland
Reinhard Kulessa	Instytut Fizyki Jądrowej, Cracow, Poland
Doris Kunschitz	Wien, Austria
Jan Kurcewicz	Warsaw, Poland
Wiktor Kurcewicz	Uniwersytet Warszawski, Warsaw, Poland
Jan Kurpeta	Politechnika Warszawska, Warsaw, Poland
Zbigniew Lewandowski	Instytut Fizyki Jądrowej, Cracow, Poland
Isabelle Licot	Universite Catholique de Louvain, Louvain-la-Neuve, Belgium

Piotr Lubiński	Uniwersytet Warszawski, Warsaw, Poland
Tomasz Ludziejewski	Instytut Problemów Jądrowych, Świerk, Poland
Jerzy Łukasik	Uniwersytet Jagielloński, Cracow, Poland
Piotr Magierski	Politechnika Warszawska, Warsaw, Poland
Maria Makowska-Rzeszutko	Instytut Fizyki Jądrowej, Cracow, Poland
Ryszard Mańka	Uniwersytet Śląski, Katowice, Poland
Andrzej Marcinkowski	Instytut Problemów Jądrowych, Warsaw, Poland
Bohdan Mariański	Instytut Problemów Jądrowych, Warsaw, Poland
Joachim Maruhn	J.W. Goethe Universität, Frankfurt, Germany
Tomasz Matulewicz	Uniwersytet Warszawski, Warsaw, Poland
Władysław Mielczarek	Instytut Problemów Jądrowych, Warsaw, Poland
Andrzej Misiejuk	Instytut Problemów Jądrowych, Świerk, Poland
Tomasz Morek	Uniwersytet Warszawski, Warsaw, Poland
Bogna Mysłek-Laurikainen	Instytut Problemów Jądrowych, Warsaw, Poland
Władysława Nawrocka	Uniwersytet Wrocławski, Wrocław, Poland
Rudolf Neu	Universität Tübingen, Tübingen, Germany
Frank Nickel	GSI, Darmstadt, Germany
Annette Nickel	Darmstadt, Germany
Gerrit van Nieuwenhuizen	Rijksuniversiteit te Utrecht, Utrecht, The Netherlands
Tomasz Niewodniczański	Bitburg, Germany
M.-L. Niewodniczański	Bitburg, Germany
Leif Nilsson	Uppsala University, Uppsala, Sweden
Heinz Oberhummer	Institut für Kernphysik, Wien, Austria
Sławomir Osuch	Uniwersytet Warszawski, Warsaw, Poland
Thomas Otto,	CERN, Geneve, Switzerland
Marcin Palacz	Instytut Problemów Jądrowych, Świerk, Poland

Zygmunt Patyk	Instytut Problemów Jądrowych, Warsaw, Poland
Marek Pfützner	Uniwersytet Warszawski, Warsaw, Poland
Wiesław Pietrzak	Instytut Problemów Jądrowych, Warsaw, Poland
Antoni Piotrowski	Instytut Problemów Jądrowych, Świerk, Poland
Roman Płaneta	Uniwersytet Jagielloński, Cracow, Poland
Marian Przytuła	Uniwersytet Łódzki, Łódź, Poland
Krzysztof Pysz	Uniwersytet Jagielloński, Cracow, Poland
Gerhard Raimann	Universität Tübingen, Tübingen, Germany
Ursel Reuter	Nürnburg, Germany
Stefan Riess	II Physikalisches Institut, Giessen, Germany
M. Rogatko	UMCS, Lublin, Poland
Stanisław G. Rohoziński	Uniwersytet Warszawski, Warsaw, Poland
Janusz Rondio	Instytut Problemów Jądrowych, Warsaw, Poland
Krzysztof Rusek	Instytut Problemów Jądrowych, Warsaw, Poland
Krzysztof Rykaczewski	Uniwersytet Warszawski, Warsaw, Poland
Thomas Schmidt	Hahn-Meitner Institut für Kernphysik, Berlin, Germany
P. V. Sedyshev	JINR, Dubna, USSR
Dariusz Seweryniak	Uniwersytet Warszawski, Warsaw, Poland
John Sharpey-Schafer	Oliver Lodge Laboratory, Liverpool, UK
Eric Sheldon	University of Lowell, Lowell, USA
Anatoly Shvedov	Institute for Nuclear Research, Kiev
Ryszard Sidor	Instytut Problemów Jądrowych, Warsaw, Poland
Rolf Siemssen	Kernfysisch Versneller Instituut, Groningen, The Netherlands
Brunon Sikora	Uniwersytet Warszawski, Warsaw, Poland
Isabelle Slypen	Universite Catholique de Louvain, Louvain-la-Neuve, Belgium

Robert Smolańczuk,	Instytut Problemów Jądrowych, Warsaw, Poland
Zbigniew Sosin	Uniwersytet Jagielloński, Cracow, Poland
Julian Srebrny	Uniwersytet Warszawski, Warsaw, Poland
Krzysztof Starosta	Uniwersytet Warszawski, Warsaw, Poland
Elżbieta Stephan	Uniwersytet Śląski, Katowice, Poland
Anna Stonert	Instytut Problemów Jądrowych, Warsaw, Poland
Ziemowid Sujkowski	Instytut Problemów Jądrowych, Świerk, Poland
Marek Surała	Uniwersytet Warszawski, Warsaw, Poland
Alicja Surowiec	Uniwersytet Śląski, Katowice, Poland
Elwira Szeflińska	Warsaw, Poland
Grażyna Szeflińska	Uniwersytet Warszawski, Warsaw, Poland
Zygmunt Szeflński	Uniwersytet Warszawski, Warsaw, Poland
Hanna Szerypo	Warsaw, Poland
Jerzy Szerypo	Uniwersytet Warszawski, Warsaw, Poland
Stanisław Szpikowski	UMCS, Lublin, Poland
Zdzisław Szymański	Uniwersytet Warszawski, Warsaw, Poland
F.-K.Thielemann	Harvard Smithsonian Center for Astrophysics, Cambrigde, USA
Jakub Tropiło	Instytut Problemów Jądrowych, Warsaw, Poland
Agnieszka Trzcińska	Uniwersytet Warszawski, Warsaw, Poland
Andrzej Turos	Instytut Problemów Jądrowych, Warsaw, Poland
Grażyna Turos	Warsaw, Poland
Youri Tsyganov	JINR, Dubna, USSR
Andrzej Tucholski	GSI, Darmstadt, Germany
Christiaan Twenhoefel	Rijksuniversiteit te Utrecht, Utrecht, The Netherlands
Jan Tys	Uniwersytet Warszawski, Warsaw, Poland
Ehrenfried Vogt	Universität München, Garching, Germany
Tomasz Werner	Uniwersytet Warszawski, Warsaw, Poland
Edmund Wesołowski	Uniwersytet Warszawski, Warsaw, Poland
Andrzej Wieloch	Uniwersytet Jagielloński, Warsaw, Poland

Zdzisław Wilhelmi	Uniwersytet Warszawski, Warsaw, Poland
Andrzej Wojtasiewicz	Uniwersytet Warszawski, Warsaw, Poland
Alicja Wolańska	Uniwersytet Warszawski, Warsaw, Poland
Huachuan Wu	Suhzon University, Suhzon, China
Sławomir Wycech	Instytut Problemów Jądrowych, Warsaw, Poland
Tadeusz Zambrzycki	Politechnika Warszawska, Warsaw, Poland
Lucjan Zemło	Uniwersytet Warszawski, Warsaw, Poland
Paweł Żuprański	Instytut Problemów Jądrowych, Warsaw, Poland
Jan Żylicz	Uniwersytet Warszawski, Warsaw, Poland

SHAPE EFFECTS IN HEAVY-ION INDUCED FISSION

J. B. Fitzgerald

Max-Planck-Institut für Kernphysik, D-6900 Heidelberg FRG

ABSTRACT

Information from γ-ray spectroscopic studies of heavy-ion fusion-fission reactions has provided estimates of the average angular momentum of fission fragments before prompt neutron and γ-ray emission. The data, analysed within the framework of a statistical scission model, show a correlation between fragment spins and the ground-state shapes of the fragments. A measurement of fragment total kinetic energy (TKE), which is closely related to the Coulomb energy at scission, has indicated that scission shapes are uniformly deformed. It is deduced that those fragments which preferentially adopt spherical g.s. shapes are colder at, and immediately following, scission, when spin excitation processes take place. The reduction in temperature is consistent with estimates of "locked-up" deformation energy. Considerations of energy balance, given a smoothly varying TKE distribution, and uniform neutron and low-energy (up to 3MeV) γ-ray emission, suggest that spherical products with g.s. masses lowered by shell-stabilization may de-excite via high-energy non-statistical radiative transitions accompanying the shape relaxation from elongated scission-point shape to near-spherical ground-state configuration. An experimental investigation of the high-energy γ-ray spectrum in heavy-ion induced fission reactions is now underway.

AVERAGE SPINS OF FISSION FRAGMENTS

High-resolution γ-ray spectroscopy studies [1] at the Nuclear Structure Facility, Daresbury UK and at the Argonne National Laboratory, Illinois USA, have provided detailed information on the relative populations of discrete states in a wide range of fission fragments from the heavy-ion induced fusion-fission reactions ^{197}Au(^{19}F,f) and ^{232}Th(^{16}O,f). Such experiments can also yield information on total γ-ray multiplicity (and hence also statistical γ-ray multiplicity) and, from fragment mass and atomic number distributions, neutron multiplicity. Hence the average spins of fragments *before* prompt neutron and γ emission have been deduced [2,3]. A simplified statistical scission model (SSSM) has been used to derive trends in the mean spins $\langle J \rangle$ of individual fragments, and predicts that for a fragment of mass A with nuclear temperature T and for constant scission-point shape, $\langle J \rangle \propto A^{5/6}T^{1/2}$. The temperature has been estimated using ground-state Q-value systematics for the fission products, and the experimental mean spins scaled accordingly to remove this mass dependence (see Figure 1).

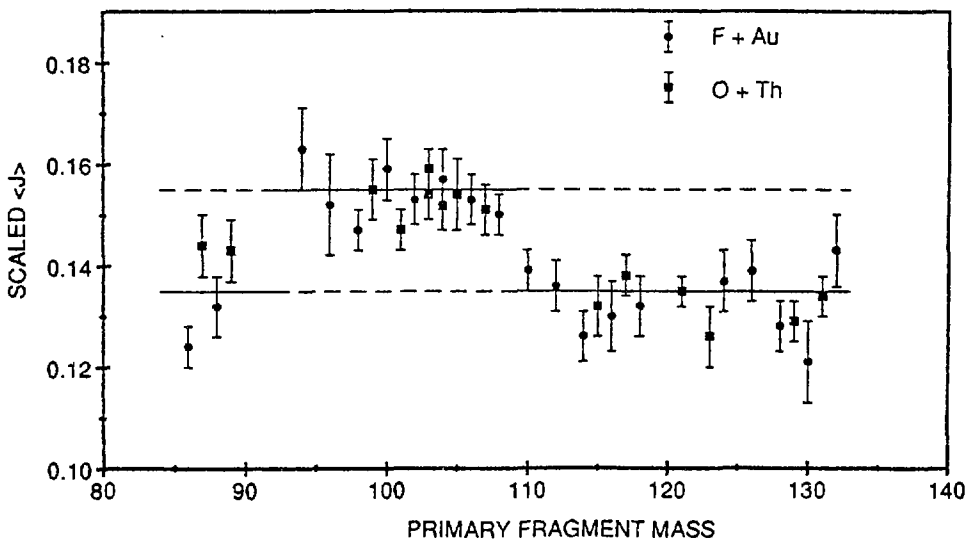

Figure 1 Scaled mean spins as a function of fragment mass

The data fall into two regions, of high and low scaled mean spin (shown by solid and dashed lines in Figure 1). These regions coincide with regions of constant ground-state shape, and it appears that within this constraint, the SSSM describes the mean spins rather well. The scaled spins of fragments spherical in their ground-states are, however, lower than those of "soft", deformed nuclei. This can be explained either (i) by fragments taking up their ground-state shapes at scission, since in the SSSM, $\langle J \rangle \propto \sqrt{\text{moment of inertia}}$ via the effect on the level-density of collective, rotational states in deformed nuclei; or (ii) by assuming a constant, elongated "liquid-drop" scission configuration for all fragments, and taking a lower nuclear temperature for those nuclei preferentially spherical in their ground-states: this can be understood in terms of a deformation energy, as well as loss of the shell-stabilization associated with preferred ground-state shape.

FISSION FRAGMENT SHAPES AT SCISSION: FISSION TKE

In order to determine the influence of the ground-state configuration on fragment angular momentum, the fission total kinetic energy (TKE) has been measured [3] for the system ^{197}Au(^{19}F,f). The TKE is predominantly determined by the Coulomb energy at scission, and thus is highly sensitive to the shape of the touching, nascent fragments. The measured TKEs are in excellent agreement with models assuming a constant scission-point configuration over all masses. Ground-state shapes at scission would result in an increase of $\sim$ 10MeV for fragments outside the $A \sim 100$ region of deformation, giving a rather broad, "top-hat" distribution.

ENERGY BALANCE: HIGH-ENERGY γs IN FISSION?

This detailed information on γ-ray and prompt neutron emission, and on the fission TKE as a function of mass, enables investigation of the energy balance in these fissioning systems. Ground-state mass evaluations show that the total energy release (after shape relaxation) is considerably more for the

shell-stabilized asymmetric (in the case of ^{197}Au(^{19}F,f) mass splits than for fissions leading to soft deformed nuclei in the $A \sim 100$ region. However, both TKE and neutron multiplicity are smoothly-varying, well-behaved functions of mass (or charge). The average neutron multiplicity, derived from the mean A/Z ratio for each element [3], agrees closely with the Maximum Excitation Energy *Sans Shells* model of charge division in fission, with a post-scission multiplicity of 4.0 ± 0.2 per fragment pair for all mass splits.

Furthermore, experimental studies [4] of such heavy-ion reactions, including ^{197}Au(^{19}F,f), have shown that the total energy carried by γ-rays of energy up to 3MeV is constant as a function of mass asymmetry ($\langle E_\gamma \rangle \langle M_\gamma \rangle$ = constant, for $E_\gamma \leq 3$MeV). This raises the question: where does the additional energy associated with forming shell-stabilized products go to?

One possibility is the decay of highly deformed scission shapes to spherical ground-states accompanied by the emission of a high-energy non-statistical γ-ray. There have been indications of such a decay mode in spontaneous fission, where a smaller fraction of events would be expected to undergo such a shape change [5]. Studies of neutron emission [6,7,8] in "hot" and "cold" fission events (i.e. low and high TKE events respectively) have suggested that the fragment excitation energy is similar in either case; this can be interpreted as evidence that the low TKE (elongated, high excitation energy) products may de-excite by radiative transitions.

An experiment has therefore recently been carried out to investigate the γ-ray spectrum at high energies in the reaction ^{197}Au(^{19}F,f), using the high-efficiency Heidelberg-Darmstadt Crystal Ball 4π γ-spectrometer. Fragment-fragment coincidences were detected by a pair of position sensitive parallel-plate avalanche counters, giving time-of-flight information and hence mass asymmetry. Around 10^7 fragment-fragment-γ coincidences were recorded. The analysis is expected to give information on the γ-ray spectra at high-energy as a function of fragment mass asymmetry.

ACKNOWLEDGEMENTS

The work referred to in this report has been carried out by a large number of scientists. In particular, I wish to mention J. L. Durell, W. R. Phillips, M. A. C. Hotchkis, A. S. Mowbray and B. J. Varley of Manchester University UK; R. V. F. Janssens and colleagues at the Argonne National Laboratory, Illinois USA; B. R. Fulton and G. Tungate of Birmingham University, UK; and the members of the Crystal Ball group at the Max–Planck–Institut für Kernphysik, Heidelberg FRG.

REFERENCES

[1] Y. Abdelrahman, J. L. Durell, W. Gelletly, W. R. Phillips, I. Ahmad, R. Holzmann, R. V. F. Janssens, T. L. Khoo, W. C. Ma and M. W. Drigert, Phys. Lett. **B199** (1987) 504

[2] J. B. Fitzgerald, Proc. Int. Conf. "50th Anniversary of Nuclear Fission", Leningrad 1989 (to be published)

[3] J. B. Fitzgerald, Ph.D. thesis, University of Manchester (1991)

[4] D. Hook, Ph.D. thesis, University of Manchester (1987)

[5] P. Glässel, R. Schmid–Fabian, D. Schwalm, D. Habs, H. U. v. Helmolt, Proc. Int. Conf on Fifty Years Research in Nuclear Fission, 1989, ed. D. Hilscher, W. von Oertzen and H. J. Krappe, Nucl. Phys. **A502** (1989) 315c

[6] P. Koczon, M. Mutterer, J. P. Theobald, P. Geltenbort, F. Gönnenwein, A. Oed, M. S. Moore, Phys. Lett. **B191** (1987) 249

[7] R. W. Hasse, All–Union Symposium on Physics and Chemistry of Fission, Obninsk, 1987

[8] H. Nifenecker, C. Signarbieux, R. Babinet, J. Poitou, Proc. IAEA Symp. on Physics and Chemistry of Fission, Rochester 1973 (IAEA, Vienna 1974), vol.II, p.117

TIDAL SYMMETRY IN SCATTERING OF POLARIZED ^{23}Na FROM ^{208}Pb

H.D. Choi, G. Tungate, C.O. Blyth, K.A. Connell*, S.E. Darden**, N.J. Davis†, S.J. Hall, O. Karban, G. Kuburas, S. Roman and A.C. Shotter†

University of Birmingham,
* SERC Daresbury Laboratory, ** University of Notre Dame, † University of Edinburgh

Abstract

The data for differential cross sections and transverse tensor analysing powers in scattering of polarized ^{23}Na from ^{208}Pb at 170 MeV were obtained for the ground, first and second excited states of ^{23}Na. The extracted data were analyzed on the basis of the tidal symmetry model and the adiabatic approximation. By comparing these results with the exact coupled channel calculations and the measured data, the validity of tidal symmetry model is discussed.

The data for differential cross sections and transverse tensor analysing powers in scattering of polarized ^{23}Na from ^{208}Pb at 170 MeV [1] were obtained for the ground, first and second excited states of ^{23}Na using the QMG/2 magnetic spectrometer at Daresbury Laboratory. The polarized ^{23}Na beams of typical currents 15 - 60 enA and of tensor polarizations t_{20} = 0.11 - 0.14 at the target were provided by the polarized heavy ion source. A ^{208}Pb self supporting target of 150 μg/cm^2 was used. The observed FWHM of the elastic peak was 170 - 300 keV, mostly due to the energy spread of the beam and target nonuniformity. A typical momentum spectrum of scattered ^{23}Na is shown in Figure 1. The peaks were fitted by Gaussians and the differential cross sections were obtained by normalizing the areas to the quasi-elastic cross sections [2].

The extracted data were analyzed on the basis of the tidal symmetry model [3] and the adiabatic approximation [4]. The ground state (g.s.) reorientation coupling together with 2-channel and 3-channel coupling scheme of ^{23}Na states have been attempted. Both nuclear and Coulomb terms were used in the reorientation and coupling potentials. The Woods-Saxon(WS) and derivative WS form factors were used for the central and coupling nuclear potential respectively. The optical model parameters were optimized by fitting only the cross sections and listed in Table 1. These results from tidal symmetry model were also compared with the exact coupled channel (CC) and adiabatic CC calculations by the code FRESCO [5]. To allow a direct comparison, the same potential strengths, form factors and coupling strengths shown in Table 1 were used. Both the nuclear and Coulomb deformation lengths were kept equal to the extracted value from the g.s. spectroscopic quadrupole moment of ^{23}Na [6].

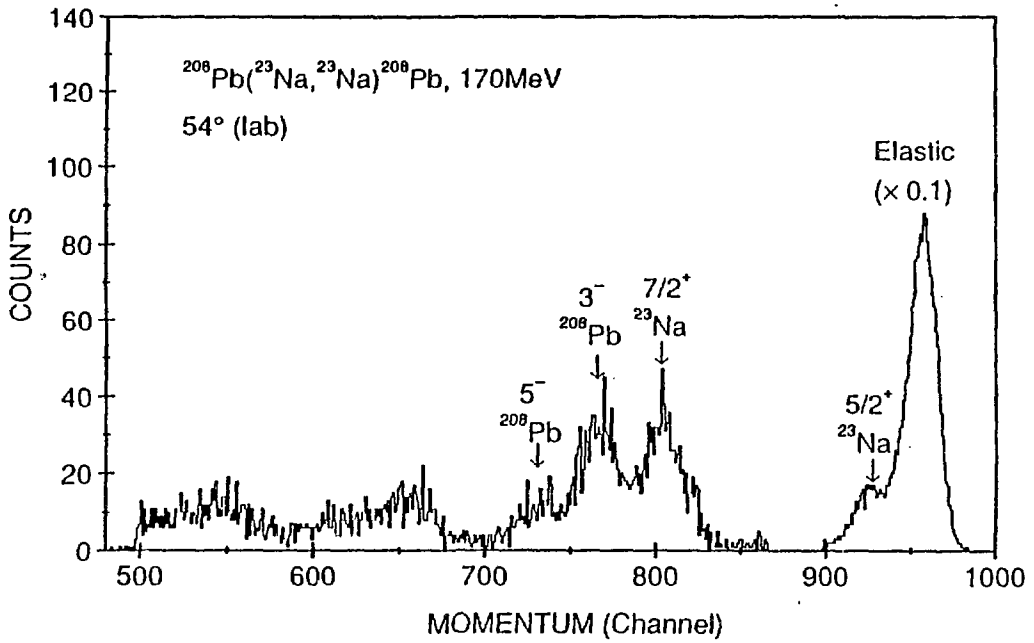

Figure 1. The momentum spectrum of scattered ^{23}Na at 54°(lab). The inelastic groups are identified. The elastic and inelastic($5/2^+$) peaks are reduced by a factor of 10.

The results of ground state reorientation coupling calculations are shown in Figure 2. The elastic cross section and the transverse analysing power from the exact CC calculation are almost identical to those given by the tidal symmetry model over the relevant angular range. In Figure 3, the results of 2-channel coupling are compared. The elastic cross section and the transverse analysing power data are well reproduced from the exact CC calculation using the potential parameters determined from the fit by the tidal symmetry model. It is notable that the exact CC calculation correctly predicts the magnitudes of the $5/2^+$ inelastic cross section at forward angles and also the transverse analysing power data.

Table 1. The used parameters of the Woods-Saxon potentials.

parameter set	V (MeV)	W (MeV)	r_0 (fm)	a (fm)	δ_2 (fm)
I	74.7	53.6	1.2	0.6	1.57
II	134.1	74.1	1.2	0.53	1.57
III	63.0	51.0	1.2	0.6	1.03
IV	63.0	51.0	1.2	0.6	1.57

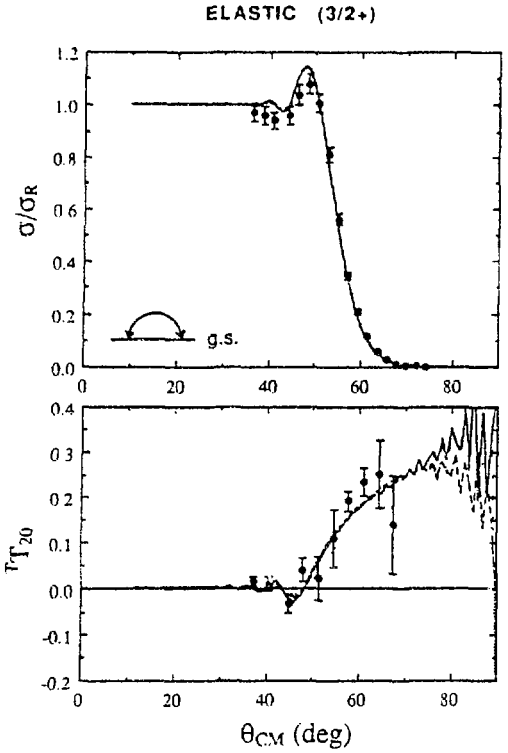

Figure 2. (Top) A fit to the elastic differential cross section by the tidal symmetry model (continuous) and the exact CC calculation (dashed) using the potential parameter set I in Table 1. (Bottom) The predicted $^{T}T_{20}(\theta)$ from both calculations compared with the data.

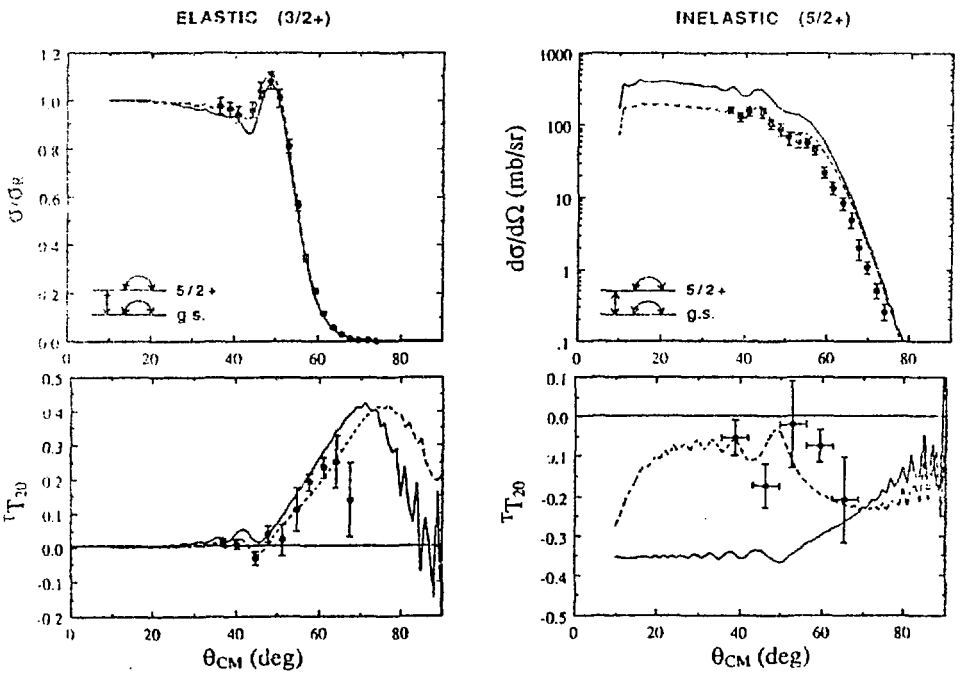

Figure 3. A fit in the tidal symmetry model to the elastic differential cross section in 2-channel coupling. The optimized potentials are listed in set II of Table 1. The results from the tidal symmetry model are shown in continuous lines. The results from exact CC calculation using the same potential parameters and deformation length are shown in dashed lines.

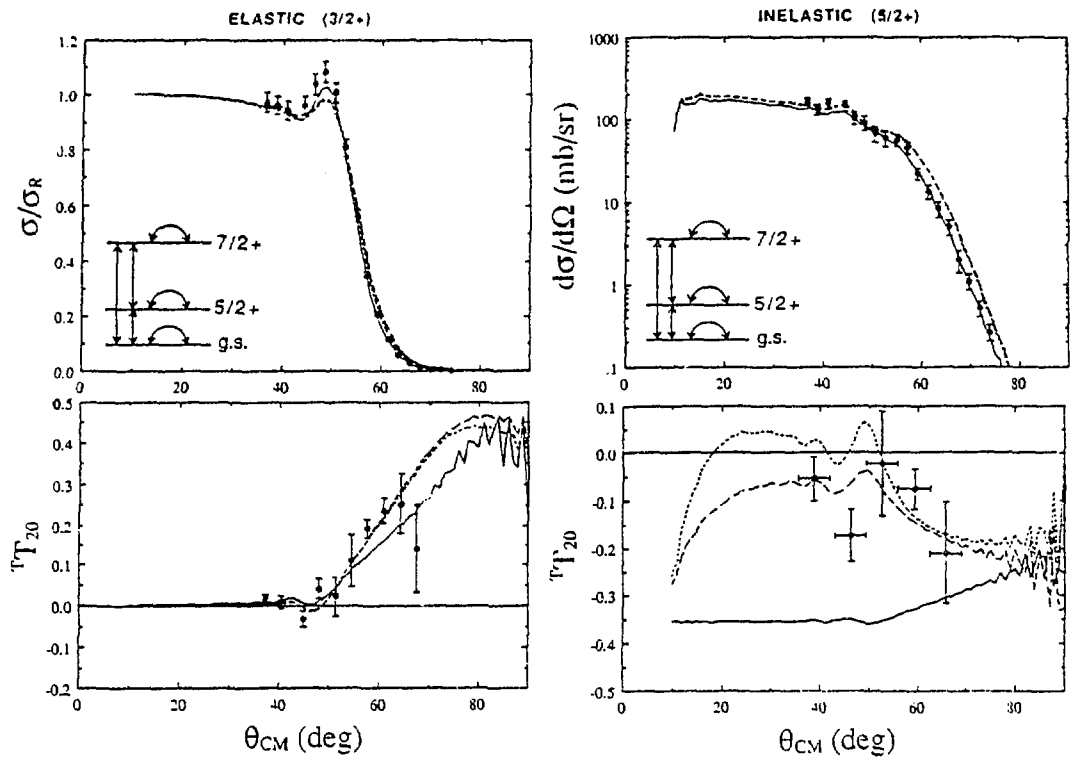

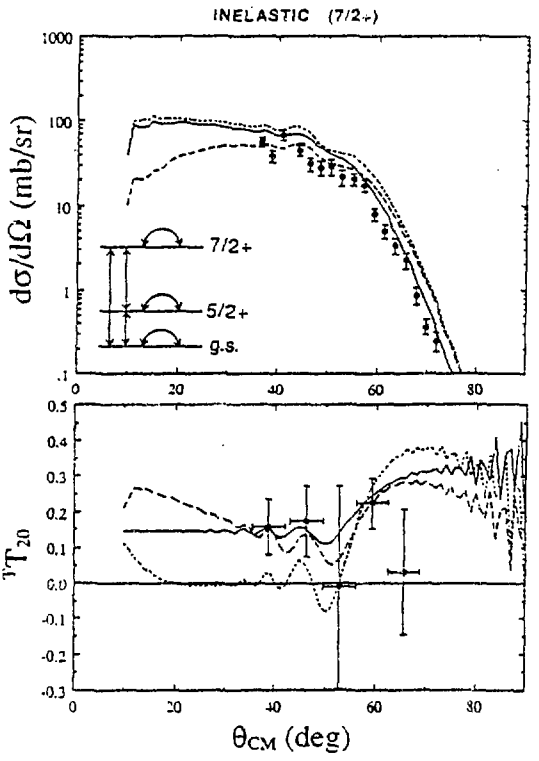

Figure 4. Results for the elastic channel, the $5/2^+$ and the $7/2^+$ inelastic channels from a 3-channel coupling calculation. The measured data are compared with the results from the tidal symmetry model (continuous lines) using the parameters of set III in Table 1. The exact CC calculations (dashed) and the adiabatic CC calculations (dotted) used the same potential parameters (set IV of Table 1) but the deformation length was fixed to the reported experimental value.

The results of 3-channel coupling are shown in Figure 4. The continuous, dashed and dotted lines are from the tidal symmetry model, exact CC and adiabatic CC calculations respectively. The potentials and coupling form factors were the same in the calculations but the deformation length was reduced by a factor of 2/3 in the tidal symmetry model calculation. Although a detailed fit was not attempted, the cross sections and transverse tensor analysing powers in the observed channels could be reproduced in the exact CC calculation. The predicted transverse tensor analysing power for the $5/2^+$ inelastic channel from the tidal symmetry model was not consistent either with the measured data or with the exact CC calculation result. It should be noted that the predicted transverse tensor analysing power for the $7/2^+$ inelastic channel was similar in both the tidal symmetry model and the exact CC calculations while the $7/2^+$ inelastic cross sections were overpredicted in the forward angle region by the tidal symmetry model. From the comparison of the calculations, the overprediction of the $7/2^+$ inelastic cross section in the tidal symmetry model was partly due to neglecting the excitation energy (2.08 MeV). The calculated elastic cross section, $5/2^+$ inelastic cross section and elastic transverse tensor analysing power were not changed appreciably by the adiabatic approximation. The discrepancy of the predictions for the inelastic channels by the tidal symmetry model is regarded as resulting from the tidal spin mixing by both the Coulomb excitation process [7] and the isocentrifugal approximation [8].

In conclusion, the tidal symmetry concept is useful only for the elastic scattering mechanism in heavy ion collisions. For the elastic scattering of the collision system in this study, the tidal symmetry model describes the measured data quantitatively and the calculated result is consistent with the exact CC calculation. In the inelastic channels, there are indications of tidal symmetry violation hence a more elaborate treatment of the problem is required.

References

[1] H.D. Choi *et al.*, Nucl. Phys. **A529** (1991) 190
[2] O. Karban *et al.*, J. Phys. **G14** (1988) L261
[3] J. Gomez-Camacho and R.C. Johnson, J. Phys. **G14** (1988) 609
[4] H.D. Choi, G. Tungate, M.A. Nagarajan and N. Rowley, J. Phys. **G15** (1989) 457
[5] I.J. Thompson, Computer Physics Report **7** (1988) 167
[6] B. Jeckelmann *et al.*, Nucl. Phys. **A408** (1983) 495
[7] Y. Sakuragi, M.A. Nagarajan and N. Rowley, J. Phys. **G15** (1989) 1855
[8] R.C. Johnson, Proc. Workshop on Heavy Ion Collisions at Energies near the Coulomb Barrier, 1990, ed. M.A. Nagarajan (IOP Publishing Ltd, Bristol, 1991) p.273

ANALYSIS OF THE INELASTIC α-^{36}Ar SCATTERING AND THE ^{39}K($\vec{p},\alpha$)^{36}Ar REACTION USING FOLDING POTENTIALS

R. Neu, K. Kocher, C. Ragutt, and G. Staudt

Physikalisches Institut der Universität Tübingen, D 7400 Tübingen
Federal Republic of Germany

ABSTRACT

The elastic α-scattering on ^{36}Ar has been analyzed in a broad range of energies using a double folded α-optical potential. The cross sections were reproduced excellently and the extracted optical potentials show a nice systematic behaviour. The inelastic scattering has been analyzed within the coupled-channel approach. Again the double-folded potentials lead to a very satisfactory description of the cross sections. The analyses proof the oblate shape of ^{36}Ar. In microscopic finite-range DWBA analyses of the ^{39}K($\vec{p},\alpha$)^{36}Ar reaction the use of the folding potential yields a good description of the differential cross sections as well as the correct absolute values.

I. INTRODUCTION

In systematic studies of the elastic and inelastic scattering on light nuclei [1,2,3] double folded α-nucleus potentials, calculated by means of a density dependent form of the nucleon-nucleon interaction [4], have been used to analyze the data. It could be shown, that the experimental data are rather well described in a broad range of energies. Considering inelastic scattering the analyses yield reliable values for the deformation and the isoscalar transition probabilities. Additionally microscopic Finite-Range DWBA analyses of (p,α) reactions, which used the double folded α-optical potential, provide the almost correct magnitude of the cross sections [5], whereas Woods-Saxon optical potentials often underestimate the absolute value by orders of magnitude.

In this context the nucleus ^{36}Ar is interesting for an investigation, because only few data exist on elastic α-scattering. There are no inelastic cross sections and the deformation is not well established up to now. Additionally the reaction ^{39}K($\vec{p},\alpha$)^{36}Ar should provide another test for the use of the folding potential.

The elastic and inelastic α-scattering was measured at the Bonn isochronous cyclotron facility at the energies 40, 48, and 54 MeV [6]. The ^{39}K($\vec{p},\alpha$)^{36}Ar reaction was measured at the injector cyclotron of the PSI (Villigen) at E_p = 35 MeV [7], which corresponds to an α-energy of about 40 MeV.

II. OPTICAL MODEL ANALYSES

First we consider the description of the elastic α-scattering in the optical-model (OM). The real part of the optical potential was deduced in the framework of the double-folding model and is described by

$$U_F(r) = \lambda_f \int d\mathbf{r}_T \int d\mathbf{r}_\alpha \quad \rho_T(\mathbf{r}_T)\rho_\alpha(\mathbf{r}_\alpha)t(E, \rho_T, \rho_\alpha, \mathbf{s} = \mathbf{r} + \mathbf{r}_\alpha - \mathbf{r}_T) \qquad (1)$$

where $\mathbf{r}$ is the separation of the centers of mass of the colliding target nucleus and the α particle, $\rho_T(\mathbf{r}_T)$ and $\rho_\alpha(\mathbf{r}_\alpha)$ are the respective nucleon densities, $t(E, s)$ is the density dependent effective interaction [4], and λ_f is an overall normalization factor. A detailed description of the computation of the potential $U_F(r)$ is given in Ref. 1. The imaginary potential was taken as a sum of a Woods-Saxon volume and surface term.

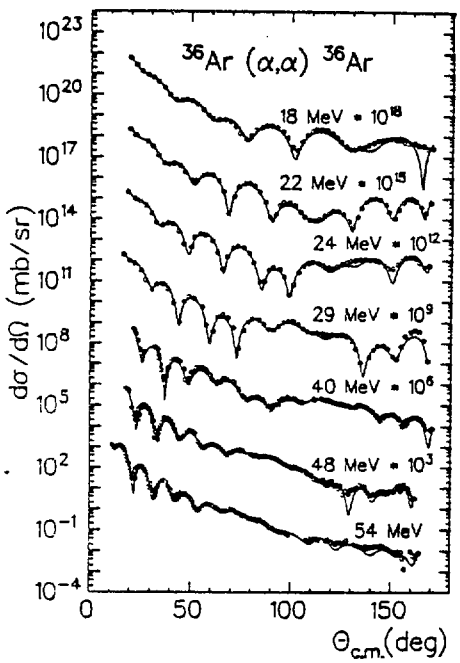

Fig. 1. Elastic α scattering on ^{36}Ar.

The results of the OM-calculations are shown in Fig. 1. The data at energies between 18-29 MeV have been taken from Gaul et al. [8]. For the whole energy range a good agreement between experimental and calculated data has been found. The volume integrals of the real part of the potential decrease with increasing energy, whereas the volume integrals and the rms radii of the imaginary potential show a marked increase with increasing energy. The rms radii of the real part are, due to the folding procedure, constant over the whole energy range. This systematic behaviour is very similar to that obtained in the case of the nuclei ^{16}O [1] and ^{24}Mg [2].

E_{Lab} [MeV]	J_R [MeV fm^3]	$< r_R^2 >^{1/2}$ [fm]	J_I [MeV fm^3]	$< r_I^2 >^{1/2}$ [fm]
18	366.9	4.11	49.3	4.37
22	363.9	4.11	48.8	4.66
24	360.9	4.11	50.6	4.55
29	366.3	4.11	60.8	4.84
40	360.1	4.11	76.7	4.73
48	355.1	4.11	95.5	4.78
54	338.7	4.11	125.7	4.78

Table I. Volume integrals and rms radii for the optical-model analyses

III. COUPLED-CHANNEL ANALYSES

In order to obtain further insight into the nature of the low-lying collective states of the ^{36}Ar nucleus, we analyzed the inelastic scattering within the Symmetric Rotor Model. To obtain an optimum reproduction of the experimental cross-section data, first the deformation parameters β_λ and the potential parameters were adjusted for each energy. Although both signs for the deformations were allowed in the analyses, only negative values for both, β_2 and β_4 resulted in a good description of the experimental data at all energies. The final results, calculated with averaged negative values for β_2 and β_4, are shown in Fig. 2.

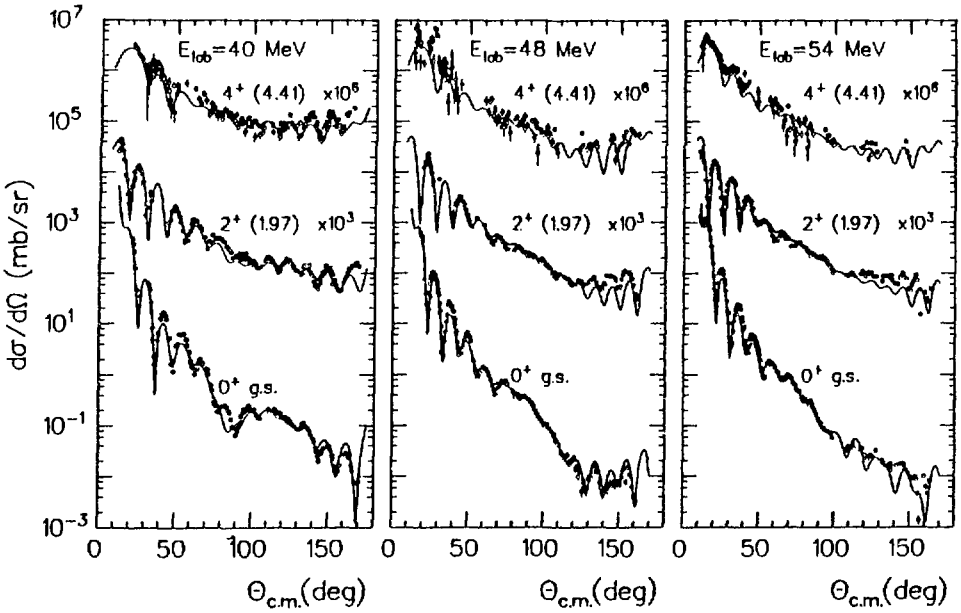

Fig. 2. Elastic and inelastic α scattering on ^{36}Ar together with CC analyses within the SRM. The deformation parameters were fixed at $\beta_2 = -0.21$, $\beta_4 = -0.08$.

Comparing the imaginary volume integrals obtained by the optical model calculations (Table I) with those from CC calculations (Table II), the latter are lower by 20-30%, due to the explicit consideration of the first excited states. The values are similar to those obtained from α-scattering on nuclei at the beginning of the *sd*-shell [1,2,3].

E_{Lab} [MeV]	J_R [MeV fm^3]	$< r_R^2 >^{1/2}$ [fm]	J_I [MeV fm^3]	$< r_I^2 >^{1/2}$ [fm]
40	356.3	4.11	57.1	4.65
48	344.0	4.11	76.0	4.60
54	333.4	4.11	89.8	4.72

Table II. Volume integrals and rms radii within the SRM.

The volume integrals of the real part of the optical potential (Table II) are lower than those obtained by OM calculations. This effect, characteristic of nuclei with an oblate shape, has already been observed by Clement et al. [9]. The deduced isoscalar transition rates $B(IS\lambda)$ are only somewhat larger than the $B(E\lambda)$ from electromagnetic probes. The resulting quadrupole moment is positive, which proves the oblate shape of ^{36}Ar.

Analyses within the pure harmonic vibrator model did not provide satisfactory results.

IV. MICROSCOPIC FINITE RANGE DWBA ANALYSES

In the analyses of the ^{39}K$(\vec{p},\alpha)^{36}$Ar reaction we used folding potentials in the proton as well in the α-channel. (dashed line in Fig. 3). The microscopic formfactor was derived from the spectroscopy of Chung Wildenthal shell model wave functions. The proton scattering data was taken from Bray et al. (25 MeV) [10] and from Fabrici et al. (35 MeV) [11]. The proton analyzing power was measured together with the (p,α) reaction [7]. The description of the α-scattering at 29 and 40 MeV is equal to that in Fig. 1. The normalization factor needed for the calculated reaction cross section is nearly one. The solid line in Fig. 3 shows the result of a simultaneous fit to all three channels, where a sum of six Fourier Bessel terms is added to the optical potentials. It turned out that minor modifications of the folded potentials improve the fit to the experimental data in entrance-, exit- and reaction channel.

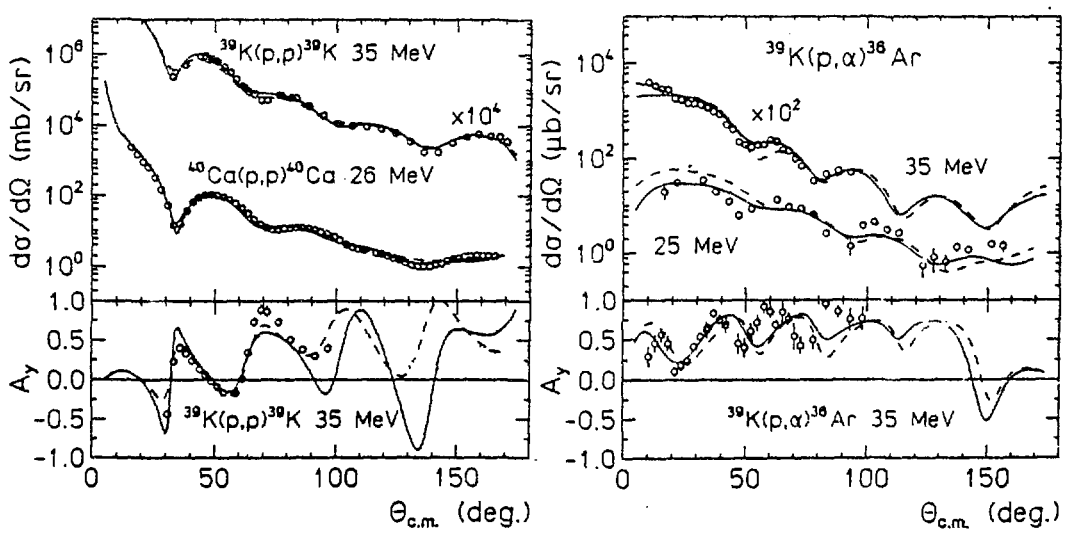

Fig. 3: p-scattering and (p,α) transfer reaction (for explanation see text).

V. CONCLUSIONS

The elastic scattering data have been analyzed in the framework of the optical model using a double folded real potential. The angular distributions are described very satisfactory for all incident energies between 18 and 54 MeV. The integral values of the optical potentials show a smooth variation with energy.

The inelastic scattering was treated in the rotational model. A negative value for β_2 as well as for β_4 is needed to fit the inelastic scattering data at all three energies. The spectroscopic quadrupole moment of the 2_1^+ state is found to be positive, thus showing the oblate shape of ^{36}Ar. The extracted isoscalar quadrupole transition strengths are only slightly higher than the e.m. values.

The microscopic FR-DWBA analyses, using the folding procedure for the proton as well for the α optical potential, give the correct absolute value for the reaction cross section. Slight modifications of the optical potentials allow an excellent description of the cross sections and analyzing powers of the entrance-, exit- and reaction channel.

ACKNOWLEDGMENTS

This work has been funded by the German Federal Minister for Research and Technology at Bundesministerium für Forschung und Technologie (BMFT) under Contract No. 06 Tü460.

REFERENCES

[1] H. Abele et al., Z. Phys. A **326**, 373 (1987).
[2] R. Neu et al.,Phys. Rev. C**39**, 2145 (1989).
[3] J. Fritze, et al., Phys. Rev. C**43**, 2307 (1991).
[4] A. M. Kobos et al., Nucl. Phys. **A425**, 205 (1984).
[5] M. Walz et al., J. Phys. G14(1988)L91
[6] K. Kocher et al., submitted to Phys. Rev. C
[7] R. Neu et al., to be published
[8] G. Gaul et al., Nucl. Phys. **A137**, 177 (1969).
[9] H. Clement et al., J. Phys. Jap.(Suppl.) **44**, 570 (1977).
[10] K.H. Bray et al., Nucl. Phys. **A167**, 57 (1971).
[11] E. Fabrici et al., Phys. Rev. C**21**, 844 (1980).

POWER LAW AND FLUCTUATIONS IN MULTIFRAGMENTATION

ANDRZEJ TUCHOLSKI

Institut für Physik, Universität Frankfurt,
D-6000 Frankfurt/Main 11, Germany
and
Institute for Nuclear Studies,
PL-05-400 Swierk, Poland

ABSTRACT

We argue that the factorial moments analysis is the very efficient in investigation of multifragmentation phenomenon. It is shown that inclusive spectrum does not determine the correlations between fragments. In particular, we show that inclusive poissonian distribution of M_{IMF}(multiplicity of intermediate mass fragments) does not determine the correlations between them.

For some time there has been an interesting question whether the multifragmentation phenomenon exhibits, from statistical point of view, the breaking mechanism analogous to that encountered in percolation. The interest in this problem started when the same power law has been observed in the fragment size distribution for both the experimental data and the percolation model [1,2]. The latter, in the critical regime, gives the following formula for the cluster size distribution $N\ (s,\varepsilon) \sim s^{-\tau}\ f(\varepsilon,\ s^{\sigma})$. Here, $f(\varepsilon,\ s^{\sigma})$ is the scaling function in which ε is a variable characterizing distance from the critical point , s is the size of the finite cluster and τ, σ are critical exponents. It was recently also discovered that for percolation at a critical point there exists a linear growth of factorial moments in charge spectrum, so it is an interesting question if the same behavior can be also observed in the experimental data. There was also another interesting question if the critical exponent $\tau = 2.15$ in charge distribution and/or the mean multiplicity of fragments dominates the correlations between fragments. In this note we first illustrate in very simple terms the idea of intermittency: we then show that an additional information can be obtained by applying this method in studies of charge distribution. Finally, we also show the limitations of the experiment in possible observation of the intermittency in relation to experimental resolution.

In statistics there are known mainly two kinds of moments: standard ones $\mu_p \equiv < n^p >$ and the factorial ones distributions $\xi_p \equiv < n(n-1)...(n-p+1) >$, here p is the rank of moment[3]. The factorial moments allow us to calculate the moments of convoluted distributions. If In experiment we observe the distribution $Q(\vec{k})$ which can be regard as the convolution of *dynamical* part $P(\vec{p})$ and the *statistical* part $B(\vec{p})$ [4]:

$$Q(\vec{k}) = \int d\vec{p} P(\vec{p}) B(\vec{p};\vec{k}). \qquad (1)$$

then, as it was shown by Białas and Peschański[4], by calculating the factorial moments of $Q(\vec{k})$ we can extract the standard moments of $P(\vec{p})$. In this way we can obtain the information about the *dynamical* fluctuations in a system. In order to find the underlying scale-invariance of physical processes it was also proposed[4] that factorial

moments should be calculated for different partitions of the system.

There are different normalizations of factorial moments due to the assumption about distribution $B(\vec{k};\vec{p})$. If we assume Poissonian like behavior we then obtain the following normalization:

$$< \tilde{F}_i >= M^{i-1} < \sum_{j=1}^{M} \frac{n_j(n_j-1)\cdots(n_j-i+1)}{< N >^i} >, \qquad (2)$$

which is appropriate for events with the mean particle multiplicity $< N >$ in the interval Δs and for a particular partition of the region of interest Δs in M bins of the size $\delta s = \Delta s/M$. In the above formula n_j is the number of particles in the jth bin and the brackets <> denote the average over many events. In our case $< N >$ is the mean number of fragments and Δs is the fragment size distribution.

The presence of fluctuations can be established by comparison of the above calculated moments to those obtained from the smooth inclusive distribution $\rho(s)$. To correct for a possible dependence of $< \tilde{F}_i >$ on the shape of $\rho(s)$ one should divide (2) by the factor:(see also: [5])

$$R_i = M^{-1}\sum_{j=1}^{M} [\ \frac{1}{\delta s_j}\int_{\delta s_j} \rho(s)\ ds]^i / [(\ \Delta s^{-1})\int_{\Delta s} \rho(s)\ ds]^i, \qquad (3)$$

and present results in the form $ln < F_i > \equiv ln\ [< \tilde{F}_i > / R_i\ ]$ vs $(-ln\ \delta s)$. For a flat distribution $\rho(s)$, the factors R_i are equal to one and hence can be neglected.

In this way we can study the dynamical fluctuations on different scales and for various sets of events. The system for which these fluctuations grow linearly with scale are called *intermittent*. Well known example of such a system is the case of turbulante flow[6].

To show that the additional information can be get by applying the method of factorial moments to charge distribution, we simulated the uncorrelated events holding the same power law dependance of charge distribution as for percolation at a critical point. We were randomly choosing the fragments from power law probability $N\ (s) \sim s^{-\tau}$ where $N(s)$ is a frequency of cluster of the size s. For total multiplicity in an event we took a poissonian distribution. We had no charge conservation in our Monte Carlo but we wanted to be free from any kind of correlations. The percolation was simulated using a simple cubic lattice bond model containing ($A = 6^3$) number of sites. Neighboring sites are connected by bonds which are randomly activated with the probability q . A fragment with size $1 < s \leq A$ is defined as an ensemble of neighboring sites connected by active bonds. The evolution of the fragment size distribution $N(s)$ in the bond percolation models depends solely on the value of the bond parameter q . The self-similarity of $N(s)$ and the intermittent pattern of its fluctuations is seen only in the narrow range of bond parameter $0.21 < q \leq 0.27$ with maximal slopes at $q \simeq 0.23$ [7]. The result of the Monte Carlo of uncorrelated events and for percolation is presented in Fig.1 We can see that for the same inclusive distribution of fragments and the same multiplicity distribution we may have different behavior of factorial moments. This intermittent behavior in fragment size distribution has been observed in full scale only for a sharp q value in percolation. For a wide range of q the factorial exponents are different from those observed for a sharp q[7]. So there was an interesting question concerning the relation between the resolution in q parameter and a possible experimental observable. We tried to look on correlation of q with some experimental observable. It was shown lately that an event selection can be done, in an experiment of heavy ions, by applying the Z_{bound} quantity (sum of all charges with $Z \geq 2$)[8]. We are presenting the dependence of q on Z_{bound} in Fig.2a for percolation model. (of the size of $A = 216$) We can see that even with only theoretically possible resolution of the order of units in Z_{bound} we have the resolution in q of the order of ~ 0.1 which is not good enough to select the sharp q around critical value. The same disadvantage concerns also other observables. (see. Fig 2b).

CONCLUSIONS.

It was shown that the poissonian distribution of fragments produced in the multifragmentation process does not determine correlations between them. By very simple Monte Carlo example it was shown that the inclusive poissonian distribution of fragments, in particular power law dependence of charge distribution, does not determine the correlations between fragments. We have also mentioned about possible experimental difficulties in selecting the sharp q value, which is connected to the problem of the possibility in observation of the second order phase transition[9] in nuclear systems.

ACKNOWLEDGEMENT

It is my pleasure to acknowledge that this work is only a part of the bigger subject we are working at together with M.Płoszajczak and P.Bożek.

My thanks are due to W.Florkowski for useful discussions and U.Lynen for encouragement to work on the subject.

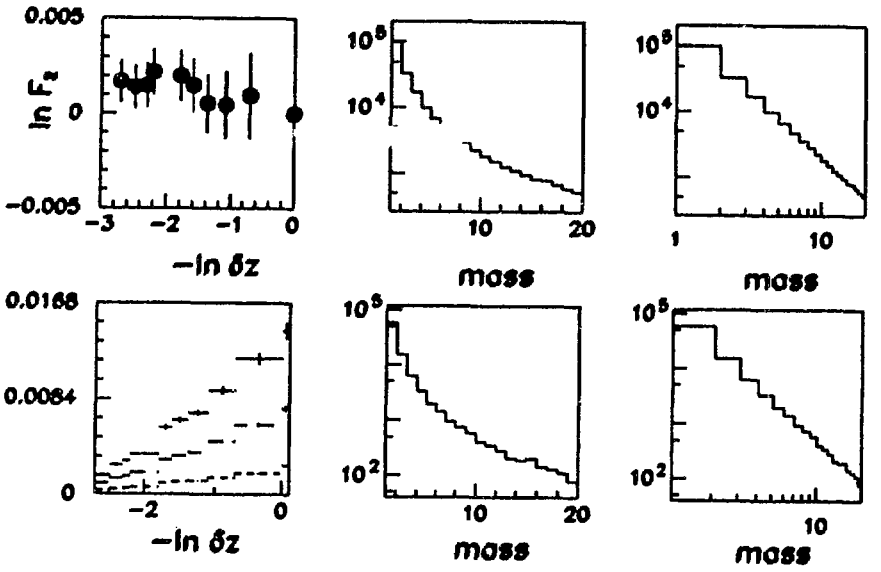

Fig.1

a) The factorial moments for poissonian distribution of multiplicity of fragments fulfilling power-law in charge distribution (three upper pictures). b) Factorial moments for poissonian distribution of multiplicity of fragments for percolation at threshold (three lower pictures).

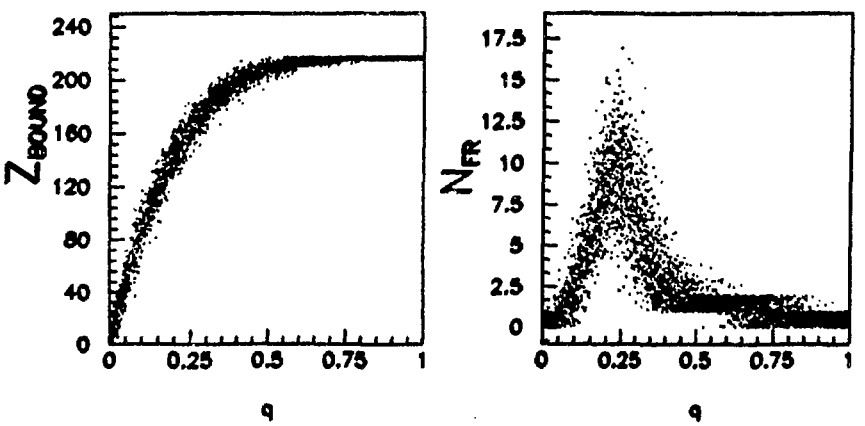

Fig.2

The correlation plots for percolation model. a) The dependence of Z_{bound} on q. b) The dependence of multiplicity of N_fr (defined as fragments with $Z \geq 3$) on bound parameter q

References

[1] X. Campi, J. Phys. A **19**, 917 (1986).

[2] W. Bauer et al., Nucl. Phys. **A452**, 699 (1986);
W. Bauer et al. Phys. Rev. Lett. **58**, 863 (1987);
J. Desbois, Nucl. Phys. **A466**, 724 (1987).

[3] P.Carruters Int.Journal of Modern Phys. A 2 1447 (1987) W.Feller, *An Introduction to Probability Theory and Its Applications*,(John Wiley and Sons, New Yourk, 1966) Vol.I.

[4] A.Białas and R.Peschanski, Nucl.Phys **B273** 703 (1986)

[5] K. Fialkowski, B. Wosiek and J. Wosiek, Acta Physica Polonica **B20**, 639 (1989).

[6] B.Mandelbrot, J.Fluid. Mech. **62** (1974) 331;
U.Frisch, P.Sulem and M.Nelkin, J.Fluid.Mech. **87** (1978) 719.

[7] M.Płoszajczak and A.Tucholski, Phys.Rev.Lett **65**, (1990) 1539;
M.Płoszajczak and A.Tucholski, Nucl.Phys. **A523** (1991) 651

[8] ALADIN collaboration Z.Phys.....
Phys.Rev.Lett...to be published

[9] M.Płoszajczak, A.Tucholski and P.Bo/.zek Phys.Lett **B262**, (1991) 383

CLUSTERING PHENOMENA IN (ALPHA, HI) REACTIONS ON ^{12}C

L.Głowacka and J.Turkiewicz

Soltan Institute for Nuclear Studies, Warsaw, Poland

O.Yu.Goryunov, A.V.Mokhnach, O.A.Ponkratenko, A.T.Rudchik,

V.K.Chernievsky and A.A.Shvedov

Institute for Nuclear Research, Kiev, USSR

and

E.I.Koshchy and Yu.G.Mashkarov

Kharkov State University, USSR

Abstract:

The $^{12}C(\alpha,^{6}Li)^{10}B$, $^{12}C(\alpha,^{7}Li)^{9}B$ and $^{12}C(\alpha,^{7}Be)^{9}Be$ reactions at 90 MeV have been applied to investigate the cluster structure of the ^{12}C nucleus. The measured angular distributions have been analyzed using the finite range DWBA formalism including both direct (pick-up) and exchange (heavy particle pick-up) processes. Absolute cross sections are satisfactorily reproduced with the cluster spectroscopic amplitudes calculated in the framework of the shell model.

The present experiment was performed using the 90 MeV alpha particle beam from the Kiev isochronous cyclotron U-240.
A self-supporting carbon foil of about 150 $\mu g/cm^2$ thickness was used as a target. A scattering chamber was used with three movable ΔE-E solid state detector telescopes which were mounted at 12.5° intervals at a distance of about 20 cm from the target. The

thickness of the transmission counters (ΔE) ranged from 20 to 50 μm and stopping counters (E) was about 1000 μm. The ΔE and E signals were amplified with active filter and biased amplifiers and then were pulse height analyzed by analog-to digital converters interfaced via CAMAC to an on-line data acquisition computer. A typical two-dimensional ΔE versus E spectrum is shown in fig.1.

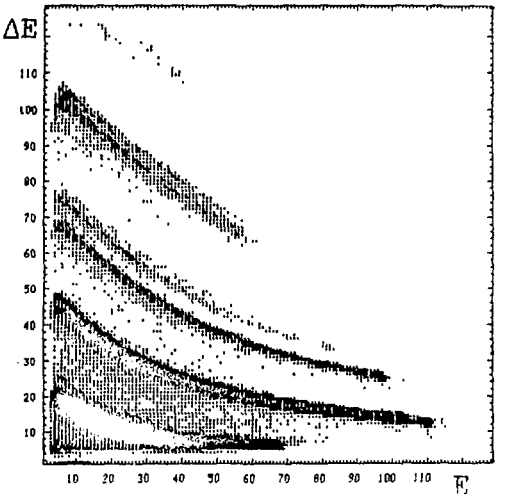

Fig.1. A typical two-dimensional ΔE versus E spectrum taken at $\theta_{LAB}=27.5^{\circ}$. The various curves are due to the He, Li, Be and B ions.

The energy resolution of our experiment was equal to 1% (mainly determined by the energy spread of the beam), which was not sufficient to resolve the first excited states of ^{7}Li and ^{7}Be from their ground states, leaving also unresolved transitions populating the ground and first excited states in the ^{10}B nucleus.

For the $^{12}C(\alpha,^{6}Li)^{10}B$ and $^{12}C(\alpha,^{7}Be)^{9}Be$ reactions one is able to measure simultaneously angular distribution in both forward and backward hemispheres by detection of a particular heavy ion (^{6}Li or ^{7}Be) or its heavier complementary product (^{10}B or ^{9}Be) at forward laboratory angles.

The finite range distorted wave Born approximation (FR DWBA) analysis of the measured angular distributions was performed according to the formalism developed by Austern *et al.* [1] using the DWUCK 5 code of Kunz [2].

Two reaction mechanisms, direct pick-up and exchange pick-up (heavy particle pick-up) (fig.2), were taken into account and their contribution to the cross sections were examined individually. In the direct process the target nucleus *A* is represented as bound state of a cluster *x* and a core *B*, and the emitted particle *b* is a composite of the transferred cluster *x* and an incident particle *a*. In the exchange process the target nucleus *A* is supposed to consist of transferred core *x'* and the emitted particle *b*.

a) b)

Fig.2. The Feynman diagrams for the pick-up (a) and heavy particle pick-up (b) mechanisms.

The essential parameters of the analysis were determined in the way described below.

1) The few-nucleon cluster spectroscopic amplitudes for the decomposition of the target nucleus or ejectile were calculated in the present work and not treated as adjustable parameters. These values have been obtained using code DESNA [3] within the framework of the of the translationally invariant shell model developed by Smirnov and Tchuvil'sky [4]. To determine the spectroscopic characteristics of the transferred clusters, and of

the initial and final nuclei, the wave functions calculated in intermediate coupling scheme by Boyarkina [5] have been used. The results of this calculation are given in the ref. [6].

ii) The bound state wave functions of the transferred cluster to the core were generated with Woods-Saxon potentials that had the geometry parameters : r_o=0.82-0.87 fm (depending on a system) and a_o=0.65 fm. The well depths were adjusted to give the correct binding energies.

iii) The distorting potential parameters used were derived from elastic scattering data. The entrance channel potential ($^{12}C + \alpha$) was provided by the global analysis of elastic scattering experiments [7]. A number of calculations were made using different sets of optical model parameters for the exit channel. It turned out that parameters which lead to satisfactory description of elastic scattering data did not work very well for transfer reactions. Satisfactory description for all investigated reactions was achieved with the parameters used to describe ^{9}Be + ^{9}Be elastic scattering cross sections [8].

The selected in this paper optical model parameters are shown in table 1, where the symbols have well known meanings.

Table 1

Optical model parameters used in distorted wave analysis

Channel	V (MeV)	r (fm)	a (fm)	W (MeV)	r_W (fm)	a_W (fm)	r_c (fm)
$\alpha + ^{12}C$	130.6	1.22	0.80	13.8	1.91	0.50	1.22
exit	110.0	0.82	0.73	20.0	1.30	0.765	0.82

The interaction radii are given by $R=rA^{1/3}$ (for entrance channel) or $R=r(B^{1/3}+b^{1/3})$ (for exit channel).

The results of the FR DWBA calculations are compared with experimental data in figs. 3-4. The contributions from the light cluster pick-up and heavy cluster pick-up processes together with their incoherent sum are shown in the figures. This simplification is partly justified by the fact that the contribution from light cluster transfer is significant for small angles and that from heavy cluster transfer, on the contrary, for large angles.

Fig.3 shows the angular distributions populating the 0.0 MeV ($3/2^-$), 2.43 MeV ($5/2^-$) and 6.76 MeV ($7/2^-$) states in the ^{9}Be nucleus compared with the FR DWBA calculations. These calculations considered both the ground and first excited states in the ^{7}Be nucleus. The contributions from ^{3}He- and ^{5}He-cluster transfers are shown separately while the solid curves present the sums of both contributions. Reasonably good agreement between the experimental data and the calculations is evident for the magnitude of the cross section and the shape of the angular distribution for the ground state of the ^{9}Be. Although the magnitude of the cross sections leading to the excited states is in rough agreement with the experimental ones, the shapes of the distributions are, however, less well reproduced.

The angular distributions for low lying states of the residual nuclei together with the results of FR DWBA calculations for the $^{12}C(\alpha,{}^{7}Li_{(gs+0.478)})^{9}B$ and $^{12}C(\alpha,{}^{6}Li)^{10}B_{(gs+0.718)}$ reactions are displayed in fig.4. Although the theoretical description appears to be not perfect, especially for the (α,^{6}Li) reaction, globally

the experimental cross sections are well reproduced.

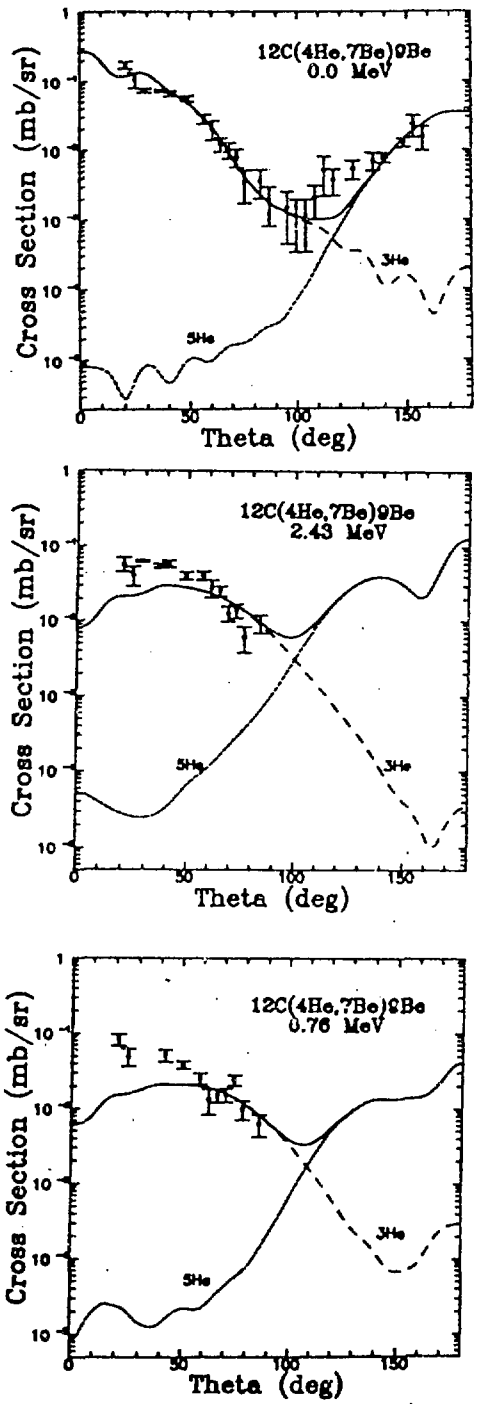

Fig.3. Comparison of the FR DWBA predictions with the experimental data for the 0.0 MeV (the top), 2.43 MeV (the middle) and 6.76 MeV (the bottom) states in ^{9}Be. Each curve is labelled by the transferred cluster.

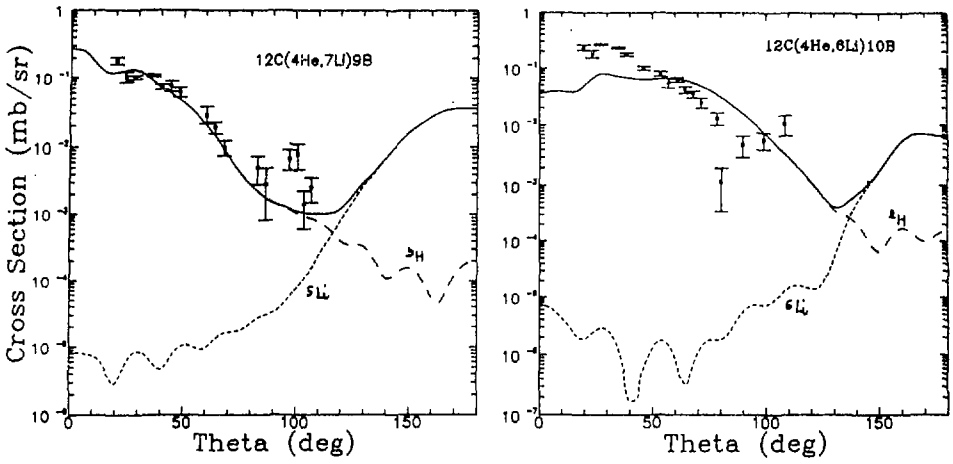

Fig.4. Comparison of the experimental angular distributions with the FR DWBA calculations.

The following conclusions can be drown from the present work.

The angular distributions of the investigated reactions can be successfully described in the framework of the FR DWBA . Together with the direct pick-up mechanism contributions from the exchange-mode mechanisms are found to be necessary for a description of the angular distributions.

The absolute magnitude of the cross sections can be satisfactorily described while using the theoretically determined shell model spectroscopic amplitudes.

Good quantitative agreement of the measured angular distributions with the theoretical predictions illustrate that from the multinucleon transfer reactions one can obtain a valuable information about cluster structure for light nuclei.

References

1. N.Austern, R.M.Drisko, E.C.Halbert and G.R.Satchler, Phys.Rev. **B133**(1964)3
2. P.D.Kunz, DWUCK5, University of Colorado (unpublished) 1980
3. A.T.Rudchik and Yu.M.Tchuvil'sky, Ukr.Phys.J. **30**(1985)819
4. Yu.F.Smirnov and Yu.M.Tchuvil'sky, Phys.Rev. **C15**(1977)84
5. A.N.Boyarkina, Structure of 1p-shell nuclei (Moscow State University, 1973)
6. L.Głowacka, J.Turkiewicz, O.Yu.Goryunov, A.V.Mokhnach, O.A.Ponkratenko, A.T.Rudchik, V.K.Chernievsky, A.A.Shvedov, E.I.Koshchy and Yu.G.Mashkarov, Nucl.Phys. (in press)
7. R.C.Barrett and D.F.Jackson in Nuclear Sizes and Structure, ed. W.Marshall and D.H.Wilkinson (Clarendon Press, Oxford, 1977) p.268
8. A.R.Omar, J.S.Eck, J.R.Leigh and T.R.Ophel, Phys.Rev. **C30** (1984)896

THE ALGEBRAIC GENERATOR COORDINATE METHOD AS A WAY TO COLLECTIVE DYNAMICS. AN APPLICATION TO THE INTERACTING BOSON MODEL.

A. Bogusz and A. Góźdź*
Institute of Physics, M. Curie-Skłodowska University,
pl. M. Curie-Skłodowskiej 1, 20-031 Lublin, Poland.

Abstract

In the paper the idea of the AGCM approach and its application to the temperature dependent IBM model has been outlined.

1. The Algebraic Generator Coordinate Method.

The Generator Coordinate Method (GCM) allows to construct the nuclear collective spaces by means of a very general ansatz for a trial function [1]:

$$|\Psi\rangle = \int dq\ u(q)\ |q\rangle \qquad (1)$$

The states (1) are pure states in the quantum mechanical sense. For many cases as for example for highly excited nuclei (hot nuclei), the heavy ions collisions and other phenomena where a statistical approach is required the ansatz (1) is not sufficient and does not provide the appropriate formalism. One needs to extend the GCM approach to the mixed states generated from a given density matrix, the approach we call the Algebraic Generator Coordinate Method (AGCM) [2]. The collective variables we introduce by means of the appropriate group of motions which defines the possible types of excitations in the physical system.

The main object in the procedure of the construction of the collective

---

* Work supported by the Polish Ministry of Education, grant No. II.1.1.P/04/399.

space generated by a density operator ρ and a given group of motions G is an *-algebra $L^2(G)$ and the space of functionals (metastates) on it [3]. The metastate on the algebra $L^2(G)$ is chosen as the following integral:

$$\langle \rho; u \rangle = \int_G dg\ u(g)\ Tr(\rho T(g)), \tag{2}$$

where T(g) is a unitary representation of the group of motion G. Following the standard GNS [3] procedure one can obtain the collective space $\mathcal{K}$ with the scalar product defined by the metastate:

$$(u|v)_{\mathcal{K}} \equiv \langle \rho; u^{\#*} v \rangle = \int_G dg' \int_G dg\ u^*(g') Tr(\rho T(g'^{-1} g)) v(g). \tag{3}$$

This formula shows that the scalar product generated by the density operator is nonlocal, where the nonlocal kernel function is the generalized overlap function, which is a measure of coupling between 'deformations' g an g'. One can obtain the standard GCM approach using the density matrix corresponding to a pure state $\rho = |\rangle\langle|$.

For simplicity we consider here a special but often met case:

$$H|\mu\ A\ a\rangle = E(\mu A a)\ |\mu A a\rangle \quad \& \quad \rho|\mu\ A\ a\rangle = \rho(\mu A a)\ |\mu A a\rangle\ , \tag{4}$$

where μ denotes an invariant in respect of G set of quantum numbers, 'A' labels the ir. r. of G and 'a' denotes a set of remaining quantum numbers required for unique specification of the basis for ir. r. 'A' of G. In this case the collective hamiltonian obtained by projection of H onto the collective space $\mathcal{K}$ has the following spectrum of the collective energies:

$$\mathcal{E}_{Aaa'} = \frac{\sum_{\mu} \rho(\mu A a')\ E(\mu A a)}{\sum_{\mu} \rho(\mu A a')}\ . \tag{5}$$

The additional quantum label 'a' describes some internal motions of the system. The well known example of a such type of quantum number is the number K representing a projection of the angular momentum vector onto an internal axe in the asymmetric top.

2. An example: the 'temperature' dependent IBM model.

In this chapter we would like to show how the method works in a popular model of interacting bosons (IBM-1) [4]. In the model the total number of bosons N for a given nucleus is fixed. We propose here to consider the case of a 'soft core' that allows for 'evaporation' of pairs of nucleons 'coupled' into bosons. This means that the number of bosons can change from N_{min} connected with half the number of valence nucleons or holes to a possible maximum value of N which is not larger than the half of the total number of nucleons in the given nucleus. In the following we choose the so called vibrational limit defined by the following group chain:

$$\begin{array}{ccccccc} SU(6) & \supset & SU(5) & \supset & SO(5) & \supset & SO(3) \\ \downarrow & & \downarrow & & \downarrow & \downarrow & \downarrow \\ N & & n & & v & x & L,M \end{array} \qquad (6)$$

We define the metastate using the canonical density matrix $\rho \equiv Z^{-1}\exp(-\theta H)$, where H is the boson hamiltonian diagonal in (6).

In fig.1 one can notice the origin of the levels: some of them are generated from the ground state by the rotational group SO(3), some by SO(5) and some "require" SU(5) to be excited. This property can be used as a basis of a new group theoretical classification of collective excitations.

In fig.2 there is plotted a behaviour of the collective energies for ^{110}Cd nucleus as a function of the boson temperature $T=1/\theta$. The temperature dependent spectrum should be interpreted as an effective spectrum. On the other hand, the parameter T can be treated as a new free parameter of the theory describing some softness of the core and, in this case, it should be fitted to the experimental data together with the hamiltonian parameters to choose the appropriate collective space.

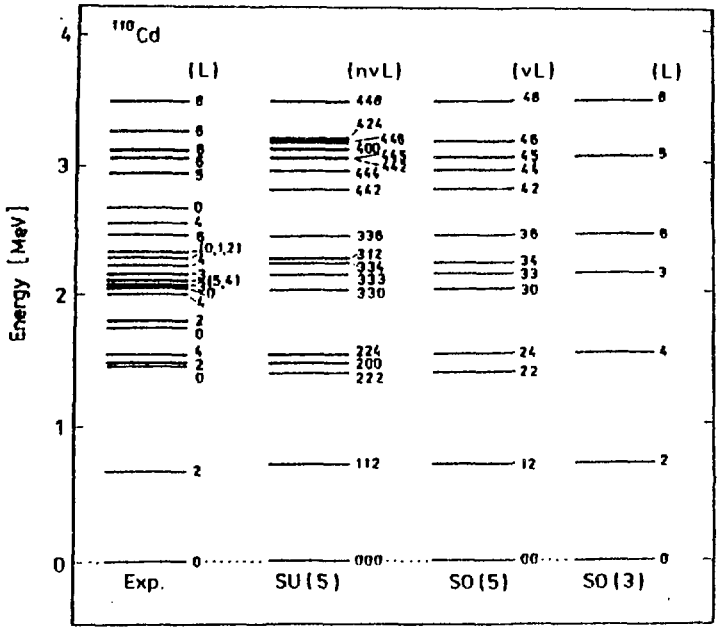

Fig. 1. The AGCM classification of the energy levels of ^{110}Cd in the IBM vibrational limit.

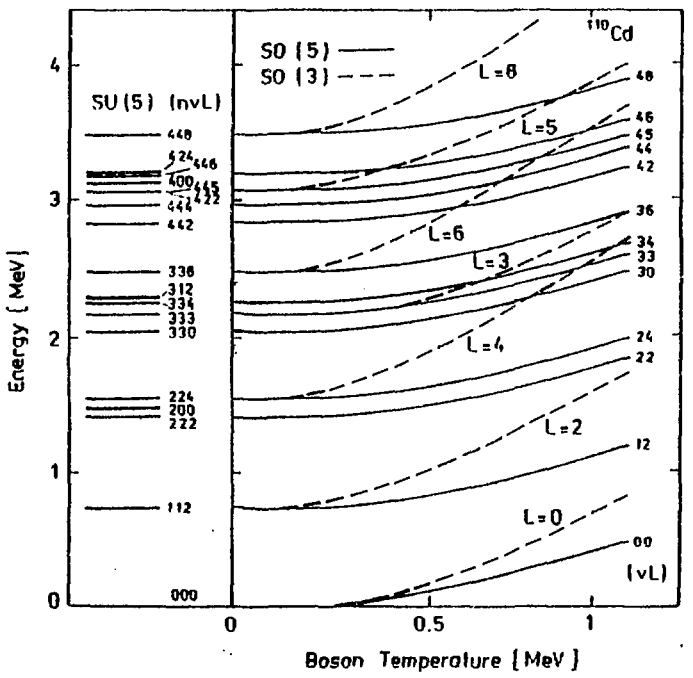

Fig. 2. A dependence of the spectrum of ^{110}Cd on the boson temperature.

3. Conclusions

The AGCM method allows for construction of the collective spaces generated by a density matrix and a given group of motions. The structure of the collective space is dependent on the shape of the metastate which, in turn, can be dependent on some external parameters. This property of the formalism allows for description of the phenomena with the variable state space.

This algebraical approach gives a tool for classification of the energy spectra with respect to subgroups of the group of motions giving also information about the states internal structure. The reduction of degrees of freedom allows to ascertain which kind of motion is responsible for the given energy level. In addition, in some cases one can obtain a double set of quantum numbers generated by the group of motion G - the second set is responsible for some internal structure of the physical system and allows for appearance of some extra bands, like rotational K-bands in the asymmetric top.

Using AGCM in the numerical codes for GCM GHW equations or in GOA approximation it is enough to change the overlap function and the reduced energy kernel.

References

1. D.L.Hill, J.A.Wheeler: Phys.Rev. 89 (1953) 112; J.J.Griffin and J.A.Wheeler: Phys.Rev. 108(1957)311.

2. A.Bogusz and A.Góźdź: The Algebraic Generator Coordinate Method as the Constrained Quantum Mechanics (in preparation).

3. G.G.Emch: Algebraic Methods in Statistical Mechanics and Quantum Field Theory, Willey-Interscience, 1972; O.Bratteli and D.W.Robinson, Operator Algebras and Quantum Statistical Mechanics 1, Springer-Verlag, New York, 1979.

4. A.Arima, F.Iachello: Ann.Phys. 99 (1976) 253.

Statistical Decay Out of the Super-Deformed Yrast Bands ?

M. Palacz Z. Sujkowski
Soltan Institute for Nuclear Studies, PL 05-400 Świerk, Poland

Abstract

The experimental data on super-deformed yrast bands in ^{132}Ce, ^{152}Dy, ^{192}Hg are used to calculate the parameters of transmission coefficient through the potential energy barrier between states of two deformations. It is found that the simplest form of transmission coefficient, together with the standard expressions for transition strengths, allow to reproduce the experimental intensity of super-deformed bands reasonably well.

The existence of discrete super-deformed (SD) bands in the region of high (a few MeV) excitation energy (relatively to normal deformed (ND) yrast line) indicates strong hindrance of statistical out-of-SD-band transitions. This hindrance is often described [1] in terms of penetration through potential energy barrier between states of two different deformations. Another conspicuous feature of the SD bands is their sudden decay out. In this work we attempt to calculate the transmission coefficient through the barrier and its spin dependence needed to describe the changes of experimental intensity [2,3,4] of SD yrast bands. This is done for 3 nuclei from different regions, the simplest form of the transmission coefficient is assumed and standard expressions for transition strengths are used.

The transition probabilities were calculated with standard strength assumptions for the rotational transitions within the SD band and for the statistical out-of-band transitions (fig. 1). The following formulas (from program GAMBLE [5]) have been used:
The statistical out-of-band transition probability:

$$P_{E1}(I) = \int_0^{E_{xSD}(I)} s_{E1} E_\gamma^3 \rho(E_{xSD} - E_\gamma) dE_\gamma,$$

where:

s_{E1} — the strength function with GDR,

$E_{xSD}(I)$ — the excitation energy of SD band relatively to ND yrast

The level density:

$$\rho(E_x) = \frac{1}{24} \frac{2I+1}{(E_x + \frac{3}{2}t)^2} \left(\frac{\hbar^2}{2J^{(2)}}\right)^{3/2} \sqrt{a}\, e^{2\sqrt{aE_x}}$$

The probability of rotational transitions in SD band:

$$P_{rotSD} = B(E2)_{SD} \times 7.346 \times 10^7 \times A^{4/3} \times E_\gamma^5$$

where E_γ is given in MeV.

Since no direct experimental information on the excitation energy of SD band is available, the value of it was chosen somewhat arbitrarily. This is the source of the main uncertainity in the calculated values. However, any reasonable value of E_{xSD} (1 MeV and higher) leads to the same conclusion that the unhindered out-of-band probabilities (for spins close to the decay region of SD band) are always a few orders of magnitude larger than in-band probabilities.

The simplest form of the barrier is one with the shape of an inverted parabola. The transmission coefficient through such a barrier is:

$$T = \frac{1}{1 + \exp\left(\frac{2\pi}{\hbar\omega_B}(E - \quad)\right)}$$

where $E_B(I)$ — height of the barrier

The parameter $\hbar\omega_B$ depends on the shape of the barrier and on the mass parameter. In the calculations presented here it was assumed that $\hbar\omega_B$ does not depend on spin. This is at varriance

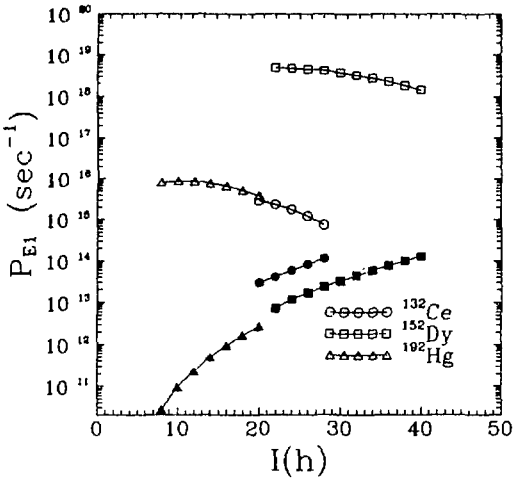

Figure 1: Out of band (open symbols) and in band (full symbols) transition probabilities.

with ref. [6], where rapid change of mass parameter due to onset of pairing was suggested as a reason of the sudden decay of SD band.

Taking into account the fact that T must be much smaller than 1 and assuming the linear dependance of E_B on spin, the formula for T may be simplified:

$$T = Ce^{-\alpha I}$$

Both C and α should be fitted to experimental data. However, the parameters of the transmission coefficient are sensitive to the intensity of only a few (3-7) transitions. Moreover, it was found that C and α are strongly correlated, hence they can not be independently determined from the fit, even if the number of the fitted points is sufficient. It was decided then to assume $C = 1$ and leave only one free parameter — α. This implies the assumption that the barrier vanishes for spin 0.

The transmission coefficient quoted above does not take into account the difference in energy between the initial and final state. In calculations of [1] the problem was solved by the assumption of sequential nature of the process of decay of superdeformed band, i.e. the barrier penetration without energy change was followed by the statistical decay in the normal-deformed well. One may argue that this does not reflect the physical situation and, more important, it requires large level density of the initial state, which is not the case for transitions from super-deformed yrast bands. A recipe for calculation of T' (the transmission coefficient including difference in energy between the initial and final state), on the basis of overlap of wave-functions in 2 wells was presented in [7]. The resulting formulas are, however, rather complex, especially to be used for fit. An approximate formula was used (compare [7]):

$$T' = \frac{KT}{(E_\gamma^2 + K)} \qquad K \cong 0.006$$

As was mentioned before, the excitation energy of SD bands is unknown. In the case of ^{152}Dy there are arguments [3] that SD band becomes yrast around I=54 — this corresponds to $E_{xSD}(I = 22) = 5.26$ MeV. The parameter α was calulated assuming such E_{xSD}. For other nuclei, value of the α of ^{152}Dy was assumed and then the E_{xSD} calculated. This procedure was repeated for various values of E_{xSD} in ^{152}Dy. The results of calculations are presented in fig. 2 and table 1 (curves in the figure correspond to row 1 in the table).

Conclusion: The decay out of the super-deformed band may be acceptably described by statistical transitions through the energy barrier between the SD and ND states with only one free parameter, corresponding to linear dependence of the berrier height on spin. The same value of the parameter may be used for different nuclei, if the excitation energy of SD band is adjusted. This is obtained with rather slow variation of the barrier height, similarly as calculated in [8] (however, in opposite to [8], $E_B(I = 0) = 0$ is assumed).

		^{132}Ce $(I=18)^{a)}$	^{152}Dy $(I=22)^{a)}$	^{192}Hg $(I=8)^{a)}$
1.	α	0.26	0.26	0.26
	E_{xSD} $[MeV]$	4.61	5.26	1.36
	χ^2/n	0.68	1.21	1.34
2.	α	0.19	0.19	0.19
	E_{xSD} $[MeV]$	3.82	4.26	1.14
	χ^2/n	0.77	1.65	1.82
3.	α	0.23	0.23	0.23
	E_{xSD} $[MeV]$	4.26	4.76	1.26
	χ^2/n	0.72	1.40	1.54
4.	α	0.29	0.29	0.29
	E_{xSD} $[MeV]$	4.97	5.76	1.46
	χ^2/n	0.64	0.50	1.16

[a] spin of the lowest observed SD state

Table 1:

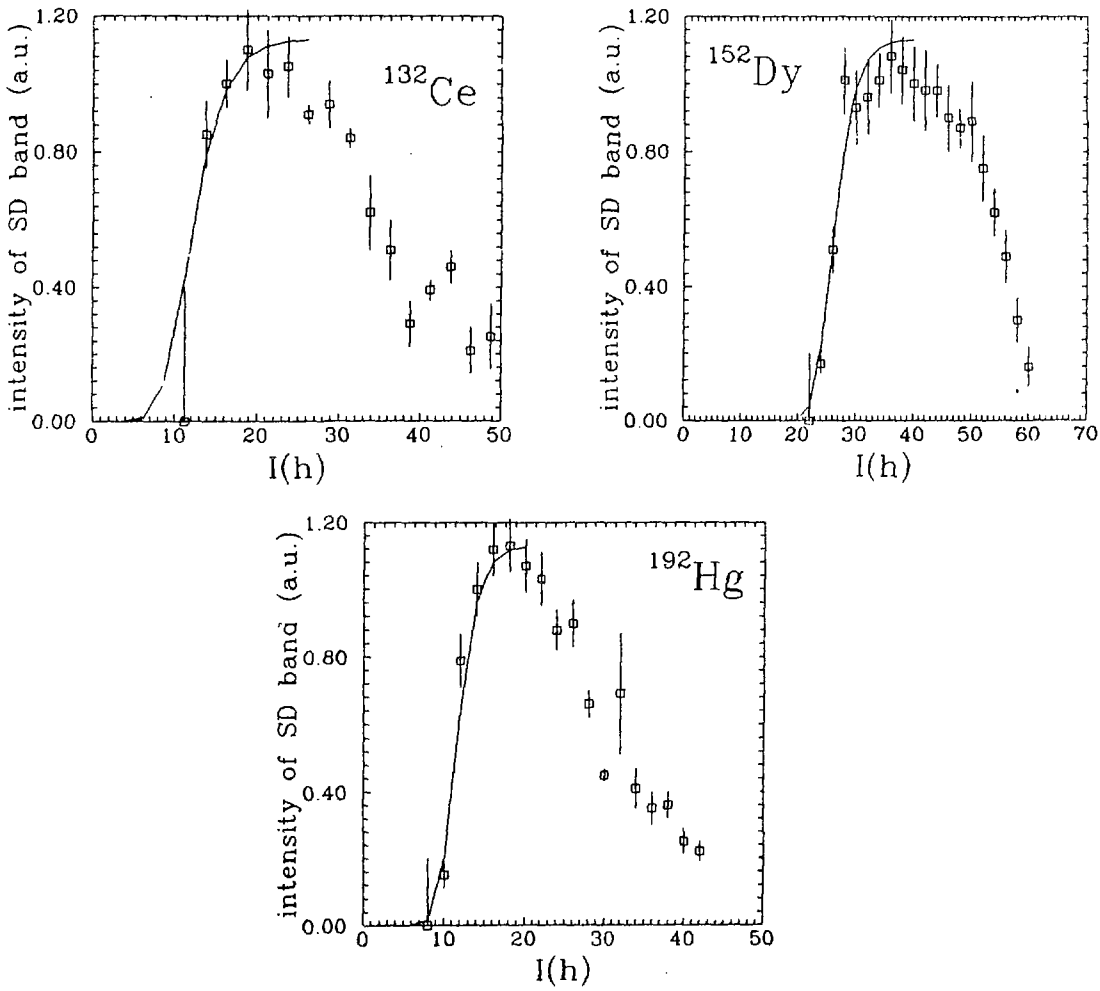

Figure 2: Intensity of transitions in SD (yrast) bands.

References

[1] I. Ragnarsson, S. Aberg Phys. Lett. **B180** (1986) 191
B. Herskind, K. Shiffer "Superdeformed ^{152}Dy — Population and Decay" in proc of "Trends in Nuclear Physics", Corso 1989

[2] A. J. Kirwan et al. Phys. Rev. Lett. **58** (1987) 467

[3] A. B. Bentley et al. J. Phys. **G17** (1991) 481

[4] H. Hübel et al. Nucl. Phys. **A453** (1986) 316
J. A. Becker et al. Phys. Rev. bf C41(1990) R9
D. Ye et al. Phys. Rev. **C41** (1990) R13

[5] G.A. Leander Comp. Phys. Comm. **47** (1987) 311

[6] J. Dudek et al. Phys. Rev. **C 38** (1988) 940

[7] S. Bjørnholm, J. E. Lynn Rev. Mod. Phys. **52** 725

[8] I. Ragnarsson et al., Nucl. Phys. **347** (1980) 287

THE ASTROPHYSICAL RELEVANT REACTION $^{19}F(p,\alpha)^{16}O$ AT SUB-COULOMB ENERGIES

S. Ambacher†, U. Atzrott*, H. Abele*, A. Denker†, J.W. Hammer†, H. Herndl‡, R. Neu*, H. Oberhummer‡, G. Staudt*

† Institut für Strahlenphysik, Universität Stuttgart, D - 7000 Stuttgart, Fed. Rep. of Germany

* Physikalisches Institut, Universität Tübingen, D - 7400 Tübingen, Fed. Rep. of Germany

‡ Institut für Kernphysik, Technische Universität Wien, A - 1040 Wien, Austria

Abstract

New results are given for the reaction $^{19}F(p,\alpha)^{16}O$. A DWBA analysis for $^{19}F(p,\alpha_0)^{16}O$ has been carried out using a double folding α optical potential. Excitation functions of $^{19}F(p,\alpha_{2,3,4})^{16}O^*$ have been measured at 12 angles at energies between E_{cm} = 175 keV and 1 MeV.

I. INTRODUCTION

The main energy source of stars is the nuclear burning in their interior. In hydrogen burning of main-sequence stars there are two dominant processes: the p-p chain and the CNO cycle. In the fourth branch of the CNO cycle the nuclear reactions $^{18}O(p,\gamma)^{19}F$, $^{19}F(p,\alpha)^{16}O$ and $^{19}F(p,\gamma)^{20}Ne$ are observed. In order to reproduce the fluorine abundance in the universe by a stellar evolution model, the accurate knowledge of the ^{19}F + p reaction rate is important. Therefore some work has been done concerning the reaction $^{19}F(p,\alpha_0)^{16}O$ at energies below 1 MeV [1, 2]. In Fig. 1 the transitions investigated are shown. The most remarkable result is the smooth variation of the α_0 excitation function while there are strongly resonant excitation functions for the transitions to the excited states in ^{16}O [1, 3].

In this work we analyse the $^{19}F(p,\alpha_0)^{16}O$ cross section in a wide energy range in the framework of a direct reaction mechanism (Section II). In Section III new experimental

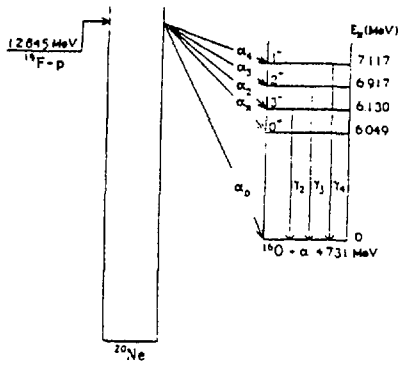

Figure 1: Energy scheme for the reactions $^{19}F(p,\alpha)^{16}O$ (g. s.), $^{19}F(p,\alpha_\pi\gamma)^{16}O^*$ and $^{19}F(p,\alpha_{2,3,4}\gamma)^{16}O^*$

results are given concerning the reaction $^{19}F(p,\alpha_2)^{16}O^*$ (E_x = 6.13 MeV, 3^-). Finally, in Section IV the results are summarized.

II. DWBA ANALYSIS OF $^{19}F(p,\alpha_0)^{16}O$ (g. s.)

The angular distributions and the absolute magnitude of the $^{19}F(p,\alpha)^{16}O$ (g. s.) cross section can be well reproduced by microscopic DWBA calculations at projectile energies greater than 9 MeV [4]. An essential improvement in the calculation of the absolute cross section for (p,α) reactions was obtained by using the double-folding procedure for the α-optical potential [5]. Recently, DWBA calculations in the energy range between 150 and 850 keV were carried out using a microscopic form factor identical to the one used for energies E > 9 MeV [3]. Good agreement was found not only for the angular distributions, but also for the absolute values of the cross sections. In Fig. 2 the results of the DWBA calculations (dashed lines) are compared with experimental data (full lines) for incident energies between 0.1 and 50 MeV. In the energy region between about 0.8 and 10 MeV where the cross section is dominated by strong compound resonances, DWBA calculations have been carried out straight forward (dotted lines).

Contrary to the g. s. transition strong resonances in the excitation functions for the α_2, α_3 and α_4 are observed for sub-Coulomb energies. It has been found that the cross section of the α_2 transition is larger by approximatly one order of magnitude than that for the g. s. transition. This observation is in agreement with the result [3] that Hauser-Feshbach (HF) calculations overestimate the cross section of the g. s. transition by a factor of 10. As discussed in [3], the reason for this discrepancy can be found in the HF ansatz, which does not account for the shell-model structures of the nuclei involved: The excited states in the compound nucleus ^{20}Ne have only a small α + ^{16}O (g. s.) component and

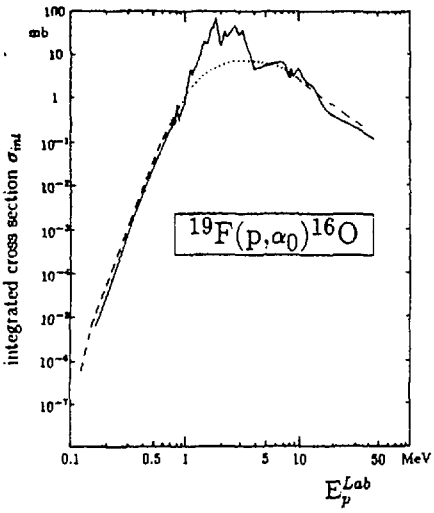

Figure 2: Comparison of experimental absolute cross sections (solid lines) with DWBA calculations (dashed and dotted lines).

therefore the decay of the compound nucleus into the ground state is strongly suppressed.

III. TRANSITIONS TO EXCITED STATES IN ^{16}O.

This argument is not valid for the transitions to the excited states of ^{16}O. Therefore one can assume that these transitions can be described as compound reactions. In a recent paper P. Aguer et al. [6] have analysed the experimental data of Bulski [2] in a R-matrix calculation. Strong interference effects between low lying 1^+ states result in a drastic change of the admitted value of the astrophysical S(E) factor. Especially the consideration of a new 1^+ level at $E_x = 12.859$ MeV (only 11.5 keV above the proton threshold) that has been recently observed by Kious in the p-transfer reaction $^{19}F(^3He,d)^{20}Ne$ [7], result in a strong influence on the $^{19}F(p,\alpha)^{16}O$ cross section in the range up to 300 keV, i. e. in the region of the Gamow peak.

In order to look for such interference effects especially in the tails of the strong resonances, we have measured the excitation function of $^{19}F(p,\alpha_{2,3,4})^{16}O$ at 12 angles in the c. m. energy range betweeen 175 and 1000 keV using inverse kinematics. The experiment was carried out at the Bochum 4 MeV Dynamitron-Tandem accelerator using a ^{19}F beam. The target was the Stuttgart supersonic windowless gastarget RHINOCEROS with a ^1H jet. For a detailed description of the target properties see [8]. The α particles were measured directly using 12 ion-implanted Si-detectors. These were mounted at fixed angles between $\theta_{Lab} = 9.3°$ and 62.7°. Fig. 3 shows a spectrum of the measurement.

The cross section was normalized through monitoring the elastic scattering $^{19}F(p,p)^{19}F$. For this a second run was done using a mixed ^{40}Ar-^{1}H jet to measure the deviation of $^{19}F(p,p)^{19}F$ from Rutherford scattering. In comparison to Bulski [2] we used an advanced set up to gain more accurate data.

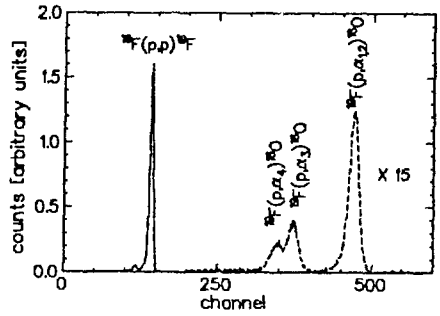

Figure 3: Typical spectrum : $E_{cm} = 824$ keV, $\theta_{Lab} = 12.8°$

Up to now only excitation functions of the α_2 group can be shown, the evaluation of the α_3 and α_4 data is still under way. In Fig. 4 the integrated cross sections for the α_2 transitions are plotted together with the data of Bulski [2]. Comparing both sets of data, the new measurement results in cross section values in the tails of the resonances which are somewhat lower than those given by Bulski. A new R-matrix calculation must show which consequences will result from these data concerning the burning stage of hydrogen in the CNO cycle.

IV. CONCLUSIONS

We have calculated the reaction $^{19}F(p,\alpha_o)^{16}O$ (g. s.) in the direct reaction model. In the DWBA calculations double-folding α potentials and a microscopic form factor were used. Excellent agreement with experimental data is obtained in the energy range from the sub-coulomb region up to about 50 MeV.

New experimental data are presented for the reaction $^{19}F(p,\alpha_2)^{16}O^*$ ($E_x = 6.13$ MeV, 3^-) in the range between 175 keV and 1 MeV. In the excitation function strong resonances are observed. Comparing the new results with older data, differences have been found especially in the tails of the resonances. An interpretation of these data concerning the hydrogen burning of ^{19}F should be carried out.

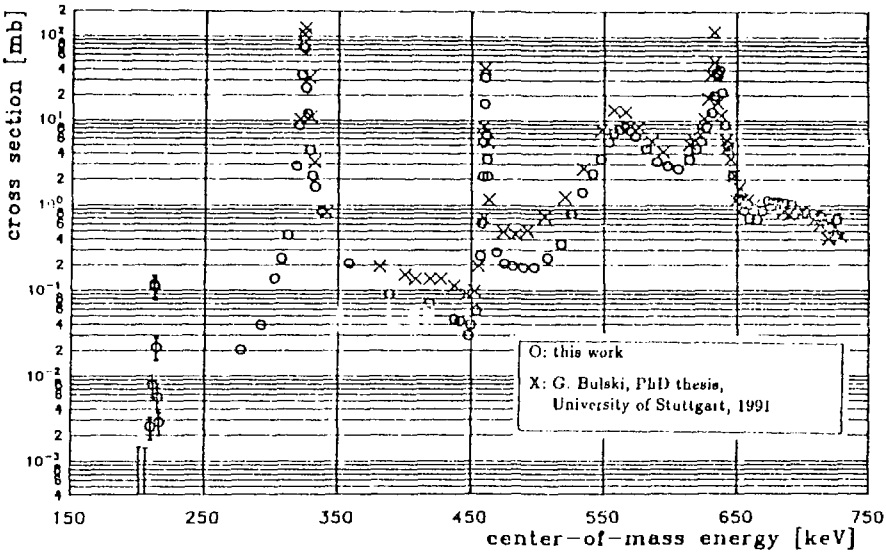

Fig. 4: Integrated cross sections for $^{19}F(p,\alpha_2)^{16}O^*$ in comparison with the data of [2].

ACKNOWLEDGMENTS

This work has been funded by the Deutsche Forschungsgemeinschaft under Contract No. Ha 962/10.

References

[1] H. Lorenz-Wirzba, PhD thesis Münster 1978

[2] G. Bulski, PhD thesis, Universtität Stuttgart, 1991

[3] H. Herndl et al. Phys. Rev. C, in press

[4] R. Neu et al., J. Phys. Soc. Jap. 58 1989 , Suppl. 574

[5] M. Walz et al., J. Phys. G 14 (1988) L91

[6] P. Aguer et al., to be published

[7] M. Kious, PhD thesis, Universite de Paris XI, 1990

[8] T. Griegel et al., J. Appl. Phys. **69** (1), 1 January 1991, pp. 19

ASTROPHYSICAL S-FACTORS OF REACTIONS RELEVANT FOR THE SOLAR NEUTRINO PROBLEM

H. Krauss, K. Grün, T. Rauscher, S. Winkler, H. Oberhummer
Institut für Kernphysik, TU Wien, Wiedner Hauptstr. 8-10, A-1040 Wien, Austria
H. Abele, R. Zwiebel, G. Staudt
Physikalisches Institut, Univ. Tübingen, Auf der Morgenstelle, D-74 Tübingen, Germany

Abstract

The astrophysical S-factors for the reactions ^{3}He(α,γ)^{7}Be and ^{7}Be(p,γ)^{8}B which are relevant for the solar neutrino problem are calculated. Excellent agreement with the experimental data is obtained.

1 Introduction

The reactions ^{3}He(^{3}He,2p)^{4}He, ^{3}He(α,γ)^{7}Be and ^{7}Be(p,γ)^{8}B determine the branching ratios between the ppI, ppII and ppIII chains in hydrogen burning of main-sequence stars. The magnitude of their reaction cross sections is of special interest for the solar neutrino problem. The reason for this is that in the ^{37}Cl neutrino experiment [1] 14% and 77%, in the Kamiokande II experiment [2] 0% and 100% and in the gallium experiments [3, 4] 26% and 11% of the detected neutrino flux stem from the high-energy neutrinos emitted in the ppII and ppIII chain, respectively [5]. Therefore, the reaction rates of the above processes determine the high-energy solar neutrino flux. In this work we investigate the last two reactions; the results for the first reaction ^{3}He(^{3}He,2p)^{4}He was published elsewhere [6].

The reactions considered in this paper have been measured by a number of authors at subCoulomb energies. The most recent data have been obtained in the energy range $E_{c.m.} = 165 - 1170$ keV for ^{3}He(α,γ)^{7}Be [7] and $E_{c.m.} = 117 - 1230$ keV for ^{7}Be(p,γ)^{7}B [8].

The dominance of the direct interaction mechanism (DI) and the validity of the description with the potential-model approach below the Coulomb barrier has been established in many light-ion reactions ([9] and references therein). In this work we apply this approach to the above reactions. In the next section we introduce the direct capture model. In Section 3 the results for the astrophysical S-factors are given and compared to the experimental data. Finally, in Section 4 the results are summarized.

2 Potential Model Approach

Potential models are based on the description of the dynamics of the reaction by a Schrödinger equation with local optical potentials in the entrance and/or exit channels. Such models are the "Distorted Wave Born Approximation" (DWBA) [10, 11, 12] for transfer or the "Direct Capture"-model (DC) [13, 14, 15] for capture reactions.

In the first order perturbation theory the expression for the differential cross section of a direct capture reaction is [16]:

$$\frac{d\sigma_{DC}}{d\Omega_\gamma} = 2\left(\frac{e^2}{\hbar c}\right)\left(\frac{mc^2}{\hbar c}\right)\left(\frac{k_\gamma}{k_a}\right)^3 \frac{1}{2I_A+1}\,\frac{1}{2S_a+1} \sum_{M_A M_a M_B \sigma} |\, T_{M_A M_a M_B,\sigma}\,|^2 \quad . \tag{1}$$

Here the I_A (M_A) and the S_a (M_a) are the spins (their projections on the z-axis) of target and projectile, respectively, σ is the polarization of the electromagnetic radiation ($\sigma = \pm 1$). The wave numbers of the emitted γ-rays and of the asymptotic relative wave function in the entrance channel are denoted by k_γ and k_a, and m is the reduced mass. The transition amplitudes $T_{M_A M_a M_B,\sigma}$ are expanded in terms of rotation matrix elements $d^\lambda_{\delta\sigma}(\theta)$ with the electromagnetic multipole λ (λ = E1, E2, M1,...),

$$T_{M_A M_a M_B,\sigma} = \sum_\lambda T^\lambda_{M_A M_a M_B,\sigma}\, d^\lambda_{\delta\sigma}(\theta) \tag{2}$$

where $\delta = M_A + M_a - M_B$ and θ is the angle between $\vec{k}_a$ and $\vec{k}_\gamma$.
The transition amplitudes are proportional to the radial integrals

$$T^\lambda \propto I^\lambda_{l_b j_b I_B; l_a j_a} = \int dr\, U_{l_b j_b I_B}(r)\, \mathcal{O}^\lambda(r)\, \chi_{l_a j_a}(r) \quad , \tag{3}$$

where $U_{l_b j_b I_B}(r)$ and $\chi_{l_a j_a}(r)$ are the radial parts of the bound state wave function and the distorted wave function in the entrance channel, respectively. The functions $\mathcal{O}^\lambda(r)$ are the radial parts of the electromagnetic multipole operators, which were taken in their approximated form

$$\mathcal{O}^{\mathrm{M1}}(r) \simeq 1, \quad \mathcal{O}^{\mathrm{E1}}(r) \simeq r, \quad \mathcal{O}^{\mathrm{E2}}(r) \simeq r^2. \tag{4}$$

We solve the radial integral (3) numerically using a single or double folding potential for the bound state potential and the real part of the optical potential:

$$U(\vec{r}) = \lambda \int d\vec{r}_A\, \rho_A(\vec{r}_A)\, t(E, \rho_A, \vec{s} = \vec{r} - \vec{r}_A) \tag{5}$$

$$U(\vec{r}) = \lambda \int d\vec{r}_A \int d\vec{r}_a\, \rho_A(\vec{r}_A)\, \rho_a(\vec{r}_a)\, t(E, \rho_A, \rho_a, \vec{s} = \vec{r} + \vec{r}_a - \vec{r}_A) \tag{6}$$

where $\vec{r}$ is the separation of the centers of mass of the bound or colliding particles, ρ_a and ρ_A are the respective nucleon densities of projectile and target and λ is the normalization constant. For the effective nucleon nucleon interaction t in the entrance and exit channels we chose the density dependent form of the M3Y interaction [17]. For the density distribution of the target nuclei we used the experimental charge distribution [18] (in the case of ^{7}Be the distribution of ^{7}Li was chosen), and for the α-particle we used a Gaussian form [19]. The normalization constants λ of the folding potentials account for the interplay of the Pauli principle and distortion and break-up effects. One of the advantages of the folding procedure lies in the fact that no open geometrical parameters exist. Therefore the form of the optical and bound-state potentials is determined uniquely.

3 Results

The numerical calculations in the DI model were performed using the direct capture code code TEDCA [20].

First we consider the reaction ^{3}He(α,γ)^{7}Be. This reaction was analyzed before in the DC model by either neglecting the nuclear potential [14] or by using different more or less phenomenological parametrisations [21]. Furthermore, many calculations exist using the resonating group method [22, 23, 24, 25, 26, 27].

In our calculation the normalization constant λ in the entrance channel was fitted to the ^{3}He+^{4}He low-energy experimental elastic scattering data [28, 29]. We obtained $\lambda = 1.47$ corresponding to a depth of the potential $V(0) = -72.3$ MeV and a volume integral of 513.9 MeV fm^3. For the bound state the depth of the folding potential was adjusted to reproduce the correct separation energy of 1.586 MeV.

The result of the DC calculation for the astrophysical S-factor in the energy range up to 1.3 MeV is compared to the experimental data in Fig. 1. For low energies the S-factor can be parametrized as $S(E) = (0.549 - 2.9 \cdot 10^{-4} E)$ keV b. As can be seen there is good agreement with the data [7].

The ^{7}Be(p,γ)^{8}B reaction is of crucial importance since it leads to the high-energy ^{8}B neutrinos. Unfortunately, there are still significant experimental uncertainties in the low-energy cross section for this reaction. The reaction was analyzed before in the DC model by either neglecting the nuclear potential [14] or by using phenomenolgical potentials [21]. Furthermore, this reaction was also analyzed with the resonating group method (RGM) [30, 31].

The normalization constant $\lambda = 0.94$ together with a small spin-orbit term ($V_{so} = 2.0$ MeV, $r_{so} = 1.54$, $a_{so} = 0.52$) reproduces the energies of the resonances due to $p_{3/2}$ and $p_{1/2}$ capture at $E_{cm} = 0.633$ MeV and $E_{cm} = 1.4$ MeV, respectively. For the bound state the depth of the folding potential was adjusted to reproduce the correct separation energy of 138 keV.

The result of the DC calculation for the astrophysical S-factor in the energy range up to 2.5 MeV is compared to the experimental data in Fig. 2. The low energy behaviour can be parametrized as $S(E) = (0.02468 - 5.6 \cdot 10^{-5} E)$ keV b. As can be seen there is excellent agreement with the data [32, 33] including the resonance energy of the 1^+ resonance at $E_{c.m.} = 633$ keV. We want to emphasize that in this calculation there is no open parameter which had to be adjusted to the reaction.

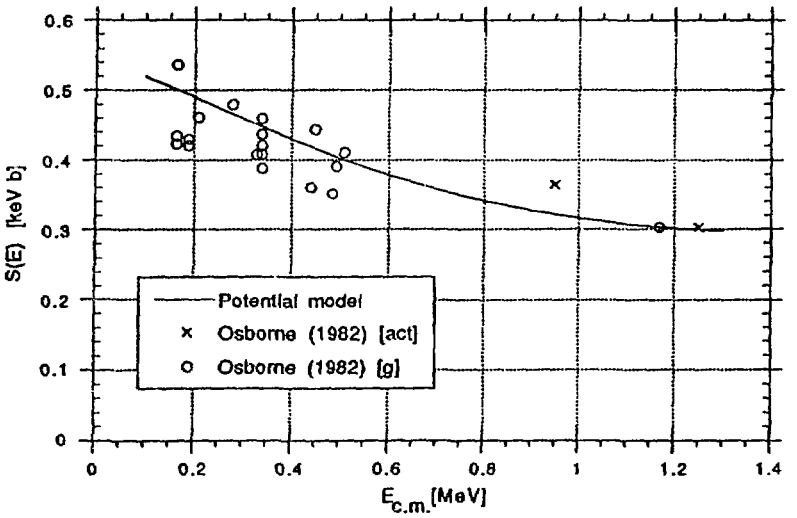

Figure 1: Astrophysical S-factor for the reaction $^3He(\alpha,\gamma)^7Be$ as a function of the c.m.-energy up to 1.3 MeV. The solid line is the result of the DC-calculation. The experimental data are taken from [7] ([g]: detection of prompt γ-rays, [act]: activation analysis).

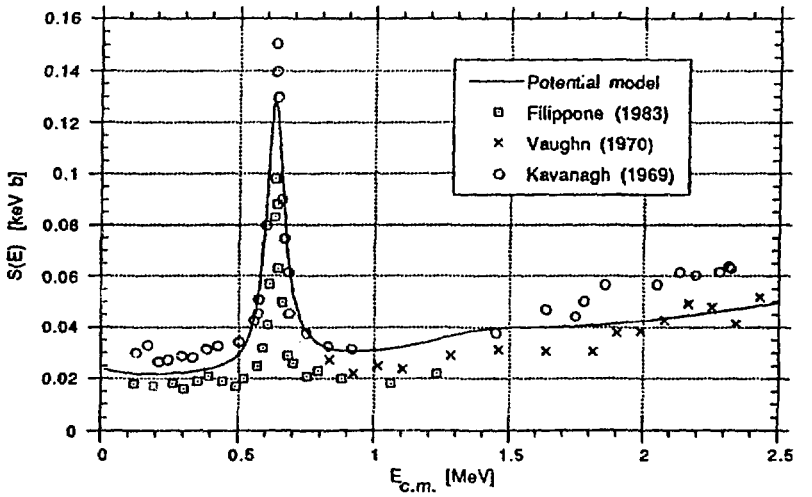

Figure 2: Astrophysical S-factor for the reaction $^7Be(p,\gamma)^8B$ as a function of the c.m.-energy up to 2.5 MeV. The solid line is the result of the DC-calculation. The experimental data are taken from [8] (squares), [32] (crosses), and [33] (circles).

4 Summary

The results relevant for the solar neutrino problem are shown in the table. The first and second rows show the astrophysical S-factors $S(0)$ and their derivatives dS/dE with respect to the energy $E=0$. The third row gives the S-factor at the effective mean energy E_0 for the thermonuclear fusion in the sun at a temperature of $T_6 = 15$. The theoretical values for the three reactions are given and compared with the experimental values including their 3σ errors using the data obtained from the original experimental papers [5]. The theoretical values for the astrophysical S-factors agree with the mean experimental values to less than 3%.

Reaction	^{3}He(^{3}He,2p)^{4}He	^{3}He(α,γ)^{7}Be	^{7}Be(p,γ)^{8}B
$S(E=0)$ [keV b]			
Theory	$5.038 \cdot 10^3$	0.549	0.02468
Experiment	$(5.15 \pm 0.88) \cdot 10^3$	0.54 ± 0.03	0.0234 ± 0.0051
$dS/dE\,(E=0)$ [b]			
Theory	-2.92	$-2.90 \cdot 10^{-4}$	$-5.5 \cdot 10^{-5}$
Experiment	-0.9	$-3.1 \cdot 10^{-4}$	$-3 \cdot 10^{-5}$
$S(E_0)$ [keV b]			
Theory	$4.980 \cdot 10^3$	0.542	0.02365
Experiment	$(5.13 \pm 0.88) \cdot 10^3$	0.53 ± 0.03	0.0237 ± 0.0053

All three reactions were calculated in a consistent way by using the potential model and the folding procedure. We want to emphasize that for the reactions ^{3}He(α,γ)^{7}Be and ^{7}Be(p,γ)^{8}B no parameters in the calculation had to be adjusted to the experimental reaction data. Still excellent agreement with the absolute values as well as the energy dependences of the experimental astrophysical S-factors was obtained.

Acknowledgement: We want to thank the Österreichische Nationalbank (project 3924) and the DFG (project Sta290/2-1) for their support.

References

[1] R. Davis Jr., A.K. Mann, L. Wolfenstein, *Ann. Rev. Nucl. Part. Sci.* **39**, 467 (1989)
[2] K.S. Hitara *et al.*, *Phys. Rev. Lett.* **63**, 16 (1989)
[3] W. Hampel, in *Proc. Workshop Neutrino Physics*, ed. by H.V. Klapdor (Spinger Verlag, Heidelberg 1988)
[4] V.N. Gavrin, in *Proc. Neutrino '88*, ed. by J. Schnepps (World Scientific, Singapore 1989)
[5] J.N. Bahcall, in *Neutrino Astrophysics* (Cambridge: Cambridge University Press 1989)
[6] S. Winkler *et al.*, in *Proceedings of Sixth Workshop in Nuclear Astrophysics, February 18-23, 1991, Ringberg Castle, Germany*, in press
[7] J.L. Osborne *et al.*, *Phys. Rev. Lett.* **48**, 1664 (1982) and *Nucl. Phys. A* **419**, 115 (1984)
[8] B.W. Filippone, A.J. Elwyn, C.N. Davids, and D.D. Koethe, *Phys. Rev. C* **28**, 2222 (1983)
[9] H. Oberhummer and G. Staudt, in *Nuclei in the Cosmos*, ed. by H. Oberhummer (Springer Verlag, Heidelberg 1991)
[10] N. Austern, *Direct Nuclear Reaction Theories* (John Wiley & Sons: New York 1970)
[11] G.R. Satchler, *Direct Nuclear Reactions* (Clarendon Press: Oxford) (1983)
[12] N.K. Glendenning, *Direct Nuclear Reactions*, (Academic Press: New York 1983)
[13] R.F. Christy and I. Duck, *Nucl. Phys. A* **24**, 89 (1961)
[14] T.A. Tombrello and P.D. Parker, *Phys. Rev.* **131**, 2582 (1963)
[15] C. Rolfs, *Nucl. Phys. A* **217**, 29 (1973)
[16] K.H. Kim, M.H. Park and B.T. Kim, *Phys. Rev. C* **35**, 1, 363 (1987)
[17] A.M. Kobos *et al.*, *Nuc. Phys. A* **425**, 205 (1984)
[18] H. de Vries, C.W. de Jager, C. de Vries, At. Data and Nucl. Data Tables **36**, 495 (1987)
[19] G.R. Satchler and W.G. Love, *Phys. Rev.* **55**, 183 (1979)

[20] H. Krauss, code TEDCA, not published
[21] B.T. Kim, T. Izumoto, and K. Nagatani, *Phys. Rev. C* **23**, 1 (1983)
[22] H. Walliser, H. Kanada, and Y.C. Tang, *Nucl. Phys. A* **419**, 133 (1984)
[23] T. Kajino and A. Arima, *Phys. Rev. Lett.*, **52**, 9, 739 (1984)
[24] K. Langanke, *Nucl. Phys. A* **457**, 351 (1986)
[25] T. Mertelmeier, H.M. Hofmann, *Nucl. Phys. A* **459**, 387 (1986)
[26] T. Kajino, *Nucl. Phys. A* **460**, 559 (1986)
[27] Q.K.K. Liu, H. Kanada, and Y.C. Tang, *Phys. Rev. C* **33**, 5, 1561 (1986)
[28] R.J. Spiger and T.A. Tombrello, *Phys. Rev.* **163**, 964 (1967)
[29] A.C.L. Barnard, C.M. Jones, and G.C. Phillips, *Nucl. Phys.* **50**, 629 (1964)
[30] P. Descouvemont ans D. Baye, *Nucl. Phys. A* **487**, 420 (1988)
[31] C.W. Johnson *et al.*, submitted to *Ap. J.* (1990)
[32] F.J. Vaughn *et al.*, *Phys. Rev. C* **2**, 1657 (1970)
[33] R.W. Kavanagh *et al.*, *Bull. Am. Phys. Soc.* **14**, 1209 (1969)

ELECTRON SCREENING IN THE REACTIONS ^{7}Li(p,α)^{4}He, ^{6}Li(d,α)^{4}He AND DWBA CALCULATIONS IN THE SUBCOULOMB REGIME [1]

G. Raimann, S. Engstler and C. Rolfs
Institut für Kernphysik, Universität Münster, FRG, and
Institut für Physik mit Ionenstrahlen, Universität Bochum, FRG

K. Grün and H. Oberhummer
Institut für Kernphysik, TU Wien, Austria

ABSTRACT

New experimental data of the reactions ^{7}Li(p,α)^{4}He and ^{6}Li(d,α)^{4}He down to approximately 10 keV center-of-mass energy were taken in Münster and Bochum recently. The measurements serve two purposes: the effect of electron screening was investigated using both solid (atomic) and gas (molecular) targets, and the new cross section or $S(E)$ data (corrected for electron screening) put the available low-energy data on a more reliable basis. In a theoretical program simultaneously carried out in Vienna and Tübingen the reaction ^{7}Li(p,α)^{4}He was investigated using the DWBA formalism for direct nuclear reactions.

1 INTRODUCTION

For astrophysical purposes it is common to extrapolate the nuclear cross section down to zero energy. Since the cross section drops steeply at subCoulomb energies (several orders of magnitude) this extrapolation is more easily done using the astrophysical $S(E)$-factor, defined by removing the strongly energy-dependent quantities of the cross section:

$$\sigma(E) = S(E)\,\frac{1}{E}\,\exp(-2\pi\eta) \quad . \tag{1}$$

The term $2\pi\eta = 31.29 \cdot Z_1 Z_2 \sqrt{\mu/E}$ is the Sommerfeld parameter, with the charge numbers Z_1 and Z_2, the reduced mass μ in amu, and the center-of-mass energy E in keV. This equation is based on the assumption of a Coulomb potential extending to infinity, i.e. on the Coulomb potential of a bare nucleus. Under laboratory conditions, however, the target material is usually in atomic or molecular composition, and the electron clouds surrounding the nuclei shield the Coulomb potential experienced by incoming charged projectiles. Hence the charged projectiles see a reduced Coulomb barrier, or equivalently, the experiment measures a cross section higher than for the case of bare nuclei. The penetration through a shielded Coulomb potential at projectile energy E is equivalent to that of bare nuclei at energy $E_{\rm eff} = E + U_{\rm e}$, if $U_{\rm e}$ is the electron screening potential (in the simple Coulomb picture $U_{\rm e}$ is given by $U_{\rm e} \simeq Z_1 Z_2 e^2/R_{\rm a}$ with $R_{\rm a}$ equal to e.g. the radius of the innermost electrons of target or projectile). For the reactions

[1] Supported in part by DFG Ro 429/18-2 and the Fond zur Förderung der wissenschaftlichen Forschung in Österreich P6760T

discussed here, $U_e \simeq 240$ eV. The enlarged cross section due to electron screening is then given by the enhancement factor

$$f_{LAB}(E) = \frac{\sigma(E_{eff})}{\sigma(E)} = \frac{E \cdot \exp(-2\pi\eta(E_{eff}))}{E_{eff} \cdot \exp(-2\pi\eta(E))} \simeq \exp\left(\pi\eta(E) \cdot \frac{U_e}{E}\right) \quad \text{for} \quad U_e \ll E \quad . \qquad (2)$$

For energies sufficiently large (e.g. $E/U_e \geq 1000$) the screening effect is negligible. Consequently, the experimental cross section (or $S(E)$-factor) is that of a bare nucleus, and polynomial fits can be used to extrapolate $S(E)$ down to zero energy. For astrophysical purposes this $S(E)$-factor of bare nuclei is the important quantity, since the effect of screening in stellar plasma involves an enhancement factor f_{plasma} different to f_{LAB} for electron screening under laboratory conditions [1].

In order to gain a deeper understanding of low-energy $S(E)$-data, it is essential that experiments continue to investigate reactions of astrophysical interest in the subCoulomb energy range. At the same time theoretical effort is required to study electron screening and to provide expressions for the cross section of bare nuclei based on nuclear models. These theoretical expressions can then be used instead of the polynomial fits presently employed. This work reports on new low-energy measurements and first results in a theoretical description of subCoulomb reactions based on a direct mechanism.

2 EXPERIMENTAL PROCEDURE AND RESULTS

A detailed description of the experimental setup will be given in [2]. Measurements were performed with solid targets and proton (or deuteron) beams, and in inverse kinematics using a hydrogen (or deuterium) gas target and lithium beams (approximate center-of-mass energy range 10 to 1500 keV).

In the data analysis of the gas target measurements the effective beam energy was corrected by the energy loss in the gas, the target thickness, the energy straggling and the calibration of the accelerator. The $S(E)$-data were corrected by the measured angular distributions $W(\theta)$. A fit of U_e (eq. 2), where the $S(E)$-factor of bare nuclei was substituted by a polynomial fit to literature data at higher energies, leads to screening potentials of $U_e = 260 \pm 50$ eV for the reaction ^{7}Li(p,α)^{4}He, and of $U_e = 290 \pm 40$ eV for ^{6}Li(d,α)^{4}He.

In the case of solid target measurements (LiF targets) the changing stoichiometry had to be detected in situ; this was mainly done by checking the two resonances in ^{19}F(p,$\alpha\gamma$)^{16}O at $E_p = 340.5$ keV and $E_p = 224.0$ keV. Details will be given in [2]. The $S(E)$-data were also corrected by the measured angular distributions $W(\theta)$. The fit of U_e leads to screening potentials of $U_e = 350 \pm 70$ eV for the reaction ^{7}Li(p,α)^{4}He, and of $U_e = 390 \pm 50$ eV for ^{6}Li(d,α)^{4}He.

The results of $S(E)$ are shown in Figs. 1 and 2. The polynomial fits leading to U_e and the literature polynomial fits are also shown. One set of gas target $S(E)$-data was absolutely determined, another gas target data set (at lower energies) and the solid target data set was determined as a relative excitation function; these data were normalized to the literature data. In the range of available literature data, the present measurements of $S(E)$ are in good agreement.

The measured angular distributions $W(\theta)$ were developed in a series of Legendre polynomials, $W(\theta) = 1 + \sum a_i P_i(\cos\theta)$; because of the symmetric angular distributions in both reactions only *even* a_i contribute. Due to the low energies the first term in the series (a_2) sufficiently describes

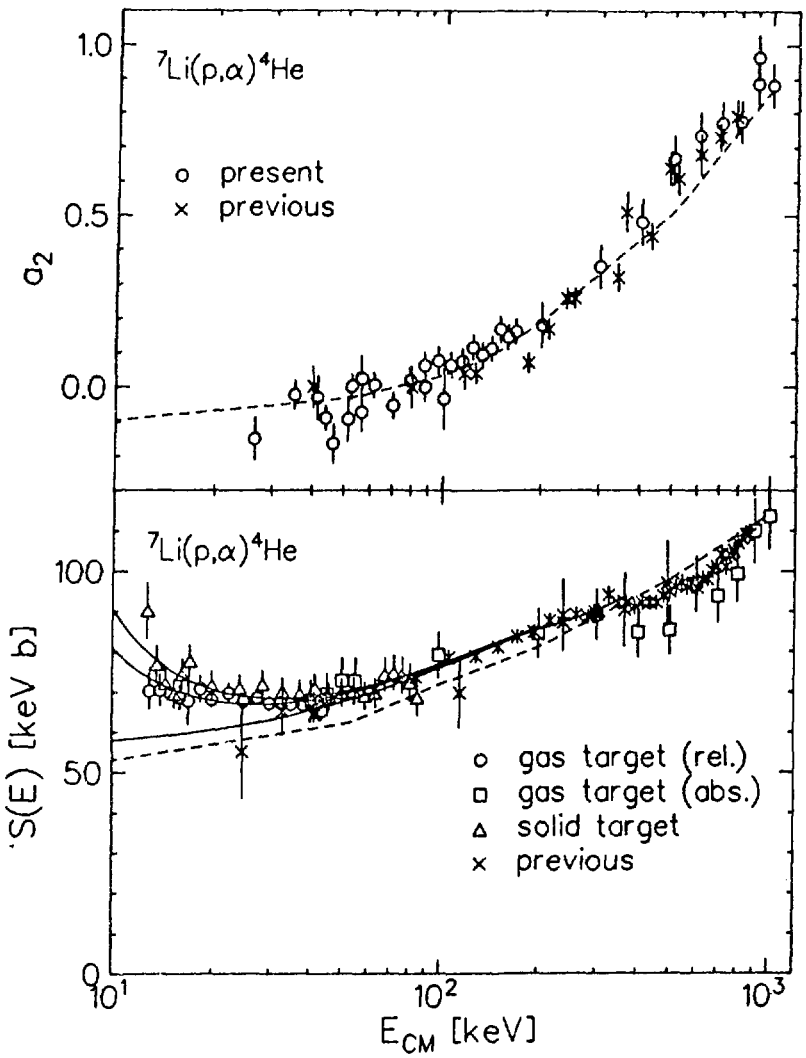

Fig. 1: Angular distribution $W(\theta) = 1 + a_2 P_2(\cos\theta)$ and excitation function $S(E)$ for the reaction ^{7}Li(p,α)^{4}He. The solid lines are the polynomial fits, the dashed curve is the DWBA calculation. Literature data are taken from [9,10].

$W(\theta)$, in fair agreement with literature. Notice the change of sign in a_1 and a_2, respectively (Figs. 1 and 2).

3 THEORETICAL CALCULATIONS

While compound nucleus mechanisms have frequently been suggested in literature as an explanation for the behaviour of subCoulomb cross sections (for the reactions discussed here, see e.g. [3,4]), the DWBA ansatz in the thermonuclear energy range (for reactions of astrophysical interest involving light ions) has been discussed recently (see e.g. [5] for an extended discussion).

A more detailed description of a first DWBA calculation for ^{7}Li(p,α)^{4}He is given in [6,7]. Briefly, a zero range calculation with a cluster form factor was attempted between 10 keV and 1 MeV center-of-mass; later it was extended up to 45 MeV [7]. In the α-channel, a double folding optical potential was used [8], in the proton channel a simple Saxon-Woods type (including spin-orbit coupling). The calculation is able to reproduce the change of sign in $W(\theta)$, the energy

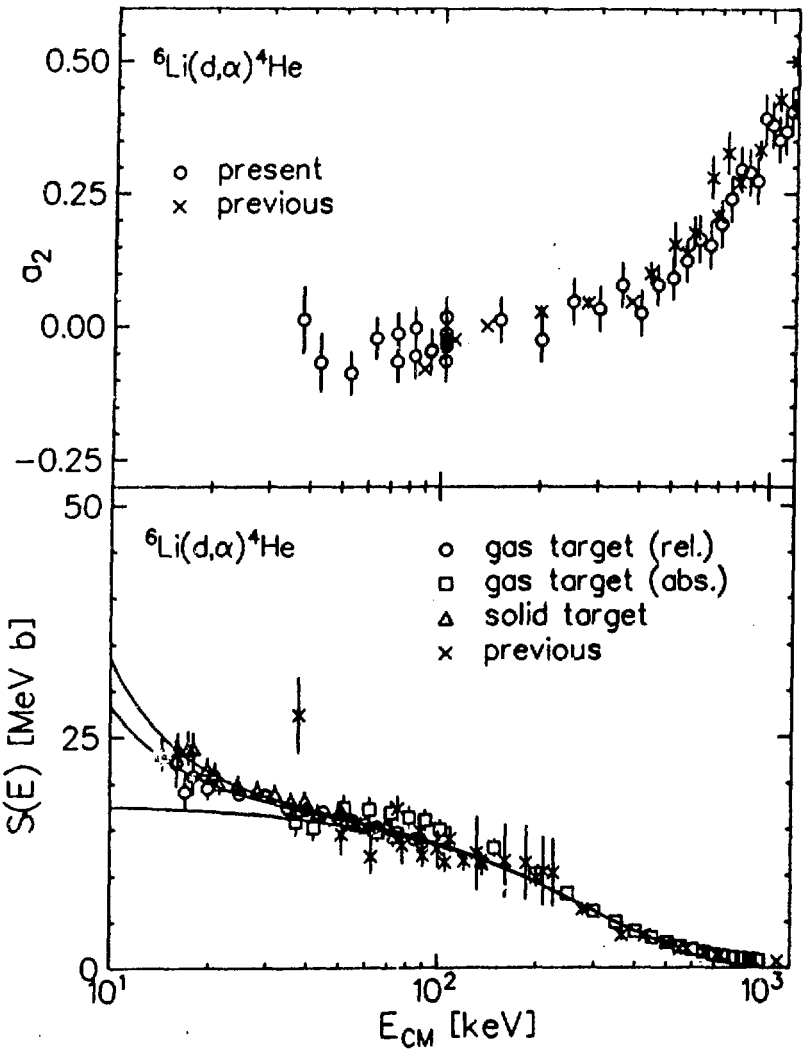

Fig. 2: Angular distribution $W(\theta) = 1 + a_2 P_2(\cos\theta)$ and excitation function $S(E)$ for the reaction ^{6}Li(d,α)^{4}He. The solid lines are the polynomial fits. Literature data are taken from [11-16].

dependance and magnitude of $W(\theta)$ and $S(E)$ up to 1 MeV and the general trend of the cross section up to 45 MeV by using one data set for the geometry of the bound state Saxon-Woods potential. The results up to 1 MeV are also shown in Figs. 1 and 2. The main advantage of DWBA over e.g. R-matrix theory is the small number of open parameters necessary for modelling the data. Further refinements of the calculation, however, are necessary and in progress (e.g. finite range, microscopic form factor, consistent use of systematically energy dependent folding potentials, knockout).

4 DISCUSSION

In the present experiments, no evidence for isotopic effects of electron screening were found, as expected. The measurements with solid (atomic) targets lead to screening potentials U_e systematically higher than the prediction of the simple Coulomb model. This discrepancy is

also observed for other reactions [2 and references therein]. Based on a still fairly simple DWBA calculation, subCoulomb cross sections and angular distributions can be theoretically described (for ^{7}Li(p,α)^{4}He). Both the experimental and the theoretical program will be continued.

5 REFERENCES

[1] H.J. Assenbaum, K. Langanke, C. Rolfs, Z. Phys. **A327** (1987) 461

[2] S. Engstler et al., to be published

[3] F.C. Barker, Ap. J. **173** (1972) 477.

[4] A.J. Elwyn, J.E. Monahan, Phys. Rev. C **19**, 6 (1979) 2114

[5] H. Oberhummer, G. Staudt, in: Nuclei in the Cosmos, ed. H. Oberhummer, Springer Verlag, to be published

[6] G. Raimann, B. Bach, K. Grün, H. Herndl, H. Oberhummer, S. Engstler, C. Rolfs, H. Abele, R. Neu, G. Staudt, Phys. Lett. B **249**, 2 (1990) 191

[7] G. Raimann, H. Abele, R. Neu, G. Staudt, B. Bach, K. Grün, H. Herndl, H. Oberhummer, S. Engstler, C. Rolfs, Proc. Int. Symp. "Nuclei in the Cosmos", ed. H. Oberhummer and W. Hillebrandt, Max-Planck Inst. f. Physik u. Astrophysik, Garching, FRG, p. 216

[8] H. Abele, PhD dissertation, University of Tübingen, FRG, 1991

[9] C. Rolfs and R.W. Kavanagh, Nucl. Phys. **A455** (1986) 179.

[10] H. Spinka, T. Tombrello and H. Winkler, Nucl. Phys. A164 (1971) 1.

[11] Z.T. Bödy, J. Szabó, M. Várnagy, Nucl. Phys. **A330** (1979) 495

[12] A.J. Elwyn, R.E. Holland, C.N. Davids, L. Meyer-Schützmeister, J.E. Monahan, F.P. Mooring, W. Ray, Phys. Rev. C **16**, 5 (1977) 1744

[13] M.S. Golovkov, V.S. Kulikauskas, V.T. Voronchev, V.M. Krasnopol'skil, V.I. Kukulin, Sov. J. Nucl. Phys. **34** (1981) 480

[14] J.M.F. Jeronymo, G.S. Mani, F. Picard, A. Sadeghi, Nucl. Phys. **38** (1962) 11

[15] M. Manalis, J.E. Henkel, Phys. Rev. **136**, 6B (1964) B1741

[16] C.R. McClenahan, R.R. Segel, Phys. Rev. C **11**, 2 (1975) 370

SECOND FORBIDDEN UNIQUE β^+ DECAY AND COSMIC RAY HALF-LIFE OF ^{54}Mn

A. Wolańska, T. Batsch, Z. Janas, W. Kurcewicz,

D. Seweryniak, B. Szweryn

Institute of Experimental Physics, Warsaw University,

00-681 Warsaw, Poland

Abstract

The second forbidden unique β^+ decay of ^{54}Mn has been investigated in the laboratory. An upper limit of $1.4 \cdot 10^{-7}$ for the β^+ branching ratio was achieved. This corresponds to the lower limit of $6.1 \cdot 10^6$ years for the partial half-life and value of 12.8 for the lower limit of logft of this second forbidden unique transition.

1 INTRODUCTION

In the laboratory conditions ^{54}Mn decays via an allowed electron capture (EC) transition to the 835 keV level in ^{54}Cr with half-life of 312 days. In cosmic rays at relativistic energies atoms of ^{54}Mn are fully stripped of theirs orbital electrons, so

^{54}Mn cannot decay through EC channel [1]. If decay of ^{54}Mn is possible at all in cosmic space, the only chance is decay via second forbidden unique transitions to the ground states of ^{54}Cr (β^+) or ^{54}Fe (β^-) - see Fig.1.

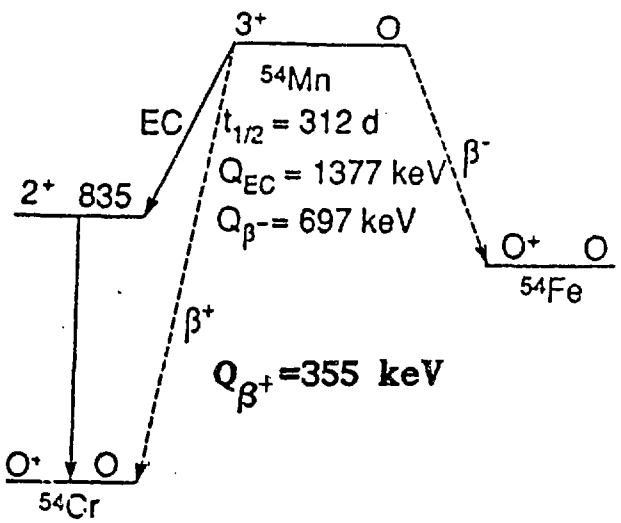

Figure 1: *Decay scheme of ^{54}Mn*

The end points of corresponding β^+ and β^- spectra are 355 keV and 697 keV, respectively. From systematics of the 3^+-0^+ transitions the estimated half-life for these decay modes of ^{54}Mn are the following [2]: $8.4{\cdot}10^7\text{y}<T_{1/2}(\beta^+)<6.0{\cdot}10^9\text{y}$ and $9.2{\cdot}10^5\text{y}<T_{1/2}(\beta^-)<6.5{\cdot}10^7\text{y}$. In order to explain the measured abundance of this long-lived radioactive isotope in cosmic rays [3] a value of $1\text{-}2{\cdot}10^6$ years for half-life of ^{54}Mn was calculated. Because of such long half-lives, the presence of ^{54}Mn in cosmic rays has been proposed as a cosmic-ray chronometer and a probe of models of an interstellar medium and cosmic ray propagation. The examination of β decays in ^{54}Mn is very important not only for astrophysics, but also for nuclear physics, because these β decays are the second forbidden unique transitions.

2 EXPERIMENTAL SET-UP

In laboratory a β^+ decay branching ratio of ^{54}Mn was measured. A source was of 1.3 MBq activity, and about one year old, allowing any short-lived activities to decay away. In a few tests (made with Ge detector) the amounts of possible contaminations of ^{65}Zn, ^{60}Co and ^{137}Cs relative to ^{54}Mn activity were found to be less than $4{\cdot}10^{-6}$, $3{\cdot}10^{-5}$ and $8{\cdot}10^{-5}$, respectively.

The ^{54}Mn source was placed in an orange type six-gap magnetic beta spectrometer with toroidal magnetic field [4]. The value of this field was controlled using Hall probe. The momentum resolution of the spectrometer was about 3.5%. The measurements were performed with a silicon ΔE-E telescope (ΔE of thickness of 165 μm, E of thickness of 1525 μm; both of them had active area of 300 mm^2). An 18 cm thick block of lead was situated between the telescope and the source [4]. This allowed to reduce significantly a background of γ rays emitted from ^{54}Mn source. Using such magnetic spectrometer as a magnetic filter it was possible to discriminate the conversion electrons from ^{54}Mn, and particles from cosmic rays.

A coincidence between the telescope elements and TAC (time to amplitude converter) was required in an electronic hardware trigger. For each such trigger the energy signals from silicon detectors and time signal between them were recorded in the event by event mode. Because of this, only the high-energy cosmic particles, which passed through the telescope contributed to the background.

3 EXPERIMENT AND RESULTS

The experimental set-up was calibrated with ^{137}Cs source. After preliminary tests the best value of energy (250 keV) for detecting positrons was found. So the positron measurement was performed for the energy of particles of 250 keV. The background spectrum was taken for the energy of 150 keV for which the transmission of the telescope was about 0. The two dimensional energy spectra for the 250 keV electrons from ^{137}Cs, 250 keV positrons of ^{54}Mn and background are shown in Figs 2a, 2b and 2c, respectively.

A distribution of events (in Figs 2b and 2c) is uniform except the region along the E-axis. These events were identified as corresponding to high-energy cosmic particles. If ^{54}Mn emits positrons with energy 250 keV the corresponding events should lay out in the same region of the ΔE-E matrix as electrons of ^{137}Cs. So the positron and background spectra were projected using the two dimensional gate shown in Fig.2a. The same window is marked in Figs 2b and 2c. In the running time of 9.3 days we observed N_1=850$\pm$29 events in the positron spectrum, whereas the number of events in the background spectrum was N_2=915$\pm$31. The result of subtraction ^{54}Mn positrons and background spectra is shown in Fig.3. The 1σ upper limit on the number of ^{54}Mn positrons detected was 42. Using our experimentally determined six-gap transmission of 1.1% and the telescope transmission of 23%, the branching ratio for β^+ decay is less than $1.4 \cdot 10^{-7}$. This corresponds to the lower limit of $6.1 \cdot 10^6$ years for the partial half-life of this decay channel and value of 12.8 for lower limit of log*ft*. This result should be compared with the upper limit $4.4 \cdot 10^{-8}$ for the branching ratio and lower limit of partial half-life about $2 \cdot 10^7$ years published recently [2]. Although the obtained result is not satisfactory we

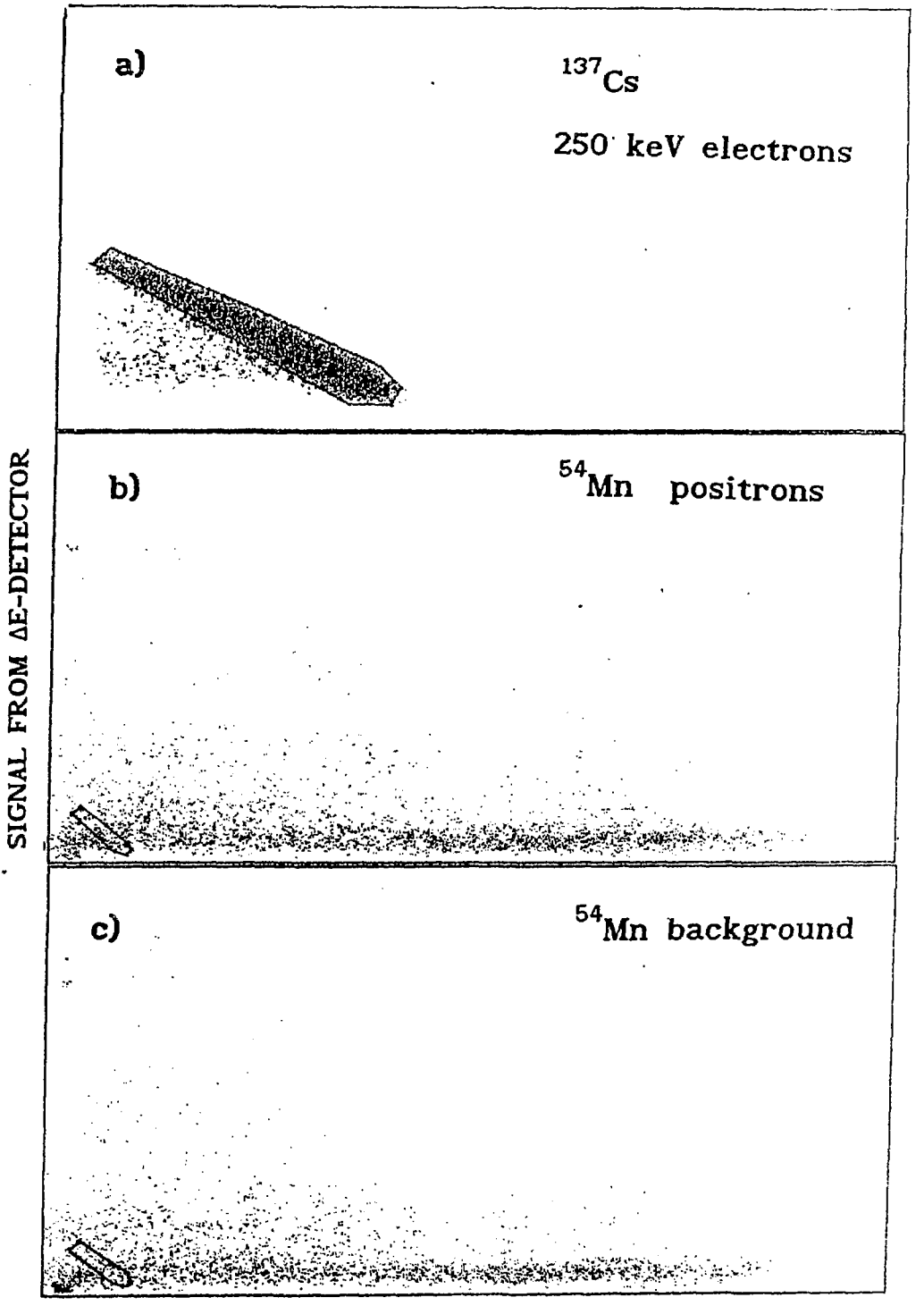

Figure 2: *ΔE-E two dimensional spectra*

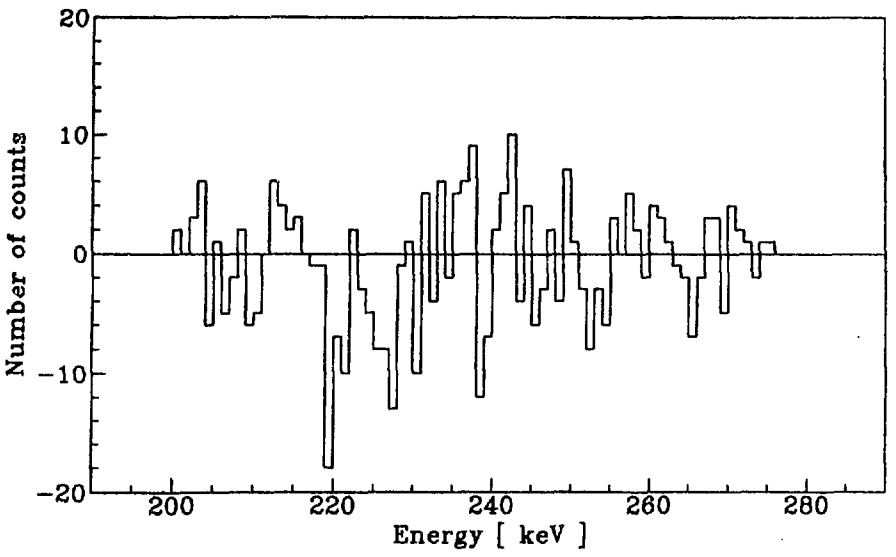

Figure 3: *Positron spectrum after background subtraction*

plan to repeat such experiment under improved conditions. The expected limit for β^+ decay branching ratio which we hope to achieve is $2{\cdot}10^{-8}$.

References

[1] M. Casse, Astrophysical Journal **180**, 623 (1973)

[2] B. Sur et al., Physical Review **C39**, 1511 (1989)

[3] L. Koch et al., Astronomy and Astrophysics **102**, L9 (1981)

[4] Z.Preibisz, W.Kurcewicz and A.Zgliński, Nukleonika **14**, 743 (1978)

[5] C. M. Lederer and V. S. Shirley, Tables of Isotopes, 7th ed., (John Wiley & Sons, New York, 1978)

[6] L. N. Zyryanova, The Beta Processes, ("Nauka", Leningrad, 1972)

MICROSCOPIC DESCRIPTION OF 2β-DECAY AND DOUBLE CHARGE EXCHANGE REACTION WITH PIONS*

A. Bobyk†, A. Fäßler‡, W. A. Kamiński†, G. Pantis♯ and J. D. Vergados♯

†Institute of Physics, Maria Curie-Skłodowska University, Lublin, Poland
‡Institut für Theoretische Physik, Eberhardt-Karls-Universität, Tübingen, Germany
♯Theoretical Physics Division, University of Ioannina, Ioannina, Greece

Abstract

Description of the pionic double charge exchange reactions and the double beta decay processes briefly discussed within the proton-neutron quasiparticle random phase approximation. The formalism allows to estimate the non-standard physics parameters: $\langle m_\nu \rangle < 7\,eV$, $\lambda < 5 \cdot 10^{-5}$, $\eta < 8 \cdot 10^{-7}$.

Introduction

Since the formulation of the standard model of electroweak interaction by Glashow, Salam and Weinberg in 1967 [1], physicists have been asking questions if this theory is the ultimate one and if there is any physics beyond it. From these questions many GUT models emerged [2], giving rise to a plethora of exotic reactions that are of great importance to astrophysics, not to mention the famous cosmological dilemma of neutrino mass and closing of our Universe [3].

There is no doubt that neutrinoless double β-decay ($0\nu 2\beta$-decay) will play the important role in shedding some light on the above problems. Firstly, it will answer the question of lepton number non-conservation, and secondly, it will show if neutrino mass eigenstates are Majorana or Dirac particles. It will also allow to find the bounds on neutrino masses and right-handed current parameters [4, 5].

Correct determination of the above parameters requires the knowledge of nuclear structure and particularly the short range two-nucleon correlations. Fortunately, thanks to the birth of meson factories during the last two decades, the physicists got a precise tool to study the depths of the nucleus — the double charge exchange (DCX) reactions. This is due to the fact that calculations of cross sections are very sensitive to the nuclear models involved, especially to the two-nucleon correlations. Moreover, both 2β-decay and DCX reaction can be described theoretically in the consistent way, based on the same nuclear model. Thus, confronting the theoretical results versus the experimental data for DCX reactions, one can test the assumptions and approximations concerning the nuclear structure.

*Work was supported in parts by Scientific Research Committee (Poland), contract no. 2.03479101 and by the Bundesministerium für Forschung und Technologie (Germany), contract no. 06TÜ90/91.

THE QRPA MODEL OF THE REACTION

Both 2β-decay and DCX reaction are two-step processes, taking place according to the following scheme (see also Fig. 1.):

$$\begin{aligned} \text{DCX:} \quad & \pi^+ + X(A,Z) \to X^*(A,Z+1) \to X^*(A,Z+2) + \pi^-, \\ 2\beta: \quad & X(A,Z) \to X^*(A,Z+1) + e^- (+\bar{\nu}) \to X^*(A,Z+2) + e^- (+\bar{\nu}). \end{aligned} \tag{1}$$

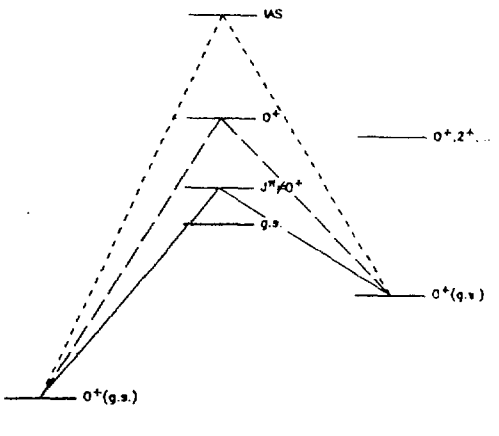

Fig. 1. Schematic diagram for two-step process from the initial nucleus (A, Z) to the final nucleus (A, Z+2) showing various paths through intermediate states.

Hence we have to know the structure not only of the inital and final nuclei, but also all the intermediate states, which must be constructed anyway. It is impossible in the case of realistic shell-model calculations, but relatively simple in the proton-neutron quasiparticle random phase approximation (pn-QRPA) [6, 7, 8]. In this framework the intermediate states $|mJM\rangle$ are two quasi - particle proton-neutron states, built on the correlated ground states of the initial ($|\text{QRPA}\rangle$) and final ($|\overline{\text{QRPA}}\rangle$) nucleus:

$$|mJ^\pi M\rangle = \sum_{pn} \left[X^m_{(pn)J} C^\dagger(pnJM) - Y^m_{(pn)J} \tilde{C}(pnJM) \right] |\text{QRPA}\rangle. \tag{2}$$

where $C^\dagger(pnJM) = [a^\dagger_p a^\dagger_n]_{JM}$, $a^\dagger$'s are the BCS quasiparticle creation operators and tilde denotes the time reversal operation. The similar expresion holds for $|\overline{mJ^\pi M}\rangle$. In general states $|mJ^\pi M\rangle$ and $|\overline{mJ^\pi M}\rangle$ do not coincide, but we expect them to be quasi-orthogonal.

The forward- and backwardgoing amplitudes $X^m_{(pn)J}$ and $Y^m_{(pn)J}$ are obtained by solving the QRPA eigenproblem:

$$\begin{pmatrix} \mathbf{A} & \mathbf{B} \\ \mathbf{B} & \mathbf{A} \end{pmatrix} \begin{pmatrix} \mathbf{X} \\ \mathbf{Y} \end{pmatrix} = E \begin{pmatrix} 1 & 0 \\ 0 & -1 \end{pmatrix} \begin{pmatrix} \mathbf{X} \\ \mathbf{Y} \end{pmatrix}, \tag{3}$$

where $\mathbf{A}$ and $\mathbf{B}$ submatrices can be calculated from the expressions:

$$\begin{aligned} A^{JM}_{\mathbf{pn},p'n'} &= \langle \text{QRPA} | C(pnJM) H_{qp} C^\dagger(p'n'JM) | \text{QRPA} \rangle, \\ B^{JM}_{\mathbf{pn},p'n'} &= \langle \text{QRPA} | C(pnJM) \tilde{C}(p'n'JM) H_{qp} | \text{QRPA} \rangle, \end{aligned} \tag{4}$$

where H_{qp} is the full nuclear hamiltonian after the quasiparticle transformation. The matrices (4) involve not only particle-hole matrix elements $\langle (pn^{-1})JM|G|(p'n'^{-1})JM\rangle$, as in

the usual RPA approach, but also particle-particle matrix elements $\langle (pn)JM|G|(p'n')JM\rangle$, which are calculated from the Bethe-Goldstone equation:

$$G(\omega) = V + V\frac{Q}{\omega - H_0}G(\omega) \tag{5}$$

and multiplied by renormalisation constants g_{ph} and g_{pp} respectively, to take into account the finiteness of the model space. In practical calculations the QRPA correlated ground states in (4) can be approximated well enough by the BCS ground states that play the role of the uncorrelated vacua.

Amplitudes of 2β-decay and DCX transitions

Due to lack of space we will not cite the full expressions describing 2β-decay and DCX transition amplitudes. They can be found e. g. in [5, 8] and [9, 10] respectively.

The $0\nu 2\beta$-decay rate can be expressed as follows:

$$[T_{1/2}(0\nu)]^{-1} = G_{01}^{0\nu}|M_{GT}^{0\nu}|^2\{\tilde{C}_1[|\chi_L|^2 + |\chi_R|^2] + \tilde{C}_4|\lambda|^2 + \tilde{C}_5|\eta|^2\}, \tag{6}$$

where $M_{GT}^{0\nu}$ is the Gamow-Teller nuclear matrix element, λ and η are the lepton number violating parameters and

$$\begin{aligned} \chi_L &= \frac{\langle m_\nu \rangle}{m_e}, \\ \chi_R &= 10^{-2} \cdot \left\langle \frac{m_p}{M_N} \right\rangle_R . \end{aligned} \tag{7}$$

Definitions of the kinematical coefficients $\tilde{C}_i$, $i = 1, \ldots, 6$ are given in [10] and $G_{01}^{0\nu}$ parameter is defined in [4].

The DCX transition amplitude has the form:

$$F(\mathbf{k}, \mathbf{k}') = \sum_J \sum_{mm'} \frac{\langle f; \pi^-(\mathbf{k}')|\hat{O}_T|\overline{m'J^\pi M}\rangle\langle\overline{m'J^\pi M}|mJ^\pi M\rangle\langle mJ^\pi M|\hat{O}_T|i; \pi^+(\mathbf{k})\rangle}{E_i + \omega_k - \frac{E_m^J + E_{m'}^J}{2}}, \tag{8}$$

where ω_k is the incoming pion total energy, $\mathbf{k}$ and $\mathbf{k}'$ are incoming and outgoing pion momenta and E_m^J are the QRPA excitation energies. The transition operator $\hat{O}_T$ is taken as a sum of the s- and p-wave hamiltonians [8]. $F(\mathbf{k}, \mathbf{k}')$ is directly connected with the DCX differential cross section:

$$\frac{d\sigma}{d\Omega}(\theta_{\mathbf{k}\mathbf{k}'}) = |F(\mathbf{k}, \mathbf{k}')|^2. \tag{9}$$

Results of the calculations

During the last two years the connection between the $0\nu 2\beta$-decay and DCX reaction were studied in some extend [11, 12, 13]. The crucial point of the above sketched approach is that we are able to calculate within it the amplitudes of both processes in the framework of the same model which has been very succesful in the description of other reactions, like

single β decay [14]. The pn-QRPA calculations utilize a realistic effective nucleon-nucleon interaction derived from the Bonn potential, but as we mentioned previously one should fit two parameters renormalizing the bare Brückner two body matrix elements to fix the nuclear structure more precisely. These are the particle-hole strength g_{ph} and the particle-particle strength g_{pp}. g_{ph} can be easily fitted to the excitation energy of the isobaric analogue state in the intermediate nucleus, which depends strongly and approximately linearly on this parameter. For tellurium isotopes one obtains $g_{ph} = 1.30$. The particle--particle strength, however, influences the amplitudes in more complex way. In the case of $0\nu 2\beta$-decay nuclear matrix elements show some reduction as g_{pp} increases but the change is not prominent [5]. For DCX reaction with low energy pions such dependence for tellurium isotopes is much stronger as shown in Fig.2. An increase of g_{pp} which, roughly speaking, is connected with an increasing role of the nucleon-nucleon correlations causes a reduction of the DCX amplitudes. Predicted cross sections come close to the experimental data for $g_{pp} > 1$. We can fix the g_{pp} values in this way and in turn calculate the $0\nu 2\beta$ matrix elements:

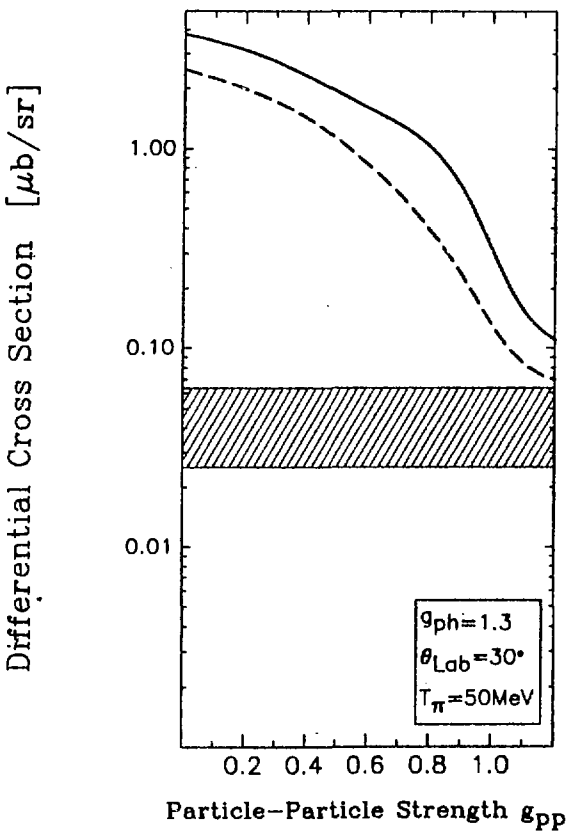

Fig. 2. Calculated differential cross sections as a function of the particle-particle strength g_{pp}. Experimental data [16] are indicated by the hatched region. Ground state transitions: ^{128}Te $\rightarrow$ ^{128}Xe (full line); ^{130}Te $\rightarrow$ ^{130}Xe (long-dashed line)

$$M_{GT}^{0\nu} = 2.30 \text{ and } 2.06 \qquad (10)$$

for ^{128}Te and ^{130}Te, respectively. Using the best presently available experimental limit for ^{130}Te isotope: $T_{1/2}^{exp}(0\nu) > 10^{21}$ y [15] we are able to extract from (7) the following limits on the lepton number violating parameters:

1. light neutrino mass

$$\langle m_\nu \rangle < 7\,\text{eV} \qquad (11)$$

2. right-handed current admixtures

$$\begin{aligned} \lambda &< 5 \cdot 10^{-5} \qquad (J_L - J_R \text{ hadronic currents}) \\ \eta &< 8 \cdot 10^{-7} \qquad (J_L - J_L \text{ hadronic currents}). \end{aligned} \qquad (12)$$

Much more realistic estimate of the non-standard model parameters needs more accurate data on the DCX processes. The low statistics of the present DCX measurements allows to set an upper limit on g_{pp} and then the lower limit of the nuclear matrix element of the 2β-decay for 0ν mode.

In conclusion, the pn-QRPA framework assures very tight connection between the DCX reaction with pions and the $2\beta 0\nu$-decay process. Due to this link we expect the best contrains will be imposed on the Standard Model in a case of more reliable DCX data.

References

[1] S. Weinberg, *Phys. Rev. Lett.* **19** (1967) 264.
[2] P. Langacker, *Phys. Reports.* **72** (1981) 185.
[3] J. D. Vergados, *Phys. Reports.* **133** (1986) 1.
[4] M. Doi, T. Kotani, E. Takasugi, *Prog. Theor. Phys. (Supp.)* **83** (1985) 1.
[5] A. Fäßler, *Progr. Part. and Nucl. Phys.* **21** (1988) 183.
[6] P. Vogel, M. R. Zirnbauer, *Phys. Rev. Lett.* **17** (1986) 3148.
[7] O. Civitarese, A. Fäßler, T. Tomoda, *Phys. Lett.* **B199** (1987) 11.
[8] A. Fäßler, W. A. Kamiński, G. Pantis, J. D. Vergados, *Phys. Rev.* **C43** (1991) R21; G. Pantis, A. Fäßler, W. A. Kamiński, J. D. Vergados, *J. of Phys.* **G**, submitted
[9] W. A. Kamiński, A. Fäßler, *Phys. Lett.* **B244** (1990) 255.
[10] W. A. Kamiński, A. Fäßler, *Nucl. Phys.* **A** (1991), in press.
[11] A. Fazely, L. C. Liu, *Phys. Rev. Lett.* **57** (1986) 968; *ibid.* **59** (1987) 2384
[12] T. Tomoda, *Phys. Rev. Lett.* **59** (1987) 2383
[13] T. -S. Ito, C. -R. Ching, *Commun. Theor. Phys.* **6**, (1987) 187
[14] J. Suhonen, T. Taigel, A. Fäßler, *Nucl. Phys.* **A486** (1988) 91
[15] Yu. G. Zdesenko et al., *Izv. Akad. Nauk (USSR), Ser. Fiz.* **45** (1981) 1856
[16] R. Bilger at al., *Phys. Rev.* **C**, to be published

FRS: A VERSATILE MAGNETIC SPECTROMETER FOR RELATIVISTIC HEAVY IONS AT GSI

F.NICKEL, H.GEISSEL, K.-H.BEHR, A.BRÜNLE, K.BURKARD, M.CHEN, H.FOLGER, B.FRANCZAK, Y.FUJITA, H.KELLER, B.LANGENBECK, E.PFENG, M.PFÜTZNER[1], E.ROECKL, K.RYKACZEWSKI[1], I.SCHALL, D.SCHARDT, CH.SCHEIDENBERGER, K.-H.SCHMIDT, TH.SCHWAB, K.SÜMMERER, M.WEBER AND G.MÜNZENBERG

GSI Darmstadt, D-6100 Darmstadt, Germany

TH.BROHM, H.-G. CLERC, M.FAUERBACH, J.-J.GAIMARD, A.GREWE, E.HANELT, B.KNÖDLER, M.STEINER, B.VOSS, J.WECKENMANN, C.ZIEGLER

Insitut fr Kernphysik, TH Darmstadt, D-6100 Darmstadt, Germany

A.MAGEL, H.WOLLNIK

Universität Gießen, D-6300 Gießen, Germany

D.J.VIEIRA

Los Alamos National Laboratory, Los Alamos, NM 87545, USA

[1]Present address: Institute of Experimental Physics, Warsaw University, Hoża 69, PL-00-681 Warszawa, Poland

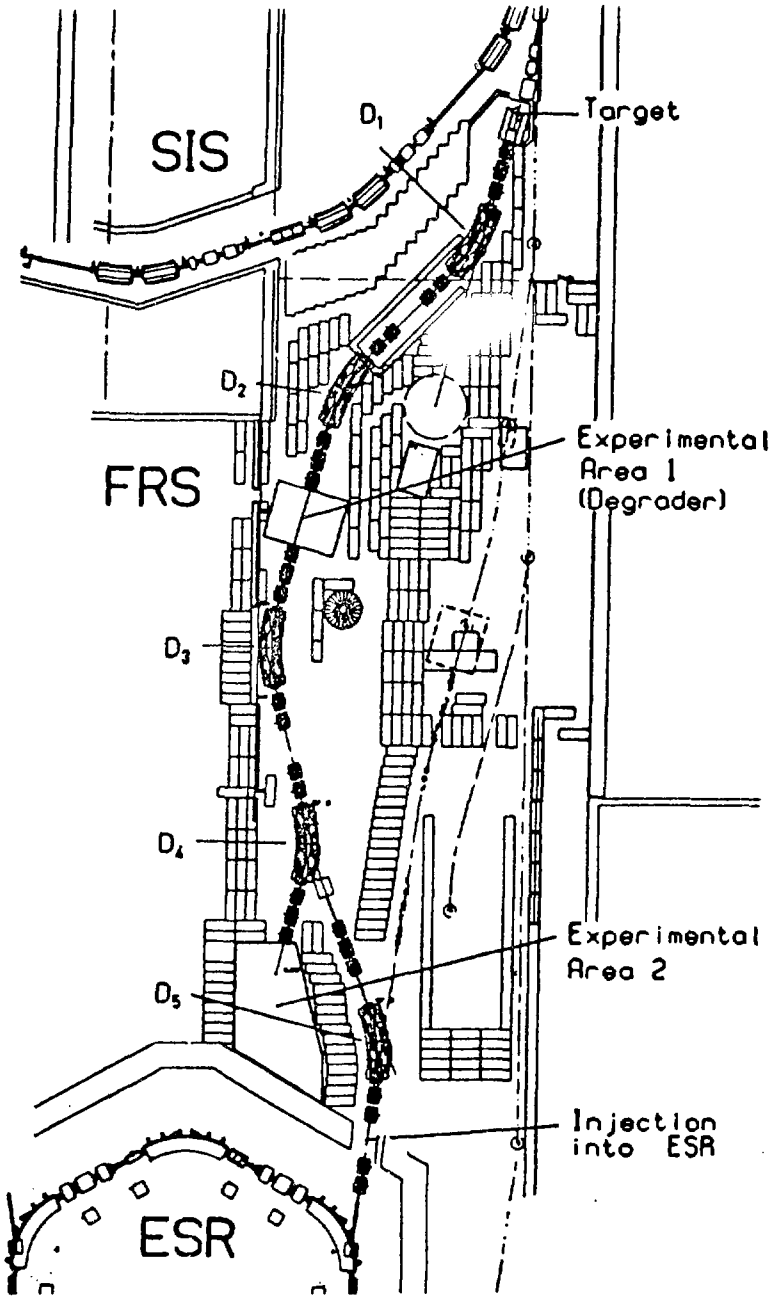

The new accelerator facilities at GSI extend heavy-ion research to relativistic energies. The fragment separator FRS, situated between the synchrotron SIS and the storage ring ESR, is a versatile magnetic spectrometer for atomic and nuclear physics experiments.

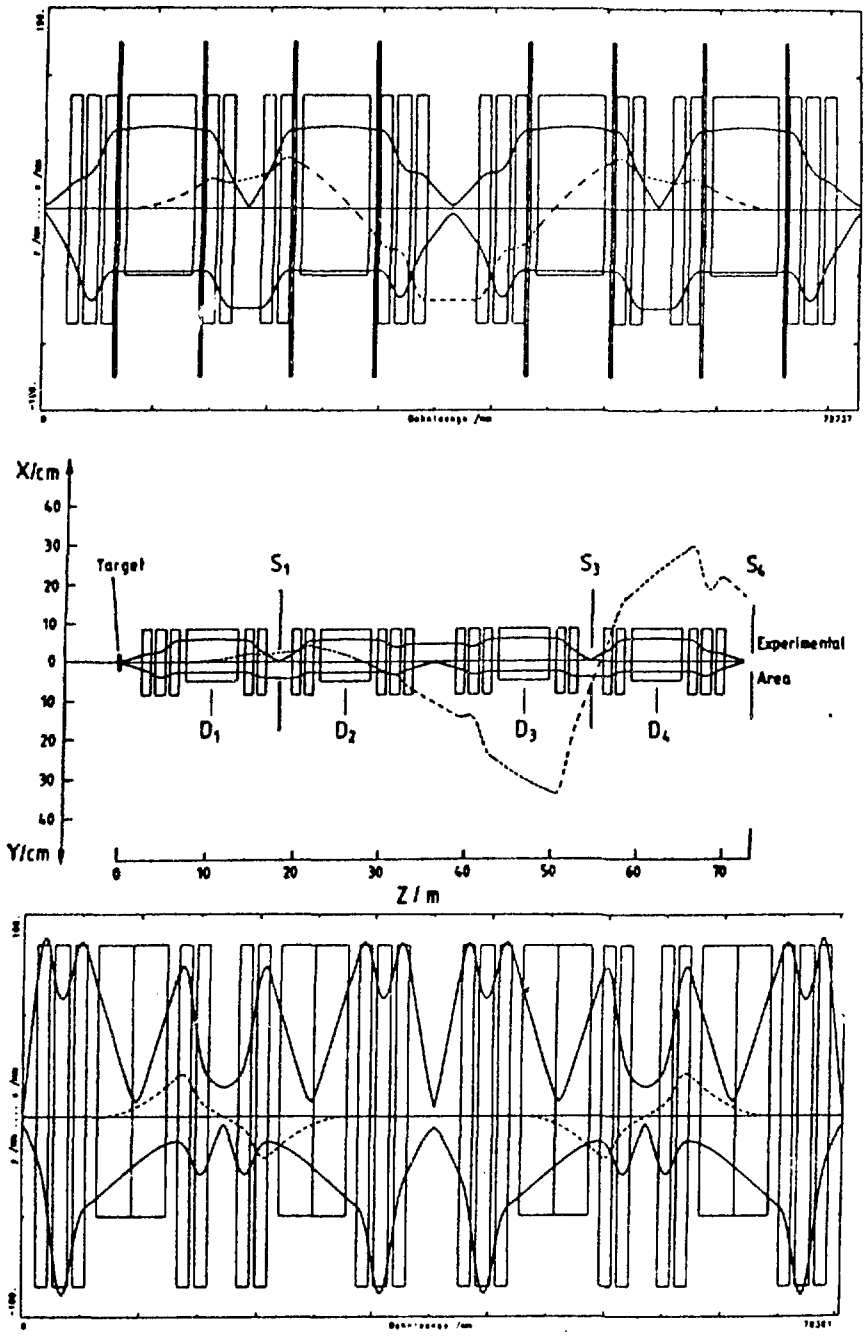

Ion optics of the FRS: The picture above shows the envelops of beams in the "normal" achromatic mode (upper part), in the middle, the mode with highest dispersion in the final focus, and below the non-dispersive mode. The dashed lines represent the dispersion lines for a $B\rho$-deviation of 1 percent.

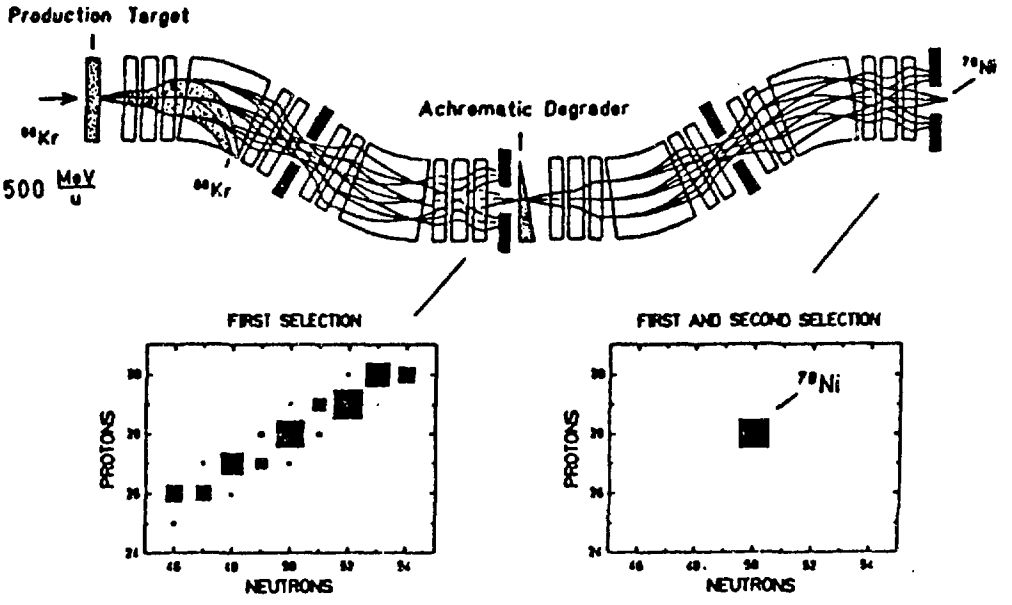

Separation principle of the FRS: The first section separates the fragments according to their magnetic rigidity. The deflection at the final focus of the system is proportional to the Z-dependent momentum-loss ratio in the intermediate degrader. The profile of the degrader preserves the achromaticity of the system which is essential for a good resolution independent of the initial momentum width. In the picture an example is given for the selection of ^{78}Ni.

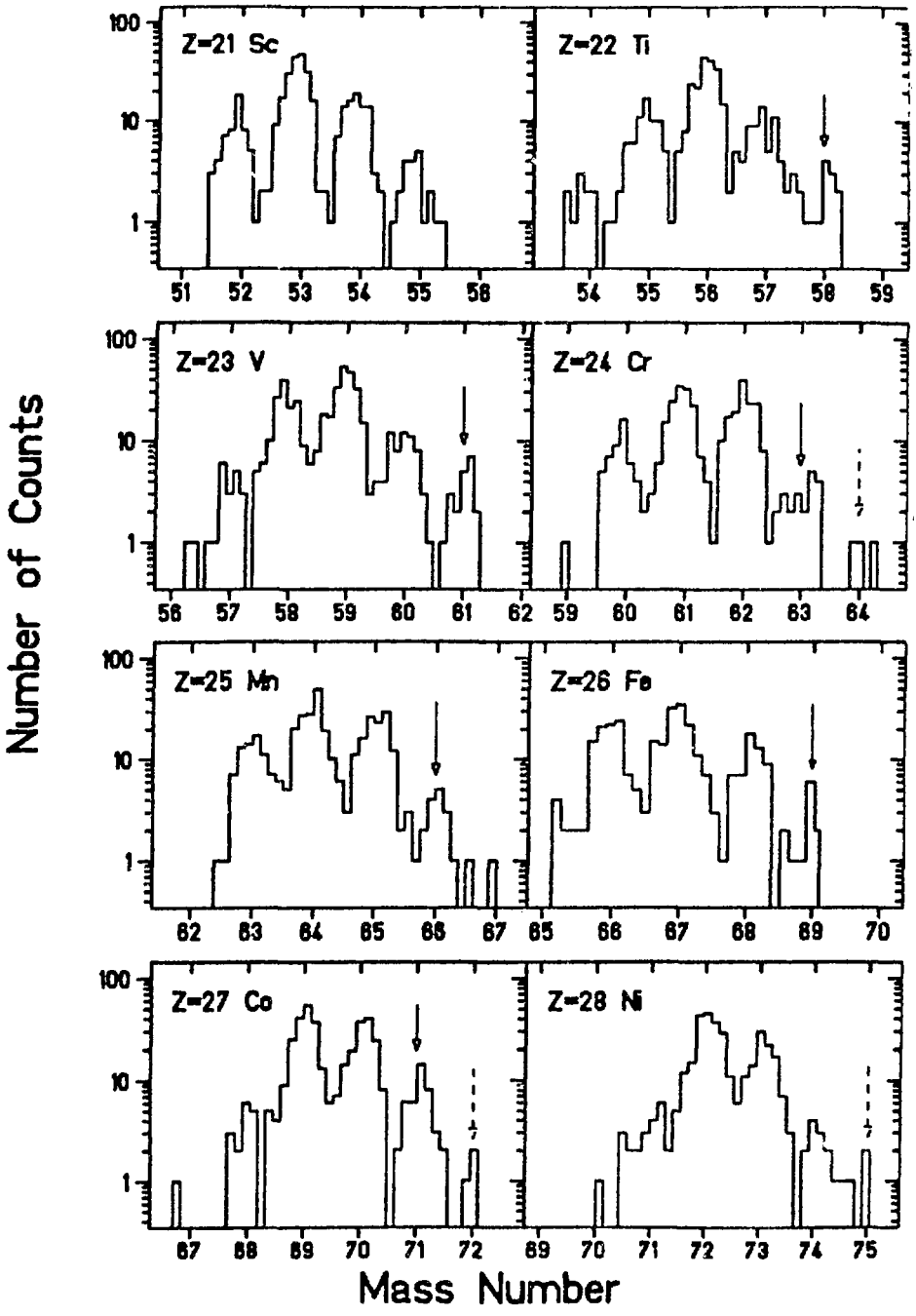

Mass distributions for fragments produced in the reaction of 500 MeV/u ^{86}Kr → Be measured at the FRS with Bρ-analysis, time-of-flight and energy-loss coincidence measurements.

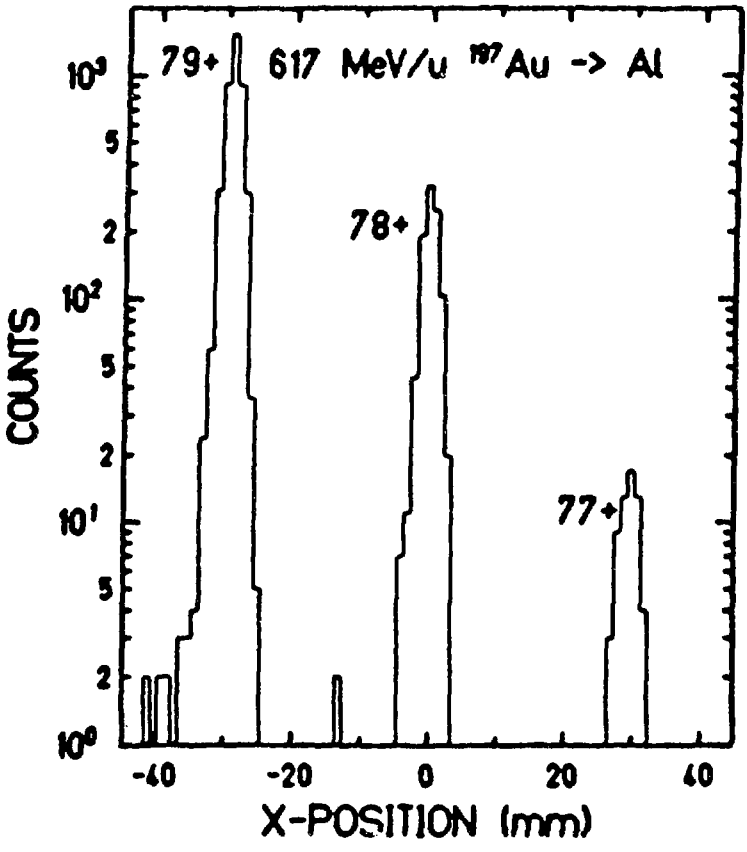

Measured charge-state spectrum of 617 MeV/u ^{197}Au ions using a 195 mg/cm^2 Al target recorded with a position-sensitive detector placed in the first focal plane.

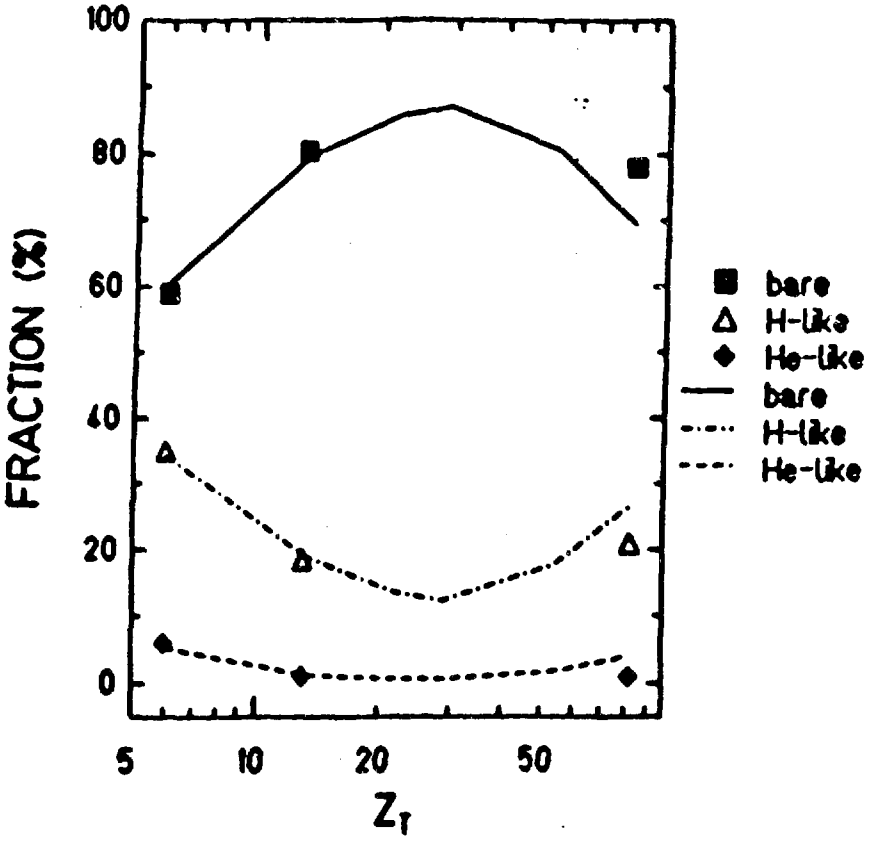

Measured yields of 617 MeV/u ^{196}Au ions in the charge states 79^+, 78^+, and 77^+ as a function of Z_T of the target.

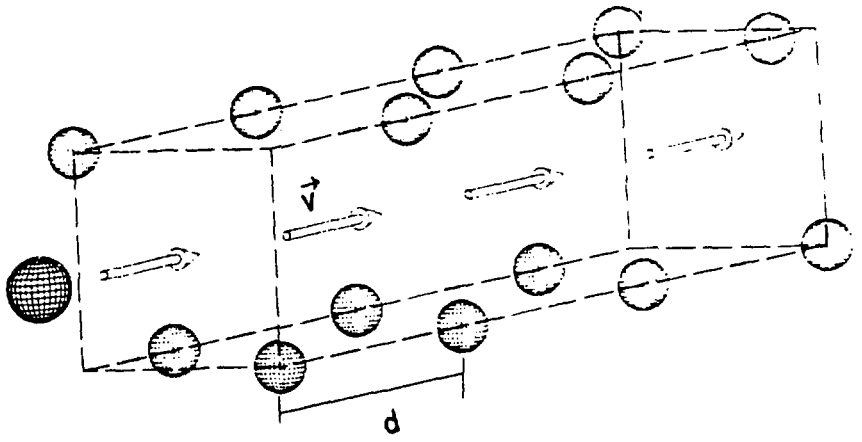

With the high-resolution mode of the FRS atomic collision processes can be studied, and channeling experiments will be possible with relativistic ions and predominantly with cooled and reinjected beams from the ESR.

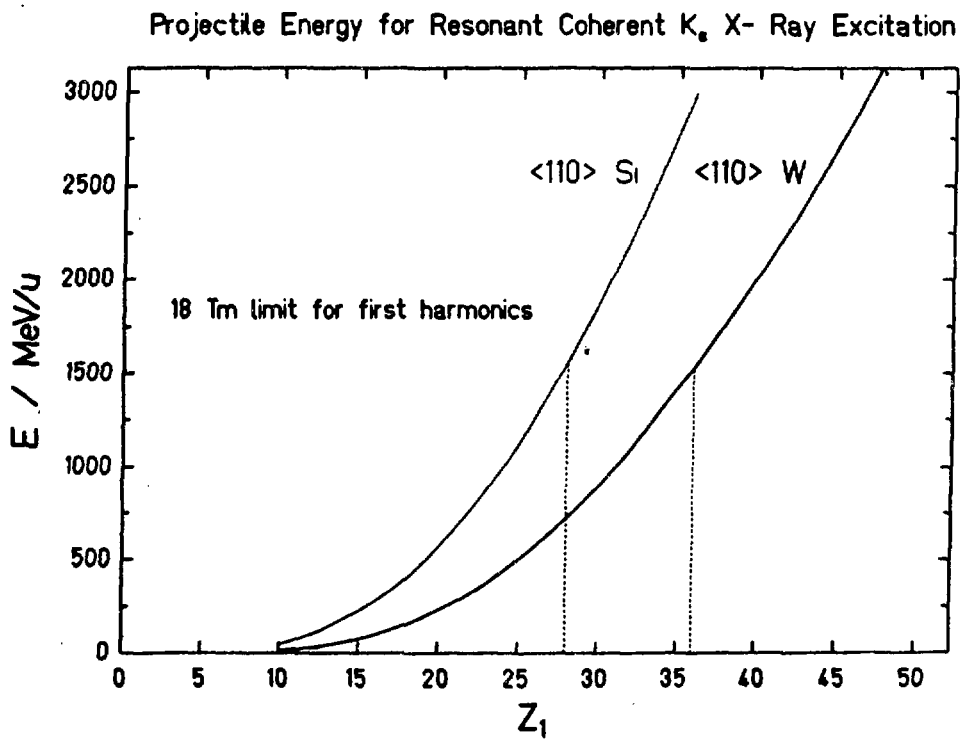

Energies for hydrogen-like projectiles needed for atomic resonant coherent excitation for the 1s → 2p transition excited by the first harmonics of the string frequency in Si and W crystals along the < 110 > axis as a function of the Z_1 of the projectile.

Plastic Barrel for the 4π Detector at SIS-ESR

E. Gierlik, G. Golakowska, M. Kirejczyk,
T. Matulewicz, B. Sikora, Z. Wilhelmi
Institute of Experimental Physics, Warsaw University
A. Gobbi, Yu. Grigorian , K.D. Hildenbrand
GSI Darmstadt, Germany
I. Belaev
ITEP, Moscow, USSR

Abstract

4π facility at SIS-ESR will be supplemented at the end of 1992 by Plastic Barrel detector consisting of 180 scintillation counters. The design and results of tests of the prototype module are discussed.

1 Design

To detect the relatively rare events of kaon emission in heavy ion collisions at SIS energies (0.1-2 GeV/u) the 4π spectrometric facility at GSI will be equipped with a double detector layer: a scintillator barrel and a Cherenkov barrel, in addition to the gas-filled drift chamber. The Bρ-ΔE-TOF-Cherenkov threshold method will identify the rare kaons among the intensive protons and charged pions composing the major part of charged particles expected backward of 30°. In addition the detector placed at large angles will increase the precision of localizing the reaction plane.

Work on the physical characteristics and mechanics of the Plastic Barrel and Cherenkov Barrel detectors to be installed in the Phase II of the 4π project on the SIS beam led to the final design [1]. The barrels consist of 180 staves (counters) each grouped in 30 modules covering $30/32 \times 2\pi$ of the azimuthal angle. The modules are mounted on a steel cylinder inserted in the yoke of the superconducting solenoid. 2 zones are not filled with counters leaving space for the rails supporting the Central Drift Chamber and Helitron detectors. The Plastic Barrel scintillators have dimensions 2400 (length) × 40 (thickness, radial) × 32 (width, azimuthal) mm^3. The modules are physically asymmetric but mechanically reflection-symmetric and can be mounted in two positions. They cover 85.4% of the azimuthal angle ϕ between 39.5° and 133° of the reaction angle θ (position I) or between 31° and 116° of θ (position II). The lightguides allow for keeping the photomultipliers in region of weaker magnetic field (~ 500 Gs). Soft iron and μ-metal shielding will reduce its strength to values below 1 Gs. Optical contacts between the detectors

and lightguides will be hard (glued) and between lightguides and photomultipliers soft (convex silicon resin RTV615 pills).

2 General Properties

Design studies of various properties of a single prototype of the Plastic Barrel detector have been performed using minimum-ionizing cosmic rays localized by the active collimator technique [2]. The most important quantity measured was the time resolution FWHM_{LR} of the time difference spectrum $t_{LEFT} - t_{RIGHT}$, which yields the time-of-flight resolution (assuming a perfect start counter) through the following relation

$$FWHM_{TOF} = \frac{1}{2} \times \sqrt{FWHM_{LR}^2 - FWHM_Q^2} \qquad (1)$$

where FWHM_Q is the time resolution coming from the finite size of active collimator; in our case this resolution was estimated to be about 190 ps.

The position of particle traversing the detector is linearly correlated with the time difference value of $t_{LEFT} - t_{RIGHT}$. By measuring the $t_{LEFT} - t_{RIGHT}$ spectra at different positions of the active collimators the position calibration of the detector was obtained. The linearity of this calibration is impressive, the maximum deviation from linearity does not exceed 50 ps equivalent to 4 mm. The slope gives the effective velocity of light propagation in the detector equal to 17.3 cm/ns for the Moscow-produced scintillator and 16.7 cm/ns for BC408 of BICRON. This velocity is larger than the apparent velocity of light traversing exactly at the total internal reflection angle, namely c/n^2, where c is the light velocity in vaccuum and n denotes the refraction index. The FWHM_{TOF} resolution was fairly constant along the detector and was usually around 300 ps reaching in some cases 260 ps. The corresponding position resolution is 5 cm.

3 Test at 615 A×MeV Au + Au

In order to study the properties of the detector in realistic conditions a prototype counter of the final dimensions and materials consisting of scintillator and Cherenkov layers has been tested at SIS with the Au beam of 615 A×MeV impinging on a 1% interaction Au target. The detector was placed in a close-to-final position. In the scatter plot of the time-of-flight versus energy deposit obtained with our counter at θ=40° (selected by a small additional scintillator) we have seen the separated branches of hydrogen (A=1,2,3) and helium (A=3,4) isotopes. The calibration of TOF spectrum was based on the punch-through point of protons. The analysis is in progress and further tests will be performed before the full detector will be completed by the end of 1992.

This work was partially supported by the Polish Ministry of National Education under projects CPBP 01.06 and G-MEN-116/90.

1. B. Sikora et al., NPL Annual Report 1990, p.54
2. T. Matulewicz et al., NPL Annual Report 1990, p.57

NUCLEAR STRUCTURE STUDIES FAR OFF STABILITY USING RADIOACTIVE BEAMS AND INVERSE KINEMATICS

G.Kraus, P.Egelhof, H.Geissel, W.Henning, A.Magel, G.Münzenberg, F.Nickel, K.Sümmerer, A.Weiß, D.Viera* (GSI Darmstadt)
M.Hamm, J.V.Kratz (University Mainz)
J.Friese, A.Gillitzer, H.J.Körner, M.Peter (TU München)
J.P.Schiffer (Argonne National Laboratory)
L.Chulkov, M.Golovkov, A.Ogloblin (I.V.Kurschatov Inst. Moscow)
* (on leave at absence from Los Alamos Nat. Lab. USA)

ABSTRACT:
For planned nuclear structure studies on nuclei far off stability using radioactive heavy ion beams from SIS/FRS and ESR at GSI Darmstadt the conditions and the experimental setup for the first prototype experiment p(^{56}Ni, p') are discussed. Preliminary results of a testmeasurement p(^{209}Bi, p) at 100 MeV/u are presented in comparison with a DWBA calculation.

1. INTRODUCTION

The new heavy ion synchrotron SIS in combination with the fragmentseparator FRS and the experiment storage-ring ESR [1] at GSI Darmstadt opens the possibility to perform nuclear structure studies on nuclei far off stability using radioactive heavy ion beams for light ion induced direct reactions with the method of inverse kinematics. Primary heavy ion beams with present intensities up to 10^9/s and energies of several 100 MeV/u are delivered from SIS and transferred to the FRS, where secondary radioactive beams are produced and isotopically selected. These secondary beams are then either (in special cases such as large level-spacing, extremely short lifetimes $\tau \ll 1$ sec) used directly for experiments or in cted, stored and cooled to high phasespace densities at the ESR and used for experiments at the internal gas-jet target [1].

Planned experiments are, for example, direct reactions like (p,p') and (d,p) on nuclei in the vicinity of the unstable doubly magic ^{56}Ni and ^{132}Sn and in the astrophysical interesting region around $A \approx 50$, the investigation of nuclear mass distributions in (p,p)-scattering on ^{8}He, ^{8}Li, ^{11}Li and the isospin dependence of nuclear potentials in ^{18}O(^{14}C, ^{18}O) and ^{18}O(^{14}O, ^{18}O) scattering.

Due to the favourable kinematical situation and the relatively high ^{56}Ni - rate expected already presently, the p(^{56}Ni, p') reaction was choosen as a prototype measurement.

2. THE p(^{56}Ni, p') EXPERIMENT

The motivation for this experiment is twofold: on one hand, the B(E2) matrix - element connecting the first exited 2^+ state of ^{56}Ni at 2.702 MeV to the 0^+ ground state is only poorly known [2] and its determination provides a better information on the corresponding β - value. On the other hand, the aim is to explore the feasibility of doing measurements with radioactive heavy ion beams using inverse kinematics.

The kinematical situation at 100 MeV/u is shown in fig.1. Because of the large level spacing in the low - lying region of ^{56}Ni the cross section for p(^{56}Ni, p') inelastic scattering to the 2^+ state can be determined in the vicinity of the first diffraction maximum in the angular distribution with the beam quality provided by the FRS ($\varepsilon = 20\pi$ mmmrad, $\Delta E/E \approx 1\%$), and it turns out, that for the interesting region between 78.5° and 80.9° in the laboratory frame only elastic protons and those from the inelastic scatt ring to the 2^+ state may emerge in two fairly seperated groups.

The protons will be detected by a ring of 20 silicon - detectors (2500 µm thick, 50 * 10 mm^2 active area each at a distance of 200 mm from a 1 mg/cm^2 solid

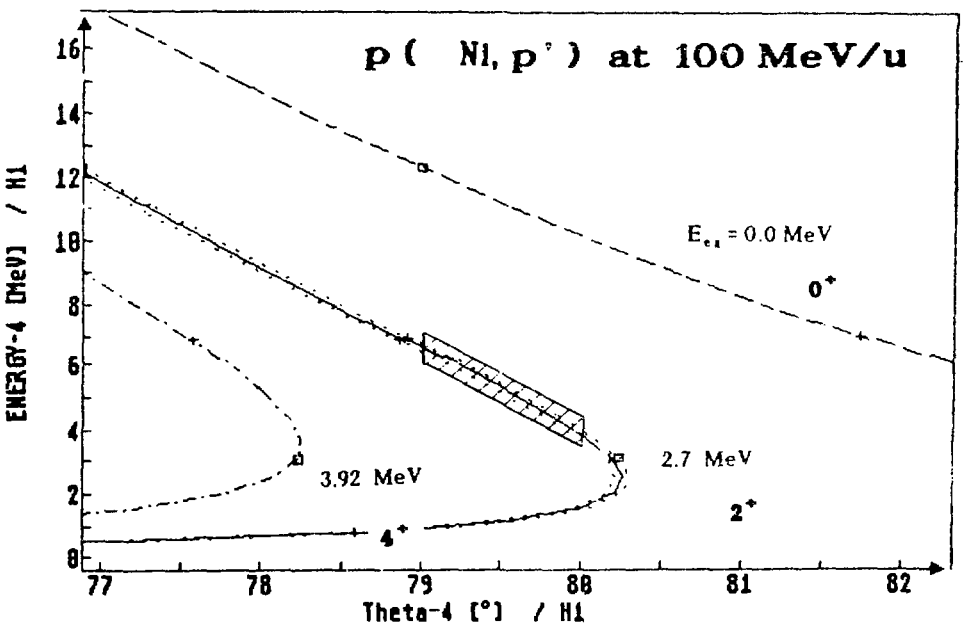

Fig.1. Kinematics for p(^{56}Ni,p'). Plotted are the proton - energies vs. laboratory angles for the groundstate and the first two exited states in ^{56}Ni. The shaded area indicates the expected maximum in the inelastic 2^+ cross section and the two dotted lines around the solid 2^+ - line represent a +- 1% variation in beam energy.

$(CH_2)_n$ target), accurately centered around the beam-axis, thus covering almost the total solid angle of interest at $\vartheta_{lab} = 79.7°$. The angular definition depends sensitively on the precise alignment of the detector slits with respect to the target and the beam-axis.

Two position-sensitive szintillation detectors [3] (500 µm thick, 200 * 200 mm^2 NE102A szintillator foil read out with 4 lightguides and PMs) mounted ≈ 2 m upstream and downstream from the target will allow tracking of the beamparticles and thus allowing to derive position and transmission-angle for the beam-particles on the target. In addition, the normalization of the measured (p, p') cross sections is delivered. The szintillation detectors have been tested to work with maximum beam intensities up to 10^6/s and a position-resolution of $\Delta x = 2$ mm has been observed. The whole setup is shown in fig. 2.

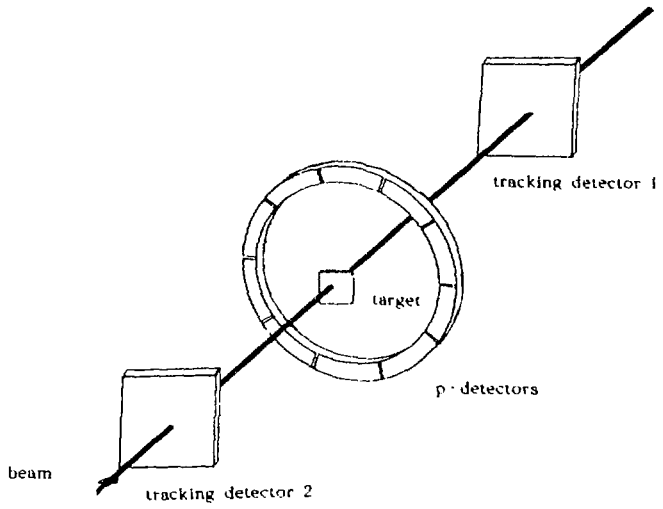

Fig. 2. Schematical view of the experimental setup.

With the described setup and a beam of 10^5 ^{56}Ni/s the expected counting rate is about 1/minute for the inelastic scattering and about five times that for the elastically scattered particles. The expected proton-background from Ni + C reactions will be monitored by using pure carbon targets and subtracted from the spectra obtained with $(CH_2)_n$ targets.

As a testexperiment for the setup and to get a quantitative information for the background situation, the reaction p(^{209}Bi, p) at 100 MeV/u has been investigated in a recent FRS-beamtime. The background originating from ^{209}Bi + ^{12}C collisions has been studied by comparing proton spectra from $(CH_2)_n$ and pure carbon targets; particle identification was done by TOF. It turns out, that essential

contributions to the proton - background arise only in an energy region below 1 MeV, while the background decreases exponentially above 1 MeV to countrates below 1/min. After discriminating the protons and subtracting the background originating from carbon, the elastic scattering cross section was determined and the preliminary results (only relative cross sections) for two of total 19 proton - detectors are shown in fig. 3 in comparison with a finite range DWBA - calculation using a potential given in [4]. The measured values are adjusted in absolute height to the calculation and the agreement of the curve with the data is satisfactory.

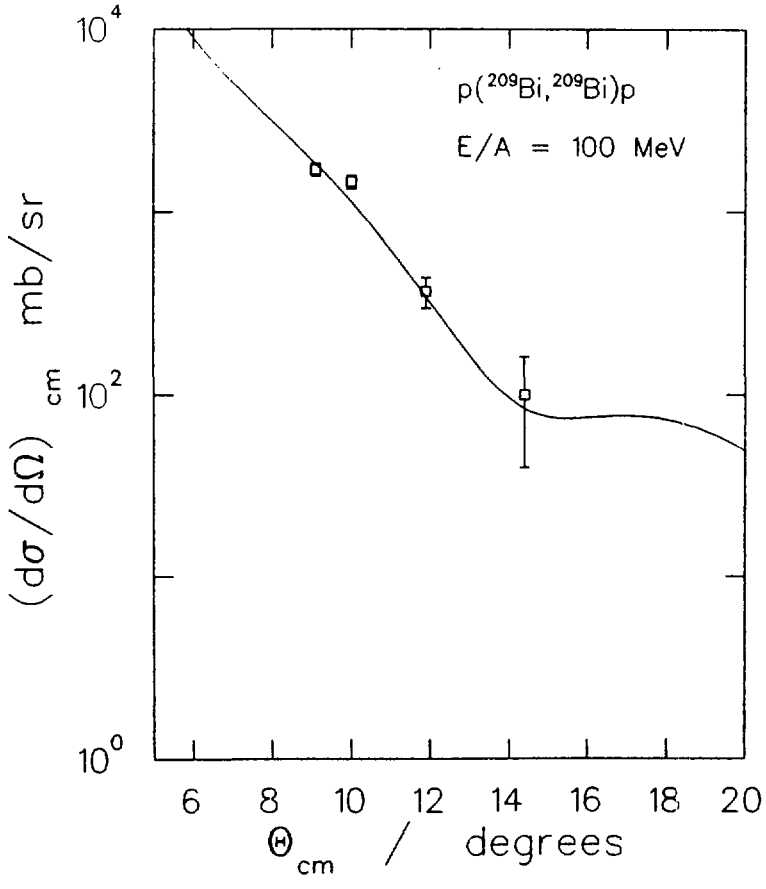

Fig. 3. Differential cross section for $p(^{209}Bi,p)$ at 100 MeV/u as function of CMS angle. The error bars are statistical. The solid line is the result of a DWBA calculation.

3. CONCLUSIONS

The p(^{56}Ni, p') reaction has been chosen for a prototype experiment with radioactive heavy ion beam using inverse kinematics. The experimental setup and the background situation has been tested with p(^{209}Bi, p) at 100 MeV/u. The proton detectors as well as the beam-tracking detectors are working satisfactory. The background turned out to be moderate for the present measurement, thus estimating a signal to background ratio better than 1:1 for the ^{56}Ni experiment, which will be performed in early 1992.

In addition, a testsetup with one silicon detector in the UHV-zone at the gas-target at the ESR has been installed and is ready to take data as soon as the design value for the density of the gas-jet target is reached.

References:

[1] P.Kienle et.al.: Phys. Bl. 46 Nr.4 (1990) 109
[2] N.Schulz et al.: Phys. Rev. C8 (1973) 1779
[3] H.Spiess et al.: to be published
[4] Comparat et.al.: Nucl. Phys. A221 (1974) 403

PENNING TRAP MASS SPECTROMETRY OF NEUTRON-DEFICIENT RB- AND SR-ISOTOPES[*]

Th. Otto[1], G. Audi[2], G. Bollen[1], H. Hartmann[1], H.-J. Kluge[1], R.B. Moore[3], G. Rouleau[3], G. Savard[1], L. Schweikhard[1], H. Stolzenberg[1] J. Szerypo[4] and the ISOLDE Collaboration[5]

[1]: Institut für Physik, Universität Mainz, Mainz, Germany

[2]: CSNSM, Laboratoire René Bernas, Orsay, France

[3]: Foster Radiation Laboratory, McGill University, Montreal, Canada

[4]: Institute for Experimental Physics, Warsaw University, Warsaw, Poland

[5]: CERN, Genève, Switzerland

ABSTRACT

We present a mass spectrometer for radioactive nuclei. The principle of measurement is the confinement of the ions in a penning trap and the subsequent determination of their cyclotron frequency ν_c which is inversely proportional to the mass. The resolution of the method is approximately 10^6, the achieved accuracy in mass determination 10^{-7}. We present some results from our survey of light Rb- and Sr-isotopes.

[*] Supported by BMFT under contract Hz-188-I

I. INTRODUCTION

The mass of a nucleus is, besides its shape, the property that can easiest be visualised in the terminology of the macroscopic world. But after 50 years of nuclear research it is not possible to calculate the mass of even the simplest nuclei from first principles. Because the mass contains the total binding energy of the nucleus, experimental mass values remain the test bed for a variety of nuclear models.

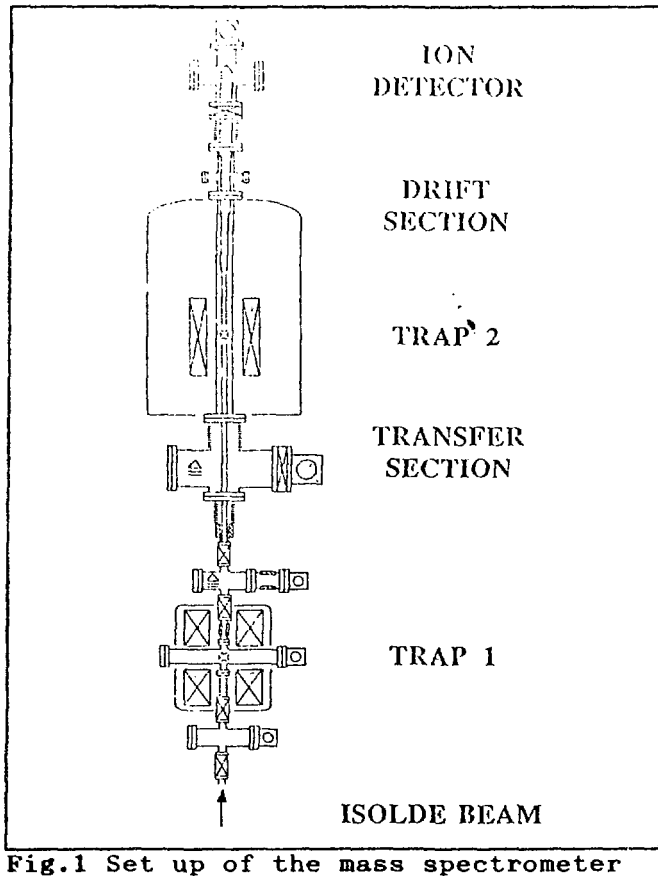

Fig.1 Set up of the mass spectrometer

The masses of stable nuclei were determined in spectrometers of the Mattauch-Herzog type. For nuclei far from stability this method was applied to Rb, Cs, and Fr in a series of experiments by the Orsay group [1],[2] but generally it is not applicable: the production yields and lifetimes do not allow the use of spectrometers with their low efficiency. The method of choice was to calculate the masses from reaction energies like total ß-decay-energies, and Q-values of different nuclear reactions. But the addition of several reaction energies led to errors and contradiction that cannot be resolved even in general adjustments of experimental results [3].

We use a method based upon the measurement of the cyclotron frequency of the ions in a strong magnetic field. The advantage of the method is the long confinement time in the penning-trap that leads to a high resolution and so to a high accuracy. After making a measurement of a long chain of Cs isotopes [4] we investigated the region of neutron deficient Rb and Sr isotopes. We find errors of only 10 keV in the investigated region.

II. PENNING TRAP

The Penning trap exploits the effect of a radially confining magnetic field and an axial binding static electrical field. If the electrostatic field has the symmetry of an axial quadrupole, the ion motions in the trap become very simple: instead of a mere rotation at the cyclotron frequency ν_c the particle undergoes a fast rotation with the reduced cyclotron frequency ν_+ superimposed on a slow magnetron drift motion with frequency ν_-. ν_+ and ν_- both depend on the trapping voltage, but their sum is independent of this quantity:

$$\nu_+ + \nu_- = \nu_c = \frac{q}{2\pi m} B$$

The sum-frequency $\nu_+ + \nu_-$ can be excited by applying an azimuthal quadrupole RF-field at this frequency in the trap [5]. This field couples the reduced cyclotron- and the magnetron-motion. In resonance, a pure magnetron motion is changed into a pure cyclotron motion of the same radius in a conversion time inversely proportional to the amplitude of the RF-field. The linewidth of the obtained resonance is inversely proportional to the interaction time with the RF-field: the 1 s interaction that we normally choose lead in the here reported region of mass 80 to a resolution of 10^6.
The change from magnetron- to cyclotron orbit is accompanied by a large increase in kinetic radial energy since $\nu_+ >> \nu_-$.

The energy pickup is detected by a time-of-flight (TOF) method [6]. After ejection from the trap the ions travel through the inhomogeneous fringe field of the solenoid that gives the trapping field. The orbital magnetic momentum - proportional to radial velocity - is converted into axial momentum. So the ions in resonance with the RF-field reach a particle detector roughly two times as fast as non-resonant ions.

The magnetic field - which enters the basic relation to calculate the nuclidic mass from the frequency ν_c - is determined from the cyclotron frequency of a nucleus with well-known mass.

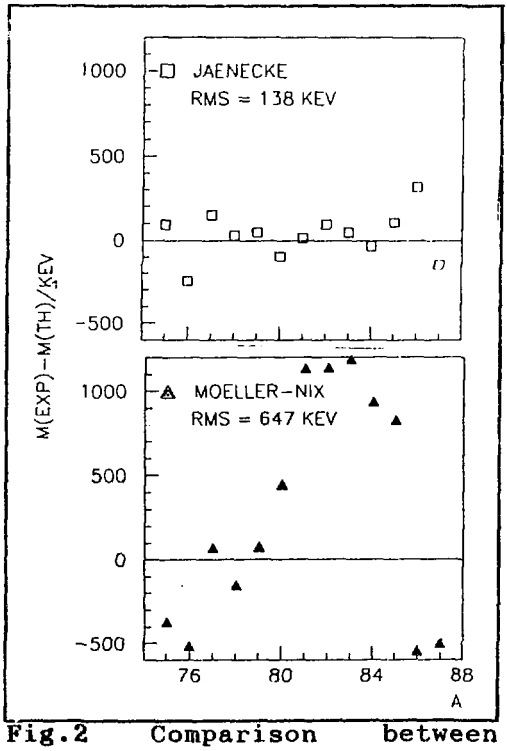

Fig.2 Comparison between theoretical and experimental results.

III. TANDEM PENNING TRAP MASS SPECTROMETER

The Tandem Penning Trap Mass Spectrometer, Fig.1, consists of a bunching and cooling trap [7] in the 0.7 T-field of an electro-magnet and the high accuracy Penning trap in the 6 T-field of a superconducting solenoid, in which the determination of ν_c is done. This trap has correction electrodes that allow for a compensation of deviations from a perfect quadrupole potential. The traps are connected with an ion-optical transfer system. For detection of the resonance by the TOF technique a drift section and a channel plate detector follow the precision trap.

IV. RESULTS FOR RB- AND SR-ISOTOPES

In a series of measurements in 1989 and 1990 we determined the mass of the nuclei $^{75-87}$Rb and $^{78-83,87}$Sr with an uncertainty of 10 keV. The mass of ^{78,79}Sr was determined for the first time experimentally. Fig. 2 shows a comparison of our new Rb-measurements with two well-known mass-formulae [8]: the model of Jaenecke and Masson is reproducing the experimental values quite well, but it only has limited predictive power since it relies on experimentally determined neighbouring masses as input parameters. On the other hand the model of Möller and Nix, a macroscopic-microscopic model constructed with a lot of physical insight, is not giving a good fit to our results. We are at the moment studying this class of models in detail to track down the deficiencies.

The resolution of the Penning trap mass spectrometer is good enough to resolve Isomers with more than 100 keV excitation energy. Here the interactions of ions with different mass have to be taken into account.

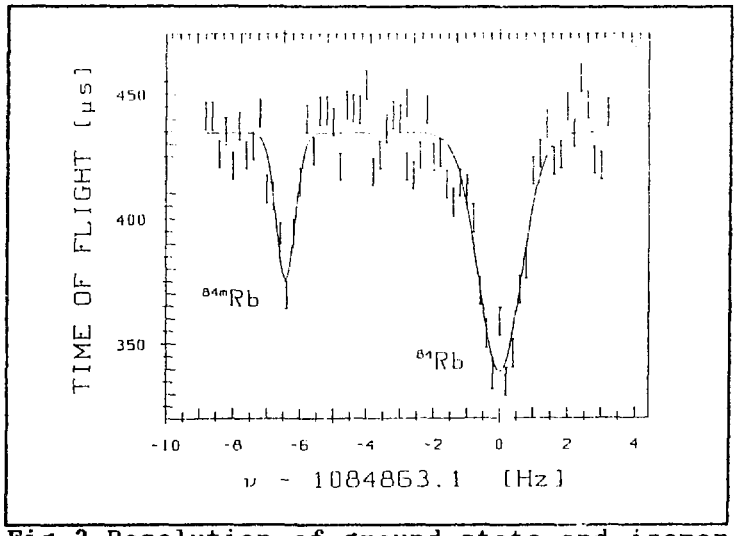

Fig. 3 Resolution of ground state and isomer of ^{84}Rb.

The mutual electromagnetic forces the ions exert on each other leads to a shift of the resonance frequency. We studied this behaviour in a series of numerical simulations and experiments. One possible way of correcting for these shifts is to perform the experiment with a very small number of ions in the trap and then to extrapolate to zero contamination. With ^{84}Rb we were able

to do this step and for the first time in mass spectrometry we achieved a resolution of ground state and isomer. Fig.3 shows the two resonances of ground- and excited state. The frequency separation corresponds exactly to the reported excitation energy of 463(10) keV.

REFERENCES

1. G. Audi et al., Nucl.Phys **A378** (1982) 443-460
2. G. Audi et al., Nucl.Phys. **A449** (1986) 1-33
3. A.H. Wapstra, G. Audi, R. Hoekstra, At.Data Nucl.Data Table **39** (1988) 290
4. H. Stolzenberg et. al., Phys.Rev.Lett. **65** (1990) 3104
5. G. Bollen et al., J.Appl.Phys. **68** (1990) 4355
6. G. Gräff, H. Kalinowsky, J. Traut, Z.Phys **A297** (1980) 35
7. G. Savard et al., to be published in Phys.Lett.A
8. P. Haustein (ed.), At.Data and Nucl.Data Tables **39** (1988) 185

MEASURED AND CALCULATED NEUTRON SCATTERING CROSS SECTIONS FOR THE ACTINIDE NUCLEI ^{232}Th , ^{238}U and ^{239}Pu

E. SHELDON*, E D ARTHUR#, J J EGAN*, G H R KEGEL*, A MITTLER* and P G YOUNG#

* *Department of Physics and Applied Physics, University of Massachussets at Lowell, 1 University Avenue Lowell, MA 01854-2881, U.S.A. [BITNET E-mail: SHELDON@RCN]*

LANL Group T-2, B 243, Los Alamos National Laboratory, P.O. Box 1663, Los Alamos, NM 78545, U.S.A. [BITNET E-mail: PGY@LANL.GOV]

1. INTRODUCTORY REMARKS

Results from the Lowell group's measurements and analyses of fast-neutron elastic and inelastic scattering cross sections on the principal actinide nuclei have been reported at previous recent Mazurian meetings (Sheldon 1989, 1986; Sheldon *et al* 1986). The current report updates the findings from these ongoing studies, presenting new results for inelastic neutron scattering from ^{232}Th and ^{238}U to collective rotational and vibrational levels up to $E^* \cong 1$ MeV in excitation energy for incident energies $E_n = 2.3 - 3.0$ MeV and for ^{239}Pu up to $E^* \cong 0.076$ MeV for $E_n = 0.57$ MeV. Preliminary results were reported at physics data conferences earlier this year (Sheldon *et al* 1991a, 1991b; Egan *et al* 1991); the results in the present paper constitute more definitively measured and calculated data, as well as new analyses and evaluations.

The experimental data on the even-A nuclei ^{232}Th and ^{238}U comprise level excitation functions [EF's] for the incident-energy range $E_n = 2.3 - 3.0$ MeV and angular distributions [AD's] at $E_n = 2.4$ and 2.8 MeV, while those for the odd-A nucleus ^{239}Pu constitute AD's at $E_n = 0.57$ MeV. These were measured using subnanosecond-resolution time-of-flight neutron spectroscopy over a 2½-metre flight-path (Aliyar 1988, Goswami *et al* 1988, Egan *et al* 1988, Kegel *et al* 1988a, 1988b, Egan *et al* 1991, Kegel *et al* 1991).

The theoretical data have been refined through the use of new vibrational-band coupling strengths and the linkage of analyses in a Lowell/Los Alamos [LANL] collaboration employing the "standard" formalisms in which Hauser-Feshbach-Moldauer compound-nucleus [CN] cross sections are incoherently added to coupled-channel distorted-wave direct-interaction [DI] contributions. To avoid inordinately long computation times and memory-capacity requirements, the more complex Hofmann-Richert-Tepel-Weidenmüller [HRTW] approach has not been utilized. The availability of very recent evaluations, in the form of ENDF/B-VI data-bank cross sections, has enabled us to make direct comparisons between experimental, theoretical and evaluated data.

2. THEORETICAL ANALYSES AND RESULTS

The close spacing of levels in these actinide nuclei rendered it impossible in some instances to resolve the separate n'-groups experimentally, even with premium resolution, and hence required that in such cases the individual contributions from the members in each group of levels be summed to

yield a "composite" cross section over a specified excitation-energy range Specifically, the data for ^{232}Th(n, n') constitute EF's and AD's for the following five groups:

(i) the 333.1-keV (6+) [K = 0+ ground-state rotational] niveau;

(ii) the pair of states at 714.25 keV (1-) [K=0- octupole vib.] and 730.10 keV (0+) [K = 0+ β- vib.];

(iii) a composite of five levels in the $E^* \approx 774 - 830$ keV range comprising the 774.1-keV (2+) [K=0+ β-vib.],774.4-keV (3-) [K=0- oct. vib.], 785.2-keV (2+) [K=2+ γ-vib.], 828.1-keV (10+) [K=0+ g.s. rot.] and 829.6-keV (3+) [K=2+ γ-vibration] states;

(iv) a combination of three levels in the $E^* = 873 - 890$ keV range consisting of the 873-keV (4+) [K=2+ β-vib.], 883.3-keV (5-) [K=0- oct. vib.] and 890.1-keV (4+) [K=2+ γ-vibration] states; and

(v) the 960.2-keV (5+) [K = 2+ γ-vibrational] level.

For ^{238}U(n, n'), the somewhat wider level spacing permitted better individualization of states into the following five groups:

(i) the 307.2-keV (6+) [K = 0+ ground-state rotational] level;

(ii) the 680.1-keV (1-) [K = 0- octupole vibrational] state;

(iii) the next 731.9-keV (3-) [K = 0 octupole vibrational] level;

(iv) the next 827.2-keV (5-) [K = 0- octupole vibrational] level; and

(v) a composite of eight levels in the $E^* = 927 - 998$ keV range consisting of the 927.2-keV (0+) [K =0+ 2-phonon γ-vib.], the 930.8-keV (1-) [K=1- oct. vib.], the next 950.0-keV (2-) [K=1- oct. vib.], the 966-keV (7-) [K = 0- oct. vib.], 966.3-keV (2+) [K = 0+ 2-phonon γ-vib.], 993-keV (0+) [K = 0+ β-vib.] and 997.5-keV (3-) [K = 1- octupole vibrational] states.

For ^{239}Pu(n,n) and (n, n') the members of the K = ½ $^+$ ground-state rotational band were paired:

(i) the 0-keV (½ +) and 7.8-keV (3/2 +) ground and first-excited states being combined; and

(ii) the 57.3-keV (5/2 +) and 75.7-keV (7/2 +) levels being combined.

For consistency, the CN + DI computations, performed at Lowell with the programmes CINDY + KARJUP and at LANL with COMNUC + DWUCK, employed the Bruyères set of optical-potential parameters and deformations (Haouat *et al* 1980, 1982), or minor modifications thereof as established by the LANL group to provide a better overall fit over the energy range E_n=1-20 MeV, as listed in Table 1.

In the CN computations, provision was made for the effect of competing n' and (radiative-capture) γ-channels and of (n, f) fission, as well as allowing for Moldauer level-width fluctuation enhancement of elastic-scattering and diminution of inelastic-scattering cross sections. For incident energies above about $E_n \cong 1$ MeV, the effect of continuum competition (using Gilbert-Cameron level-density parameters) was taken into account. The DI contributions have now been completely recalculated, using values of deformation parameters and coupling strengths as specified in Table 2. Therein, the values were either those established by the Bruyères group (Haouat *et al* 1980, 1982) from (n, n') analyses or those (β_λ) deduced from experimental studies of (d, d') or Coulomb-excitation reactions to derive reduced multipole transition probabilities B(Eλ), in accordance with the formula:

$$\beta_\lambda = \{4\pi / [3\, Z\, (r_0\, A^{1/3})^2]\}\, [B(E\lambda)]^{1/\lambda} \text{ with } r_0 = 1.2 \text{ fm.}$$

A single value of β_λ was used for all members of any given band. This procedure furnished generally better agreement with the measured data than had hitherto been achieved, though some conspicuous discrepancies remain evident in Figs. 1 - 4. No further attempt was made to secure a still closer fit through further variation of parameters -- this would have entailed inordinately long computer running times and would have obscured the basic aim of comparing the independent approaches.

In Figs. 1(a,b) are shown level EF's for ^{232}Th and ^{238}U(n, n') to E_n = 3.5 MeV, the points with error bars representing the high-energy Lowell measurements from E_n = 2.3 - 3.0 MeV by Aliyar (1988) and Kegel *et al* (1988b). The Lowell CN/DI computations with CINDY/KARJUP are depicted as solid curves, while the LANL computations with COMNUC/DWUCK and modified parameters (Egan *et al* 1986, Arthur 1986, as listed in Table 1) are displayed as broken (dashed) curves. The latest evaluated data, from ENDF/B-VI files (Bhat 1990, Weston *et al* 1990) are indicated by the dotted curves. It is evident that the variation of (n, n') cross sections with energy in this incident-energy region is fairly well represented by statistical-model/DWDI calculations and excellently fitted by the latest evaluations.

In Figs. 2(a,b) are shown the AD's for ^{232}Th(n, n') at E_n = 2.4 and 2.8 MeV, using the same graphical convention, while Figs. 3(a,b) depict those for ^{238}U(n, n') at E_n = 2.4 and 2.8 MeV, and Figs.4(a,b) present those for ^{239}Pu at E_n = 0.57 MeV. In Fig. 4 the broken curves have been omitted, since the LANL computations formed the basis for the ENDF/B-VI evaluation file and accordingly are identical with the dotted curves. As AD's are intrinsically more sensitive to reaction mechanism and choice of model parameters than EF's, it is to be expected that discrepancies between experiment

and theory will appear more pronounced in Figs 2 - 4 than in Fig 1. In particular, the AD fits to high-lying individual states (such as the $J^{\pi} = 5^{+}$ levels in Figs 2 and 3) do not provide as satisfactory an overall fit, either in magnitude or in structure as in the remaining cases. In general, it would appear that the theoretical angular variation tends to be more bland than that suggested by the measured data. Nonetheless, the over-all match of theory to experiment can be deemed acceptable.

REFERENCES

Aliyar Abobakr 1988 PhD Dissertation (University of Lowell).

Arthur E D 1986 *Bull Am Phys Soc* 31(8) 1238, Paper ED 10

Bl at M R 1990, ENDF/B-VI evaluated data files for ^{232}Th (Brookhaven: National Nuclear Data Cen)

Egan J J, Aliyar A, Horton C A, Kegel G H R, and Mittler A 1988 *Proc Int Conf on Nuclear Data for Science and Technology, Mito, Japan, May 30 - June 3, 1988* ed S. Igarasi (Tokyo: Saikon Publ. Co., 1988) pp 63 - 66.

Egan J J, Arthur E D, Kegel G, Mittler A and Shao J Q 1986, in *Proc Int Conf on Nuclear Data for Basic and Applied Science, May 1985, Santa Fe, USA*, Vol 2 (New York: Gordon and Breach, 1986) pp 1209 - 1212.

Egan J J, Kegel G H R, Yue G, Mittler A, Staples P A, DeSimone D and Woodring M L 1991, in *NUCLEAR DATA : Book of Abstracts -- Int Conf on Nuclear Data for Science and Technology, Jülich, Germany, May 13 -17, 1991* ed S.M. Qaim (Jülich: KFA, 1991) Paper A4, p 138.

Goswami G C, Egan J J, Kegel G H R, Mittler A and Sheldon E 1988 *Nucl Sci Eng* 100, 48 - 60.

Haouat G, Lagrange Ch, Lachkar J, Jary J, Patin Y and Sigaud J 1980, in *Proc Int Conf on Nuclear Cross Sections for Technology, Oct 1979, Knoxville, USA* ed J L Fowler, G H Johnson and C D Bowman, Report CP 791022 (Washington: U S Government Printing Office) pp 672 - 676.

Haouat G, Lachkar J, Lagrange Ch, Jary J, Sigaud J and Patin Y 1982, *Nucl Sci Eng* 81, 491 - 511.

Kegel G H R, Aliyar A, Chang J H, Egan J J, Horton C A and Mittler A 1988a, in *NUCLEAR DATA FOR SCIENCE AND TECHNOLOGY: Proc Int Conf on Nuclear Data for Science and Technology, Mito, Japan, May 30 - June 3, 1988*, ed S. Igarasi (Tokyo: Saikon Publ. Co., 1988), pp 399 - 402.

Kegel G H R, Aliyar A, Egan J J, Horton C A and Mittler A 1988b, *Bull Am Phys Soc* Ser II, 33(8), 1568, Paper AF 13.

Kegel Gunter H R, Dugan Patrick F, Egan James J, Jen Causon K C, Mittler Arthur and Staples Parish 1991, in *NUCLEAR DATA: Book of Abstracts -- Int Conf on Nuclear Data for Science and Technology, Jülich, Germany, May 13 - 17, 1991* ed S M Qaim (Jülich: KFA 1991) Paper O9, p 33

Schmorak M R 1982 *Nucl Data Sheets* 36, 367.

Schmorak M R 1983 *Nucl Data Sheets* 40(1), 1.

Sheldon E 1986 in *HEAVY IONS IN NUCLEAR PHYSICS: Proceedings of the 16th International Summer School in Nuclear Physics, Mikolajki, Poland, August 27 - September 8,1984* ed Z. Wilhelmi and M. Kicinska-Habior, Vol.9 of the Nuclear Science Research Conference Series (New York: Harwood Academic Publ., 1986) pp 377 - 448.

Sheldon Eric 1989 *Mikolajki 88 - Seminars, Proceedings of the 20th Mikolajki Summer School on Nuclear Physics, Mikolajki, Poland, September 1 - 11, 1988* ed Z Wilhelmi and G Szeflinska (Warsaw: University of Warsaw, 1989) pp 152 - 156.

Sheldon E, Aliyar A, Beghian L E, Egan J J, Kegel G H R, Mittler A and Arthur E D 1991a in *NUCLEAR DATA: Book of Abstracts -- Int Conf on Nuclear Data for Science and Technology, Jülich, Germany, May 13 - 17, 1991* ed S M Qaim (Jülich: KFA 1991) Paper D40, p 350.

Sheldon E, Egan J J, Goswami G C, Kegel G H R and Mittler A 1987 in *COHERENT EFFECTS IN HIGHLY EXCITED NUCLEI: Proceedings of the 18th International Summer School in Nuclear Physics, Mikolajki, Poland, September 1 - 13, 1986* ed Z Wilhelmi and G Szeflinska (New York: Harwood Academic Publ, 1987) pp 117 - 136.

Sheldon E, Egan J J, Kegel G H R, Mittler A and Aliyar A 1991b, *Bull Am Phys Soc* 36(7) 2041 - 2042, Paper S1 3.

Shurshikov E N 1988 *Nuclear Data Sheets* 53, 601.

Weston L W, Young P G and Poenitz W 1990, ENDF/B-VI Evaluated Nuclear Data File for ^{238}U (Brookhaven: National Nuclear Data Center).

Young P G and Arthur E D 1991, in *NUCLEAR DATA: Book of Abstracts -- Int Conf on Nuclear Data for Science and Technology, Jülich, Germany, May 13 -17, 1991* ed S.M. Qaim (Jülich: KFA, 1991) Paper O71, p 95.

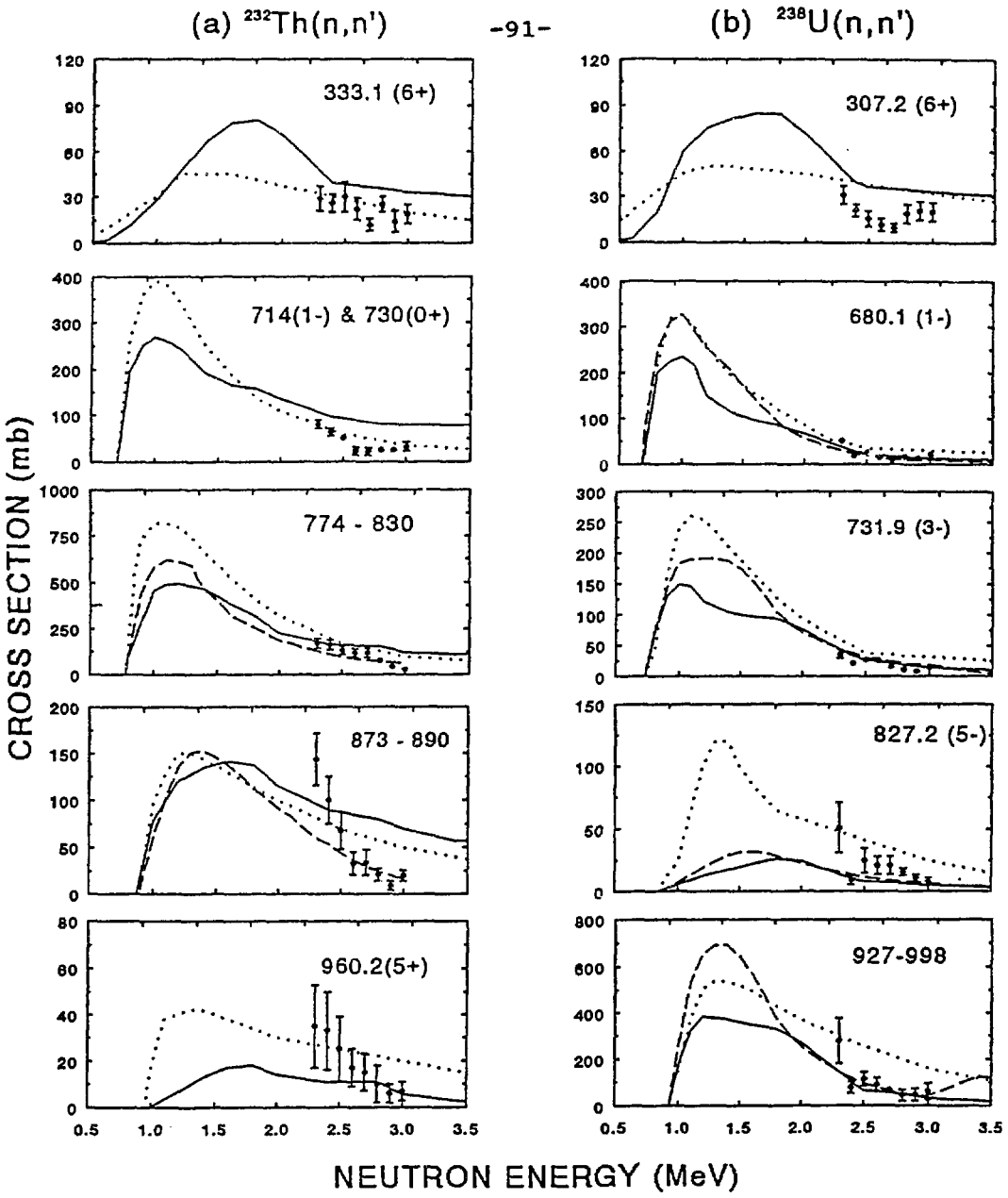

Fig. 1. Excitation functions for inelastic neutron scattering on (a) ^{232}Th and (b) ^{238}U to individual or grouped (unresolvable) levels in rotational (uppermost plots) and vibrational bands up to E*≅1,000 keV, comparing the Lowell group's measured data (points, with error bars) from 2.3 to 3.0 MeV in 0.1-MeV steps (Aliyar 1988, Kegel *et al* 1988a) with the theoretical predictions from the standard (CN+DI) formalism, as calculated at Lowell (solid curves) and Los Alamos (LANL, Egan *et al* 1986, Arthur 1986) (broken curves) to 3.5 MeV. The ENDF/B-VI evaluations by Bhat (1990) for ^{232}Th and by Weston *et al* (1990) for ^{238}U are depicted as dotted curves. In the uppermost (6+) plots, the theoretical cross sections at high energies tend to be elevated by the onset of substantial direct-interaction (DI) contributions (as compound-nucleus [CN] admixtures become vanishingly small).

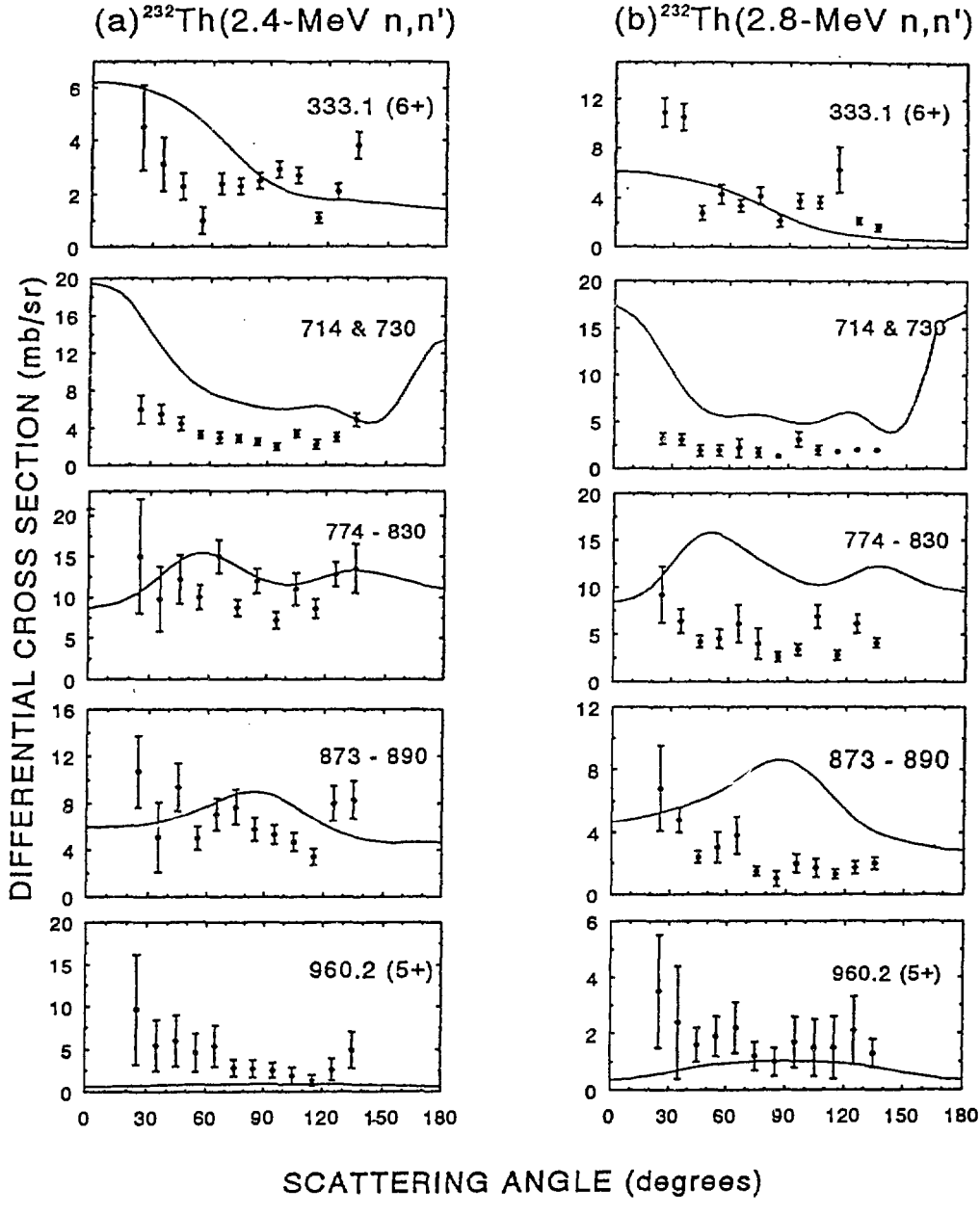

Fig. 2. Angular distributions for ^{232}Th(n, n') scattering to individual or grouped (unresolvable) levels up to $E^* = 960.2$ keV at (a) $E_n = 2.4$ MeV and (b) $E_n = 2.8$ MeV, comparing the Lowell group's measured data (points, with error bars) with theoretical (CN+DI) differential cross sections computed with the programmes CINDY/KARJUP at Lowell (solid curves), or COMNUC/DWUCK at LANL (dashed curves). As the ENDF/B-VI evaluated differential cross-section data for these levels commenced only at higher incident energies ($E_n \cong 5$ MeV), no (dotted) evaluation curves are included. The scatter of the measured data-points renders a shape-comparison difficult, but the magnitudes are in reasonably close agreement with theory (with the possible exception of the data for the 960.2-keV (5+) [K = 2+ γ-vibrational] state, for which larger DI band-coupling strengths would be beneficial; however, the experimental error limits are rather large in these cases and "fine-tuning" of the theoretical parameters would appear to be unjustified).

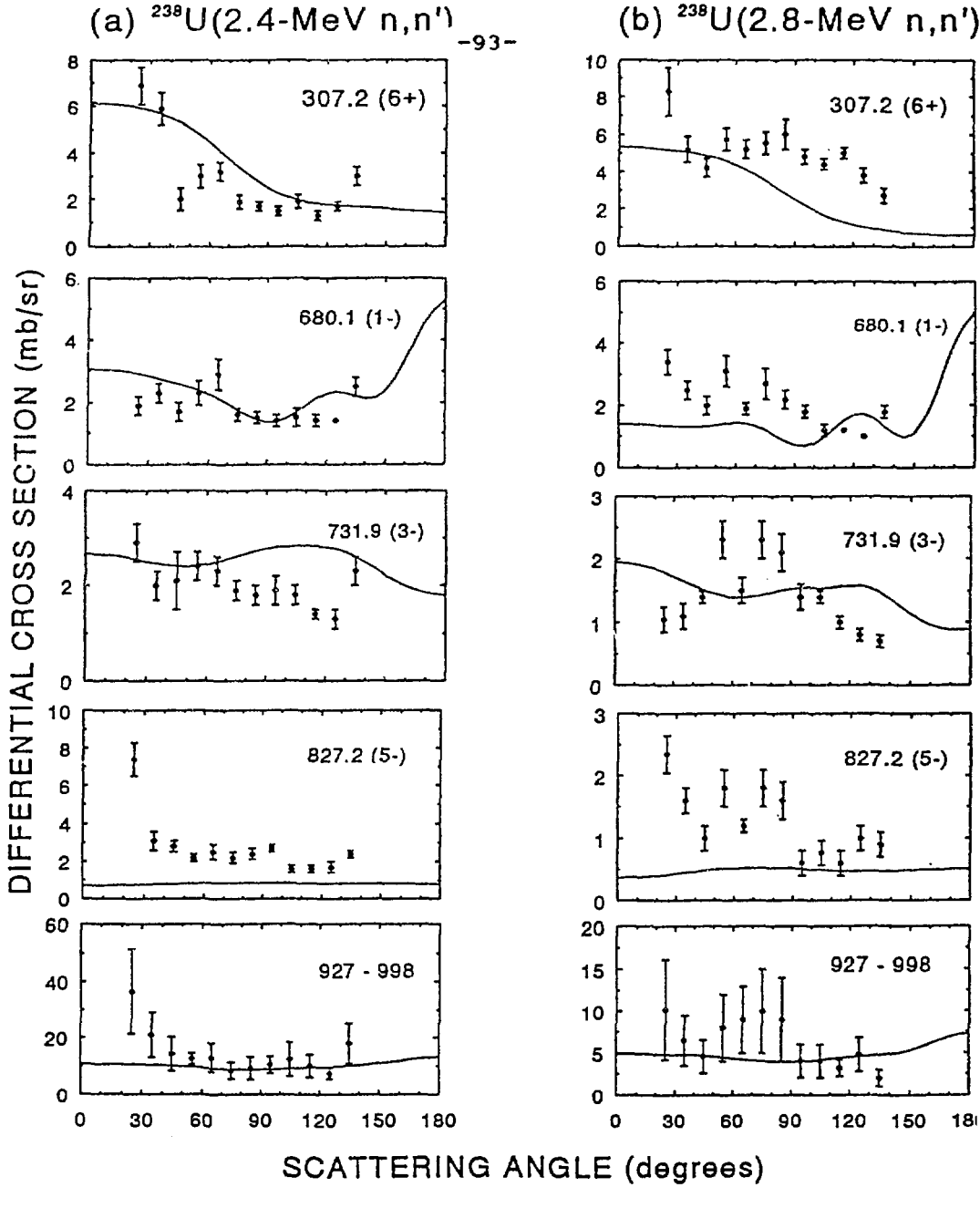

Fig. 3. Angular distributions for $^{238}U(n, n')$ to individual or composite (unresolvable) levels up to E^*=997.5 keV at (a) E_n=2.4 MeV and (b) E_n = 2.8 MeV, comparing Lowell experimental data with theoretical (CN+DI) differential cross sections. As the ENDF/B-VI evaluated differential cross-section data for these levels commenced only at higher incident energies ($E_n \cong 5$ MeV), no (dotted) evaluation curves are included. Again, the theoretical magnitudes match the measured differential cross sections quite closely, but a structural fit is unattainable. The rather poor fits in the case of the 827.2-keV (5-) [K = 0- octupole vibrational] state may be attributed to use of too small a value for the band-coupling parameter, but a larger value would have destroyed the fit to the other members of this octupole band, shown immediately above these plots.

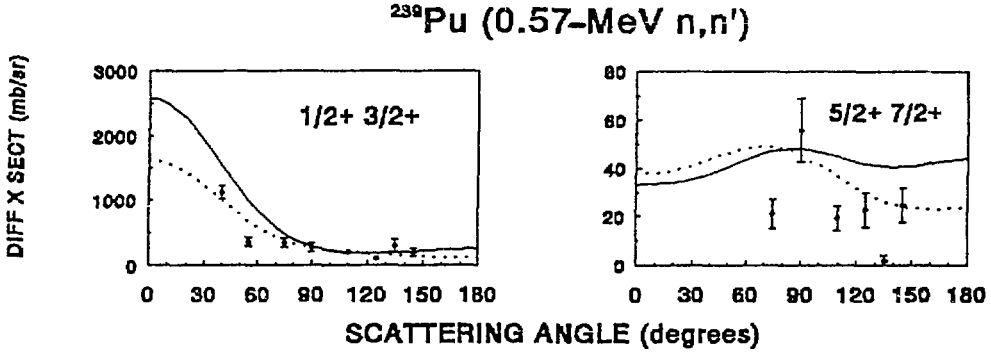

Fig. 4. Angular distributions for elastic and inelastic neutron scattering at E_n = 0.57 MeV on ^{239}Pu to paired members of the K = ½⁺ ground-state rotational band: (a) to the 0.00-keV (1/2+) and 7.8-keV (3/2+) levels, and (b) to the 57.3-keV (5/2+) and 75.7-keV (7/2+) levels, comparing Lowell experimental data (points, with error bars) with Lowell CN+DI computations (solid curves) and LANL computations, the latter being identical with ENDF/B-VI evaluations (dotted curves).

Table 1. Optical-potential parameters used in the CN/DI computations at Lowell and LANL.

Nuclide	Real Potential V	WSD Potential W	r_0	a	r_0'	a'	V_{so}	r_{so}	a_{so}	β_2	β_4
^{232}Th	46.4 - 0.3 E_n	3.6 + 0.4 E_n	1.26	0.63	1.26	0.52	6.2	1.12	0.47	0.190	0.07
^{238}U(Br/Low)	46.2 - 0.3 E_n	3.6 + 0.4 E_n	1.26	0.63	1.26	0.52	6.2	1.12	0.47	0.198	0.080
(LANL)	46.2 - 0.275 E_n	3.18 + 0.4 E_n	1.26	0.63	1.26	0.52	6.2	1.12	0.47	0.198	0.057
^{239}Pu(Br/Low)	46.2 - 0.3 E_n	3.6 + 0.4 E_n	1.26	0.63	1.26	0.52	6.2	1.12	0.47	0.220	0.070
(LANL)	46.2 - 0.3 E_n	3.3 + 0.45 E_n	1.26	0.63	1.24	0.50	6.2	1.12	0.47	0.205	0.075

Table 2. Actinide nuclear levels for which reduced multipole transition probabilities B(Eλ) have been determined and thence deformations β_λ deduced [or β assigned from (n, n') analyses], together with the levels and adopted coupling strengths featured in the present investigations.

Nucleus	E*	J^π	K^π	B(Eλ)e²	λ	β_λ	Coupl. Str.*	Reference
^{232}Th	333.1	6+	0+ g.s.rot.				$\beta_2 = 0.190$, $\beta_4 = 0.071$	Haouat *et al* 1980,1982)
	(556.9	8+	"				β_2, β_4	
	714.25	1-	0- oct.vib.				0.066	
	730.10	0+	0+ β band				0.0271	
	774.1	2+	0+ β vib.	0.10 b²	?	0.0271	0.0271	Schmorak 1982
	774.4	3-	0- oct.vib.	0.45 b³	3	0.066	0.066	Schmorak 1982
	785.2	2+	2+ γ band	0.122 b²	2	0.0299	0.0299	Schmorak 1982
	(828.1	10+	0+ g.s.rot.				β_2, β_4	)
	829.6	3+	2+ γ vib.				0.0299	
	873.0	4+	0+ β vib.				0.0271	
	883.3	5-	0- oct.vib.				0.066	
	890.1	4+	2+ γ vib.				0.0299	
	960.2	5+	2+ γ vib				0.0299	
* Deformation parameters: Range in literature: $\beta_2 = 0.183 - 0.238$; $\beta_4 = 0.049 - 0.118$; $\beta_6 = 0.009$]. Average of cited deformations: $\beta_2 = 0.208$, $\beta_4 = 0.081$, $\beta_6 = \pm 0.009$.								
^{238}U	307.2	6+	0+ g.s. rot.				$\beta_2 = 0.198$, $\beta_4 = 0.057$	Haouat 1980
	(518.3	8+	"	4.7 b²	2	0.18	β_2, β_4)	Shurshikov 1988
	680.1	1-	0- oct. vib.	0.575 b³	3	0.0685	0.0685	Shurshikov 1988
	731.9	3-	0- oct. vib.				0.0685	
	(775.7	10+	0+ g.s. rot.	5.2 b²	2	0.19	β_2, β_4)	Shurshikov 1988
	827.2	5-	0- oct. vib.				0.0685	
	927.2	0+	0+ 2-ph. γ	0.017 b²	2	0.011	0.011	Shurshikov 1988
	930.8	1-	1- oct. vib.				0.0486	
	950.0	2-	1- oct. vib.				0.0486	
	966	7-	0- oct. vib.				0.0685	
	966.3	2+	0+ 2-ph. γ				0.011	
	993	0+	0+ β-band				0.018	
	997.5	3-	1- oct. vib.	0.206 b³	3	0.0486	0.0486	Shurshikov 1988
	(1037.3	2+	0+ β vib.	.037/.048/.063 b²	2	.016/.018/.021	0.018	Shurshikov 1988)
* Deformation parameters: Range in literature: $\beta_2 = 0.198 - 0.27$; $\beta_4 = 0.017$-0.103; $\beta_6 = 0$ -> -0.015]. Average of cited deformations: $\beta_2 = 0.236$, $\beta_4 = 0.049$, $\beta_6 = -0.011$.								
^{239}Pu	0.0	1/2+	g.s. rot				$\beta_2 = 0.220$, $\beta_4 = 0.070$	Haouat 1980
	0.0	1/2+	g.s. rot				$\beta_2 = 0.205$, $\beta_4 = 0.075$	Young 1991
	0.0	1/2+	"			0.29	β_2, β_4	Schmorak 1983
	7.8	3/2+	"				β_2, β_4	
	57.3	5/2+	"	4.4 b²	2	0.169	β_2, β_4	Schmorak 1983
	75.7	7/2+	"				β_2, β_4	
	505.5	5/2-	1/2[631]		3	0.039		Young and
	556.1	7/2-	"		3	0.045		Arthur 1991
	939	3/2+			2	0.020		"
	1001	5/2-			3	0.043		"
	1135	5/2+			2	0.024		"
	1282	7/2-			3	0.050		"

INTERNAL CONVERSION IN HIGHLY STRIPPED ^{83}KR IONS

J. Copnell, W.R. Phillips and A.R. Barnett

Department of Physics, University of Manchester,

Manchester, M13 9PL, England

K.E. Rehm, I. Ahmad, B.G. Glagola, W. Kutscherra,

R.C. Pardo and J.P. Schiffer

Argonne National Laboratory, Argonne, Illinois, 90439, U.S.A.

ABSTRACT

The L-conversion coefficients of the 9.4 keV transition between the first excited state of $J^\pi = 7/2^+$ and the $9/2^+$ ground state of ^{83}Kr have been measured in ions of ionicity q from 28 to 33. These coefficients are sensitive to changes in L-shell wave functions as electrons are successively removed. Preliminary results are $\alpha_L(q) = 14.7(10)$, 14.8(10), 14.1(8), 14.7(10), 15.1(22) and 19.4(80) for q = 28, 29, 30, 31, 32 and 33 respectively.

Results of a preliminary experiment to measure L-shell internal conversion coefficients $\alpha_L(q)$ in highly stripped ^{83}Kr ions of charge state q are presented. The transition between the 9.4 keV first excited state and ground state of ^{83}Kr is predominantly [1] magnetic dipole (electric quadrupole to magnetic dipole intensity ratio = $1.7(2) \times 10^{-4}$) and is highly converted, chiefly in the L-shell with a small fraction in the M-shell. The total conversion coefficient $\alpha \simeq 19.5(15)$ with predicted [2] $\alpha_L/\alpha \sim 0.86$. Measurements of $\alpha_L(q)$ for q = 28 to 33 give information on changes in L-shell electron wave functions as L-shell electrons are successively removed, and thus provide tests of relativistic mean field predictions of electron orbitals. If measurements can be made with sufficient accuracy corrections from QED effects can be probed.

The technique used to measure the $\alpha_L(q)$ values is similar to that used [3] in experiments on the isomeric state in ^{57}Fe. A secondary beam of ^{83}Kr, in which a fraction of

the nuclei was in the excited 9.4 keV state, was produced by Coulomb excitation of i
cident 650 MeV ^{83}Kr ions from the ATLAS accelerator at the Argonne Laboratory. Th
secondary beam, scattered from a 300 μg cm^{-2} Au target at various laboratory angl
θ_L forward of the angle for nuclear grazing collisions, was analysed in an Enge magnet
spectrometer. The numbers of excited nuclei decaying during passage of the spectromet
were deduced from the patterns of events observed in the spectrometer focal plane. A
example is shown in figure 1. The pattern is simpler in this experiment than in that c
^{57}Fe because of the absence of $\Delta q = +2$ events, which are energetically impossible for ^{83}K
ions with no electrons in the M-shell ($q \geq 26$).

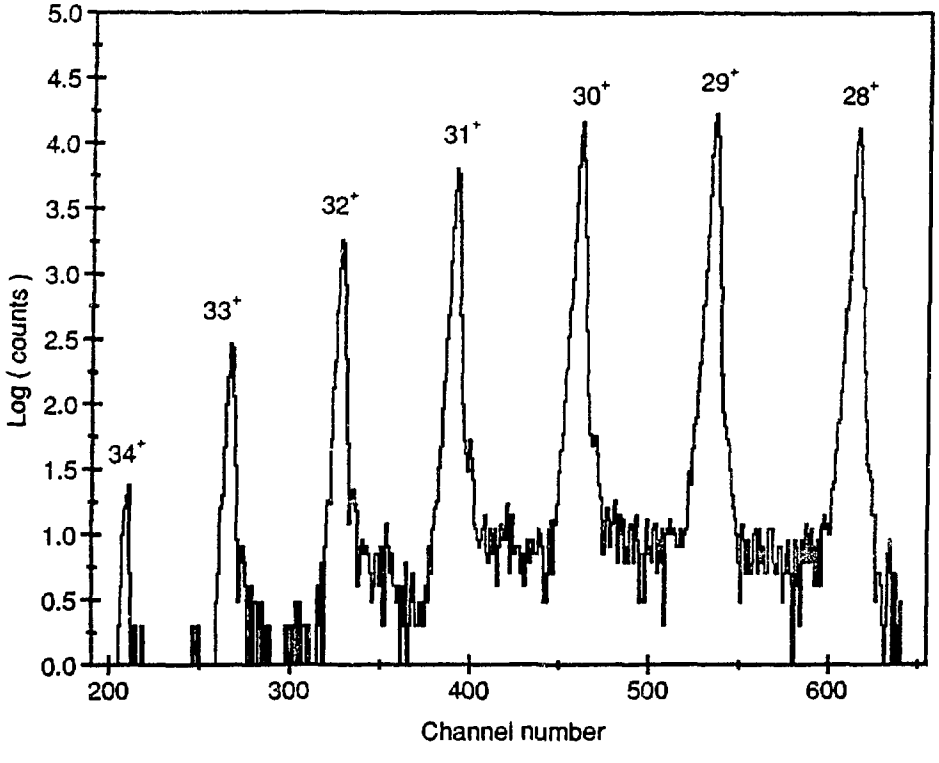

Figure 1 — An experimental spectrum (see text).

The fractions f_0 of excited ^{83}Kr nuclei leaving the target at different θ_L were deter
mined from the total numbers of ions which decayed in the magnet, and the total number
in the unchanged charge peaks. In this experiment f_0 equalled 0.07(1) at $\theta_L = 25°$, and

0.11(1) at 30°. The analysis to deduce $\alpha_L(q)$ from the numbers observed along the focal plane then followed the procedure outlined for ^{57}Fe, although simplified by the presence only of $\Delta q = +1$ events. The position spectra obtained at $\theta_L = 25°$ and 30° were analysed by performing a multi-dimensional χ^2 minimisation between the spectra and Monte-Carlo simulations of the experiment incorporating the ion-optical code RAYTRACE [4] modified to include $\Delta q = +1$ charge changes. Self-consistency was preserved by including a factor dependent on the difference between the lifetimes used as inputs to the simulations, and those deduced from the numbers produced by the simulations.

Figure 2 shows the residuals from the best fit simulation to the data of figure 1. The table shows the results obtained for $\alpha_L(q)$ from data at $\theta_L = 25°$ and 30°.

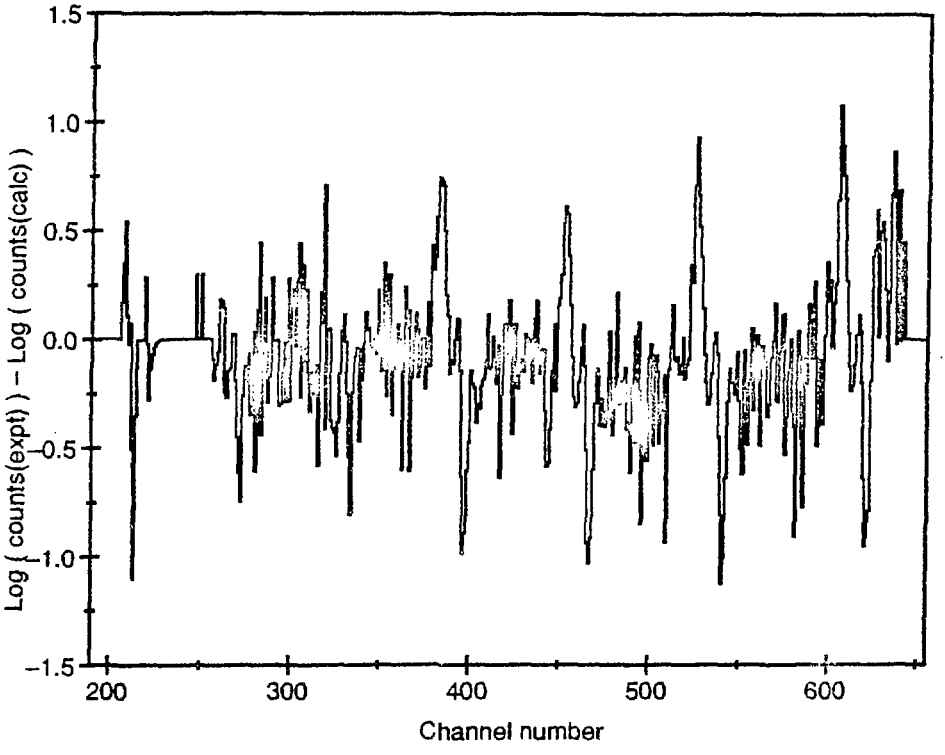

Figure 2 — The difference between the experimental and calculated spectra.

Ionic Charge q	25°	30°
28	15.1(13)	14.2(14)
29	14.4(12)	15.4(15)
30	13.9(10)	14.6(15)
31	14.5(11)	15.3(23)
32	14.4(26)	16.8(40)
33	17.2(99)	23.5(136)

Table — Extracted $\alpha_L(q)$

For $q = 33$, the F=3 ionic charge–state is expected to have a much lower α_L tha the F=4 state. (Angular momentum conservation requires a d–state free electron afte conversion in the F=3 state, and the d–electron wavefunction has small amplitude a the nucleus). In the analysis it was assumed that $\alpha_L(33)$[F=3] was zero, and that th population of ions in the $q = 33$ charge–state was statistically distributed between the tw F–states. The $\alpha_L(33)$ value obtained from the analysis is thus $\alpha_L(33)$[F=4], to a goo approximation.

Simple considerations suggest that

$$\alpha_L(33)[\mathrm{F} = 4] = \frac{8}{9}\,\alpha_L(32). \qquad (1$$

The results of the present preliminary experiment are of insufficient accuracy to probe thi prediction, or to test changes in electron wave functions as L–shell electrons are removed However, the results do show that the technique is capable of measuring those effects wit an experiment of higher statistical accuracy.

This work was supported in part by NATO grant No. 0210–87, by grants from the U.S Department of Energy, Nuclear Physics Division, under contract No. W–31–109–ENG–38 and by the Science and Engineering Research Council of the U.K.

REFERENCES

[1] J. Müller,
Nucl. Data Sheets, **49** (1986) 579

[2] R.S. Hager and E.C. Seltzer,
Nucl. Data **A4** (1968) 1

[3] W.R. Phillips et al.,
Phys. Rev. Lett. **62** (1989) 1025

[4] S. Kowalski and H.A. Enge,
MIT, 1986 version of RAYTRACE unpublished

Heavy ion induced Kα X-ray spectra of Tb studied by means of bent-crystal spectrometer

T.Ludziejewski, P.Rymuza, Z.Sujkowski
Soltan Institute for Nuclear Studies, 05-400 Świerk, Poland
D.Anagnostopoulos*, G. Borchert
Institut für Kernphysik, Forschungszentrum Jülich, D-5170 Jülich, Germany
M.Carlen, J.-Cl.Dousse, Ch.Rhême
Phys. Department, University of Fribourg, CH-1700 Fribourg, Switzerland
A.Drentje
Kernfysisch Versneller Instituut, University of Groningen, Zernikelaan 25, 9747 AA Groningen, The Netherlands

Abstract

A diffraction spectrometer with a quartz crystal bent to the radius of 4.64 m has been installed at the beam line of KVI variable energy cyclotron. The instrument is intended for a detailed study of KX-rays from multiply ionized atoms with $Z > 56$. The KX-ray spectra of Tb produced during the bombardment with 15 MeV/amu ^{4}He and ^{20}Ne beams are presented along with the Kα X-ray calibration spectrum of ^{170}Yb. The L-shell ionization probabilities in near central collisions are deduced from the measured L-satellite yield distribution. The procedure to extract the ionization probabilities from the measured satellite spectra is discussed.

In a single ion - atom collision the rapidly changing Coulomb field causes multiple removal of target inner shell electrons. For instance, several L-shell vacancies can be produced simultaneously with a single K-shell hole. Each vacancy in the L-shell reduces the screening of the remaining target electrons. As a result, energies of the $K\alpha$ X-rays following such a collision increase approximately linearly with the number of holes in the L-shell. The energy increment per each spectator hole in the L-shell is larger than the natural line width for any Z. In a consequence, the KX-ray spectrum from a statistically populated sample exhibits a composite (satellite) structure, where each satellite corresponds to a particular number of L-shell vacancies. A measurement of the relative yields of these lines gives directly the population of the L-shell vacancies at the time of the KX-ray emission and indirectly the L-shell ionization probability for the K-shell ionizing events. The latter ones can be considered as central collisions on the L-shell scale. Thus an observation of Kα satellites corresponds to measuring the L-shell ionization yields for small impact parameters. The complexity of the KX-ray spectra requires, however, that the instrumental energy resolution is comparable to the natural line width. This is only achievable with a diffraction crystal spectrometer.

The $K\alpha$ satellite spectra have been extensively investigated in the past for heavy-ion induced ionization in atoms with $Z < 30$ [1,2,3], using diffraction spectrometers in a reflection mode. Recently, this technique has also been applied to heavier elements, with the use of bent crystal spectrometers in the transmission mode, installed in-beam at the cyclotrons of PSI, Villigen [4,5] and of KFA, Jülich [6,7]. The present note describes the installation of the Jülich spectrometer [8] at the KVI, Groningen, envisaged as a continuation and extension of the PSI and KFA work. The first experimental results for Tb bombarded with 15 MeV/amu ^{4}He and ^{20}Ne ions are presented and the procedure to extract the L-shell ionization probabilities in near central collisions from the measured satellite yields is discussed.

The spectrometer uses the (110) planes of a 4 mm thick quartz crystal bent to the radius of 4.64 m. It is installed at 90° with respect to the beam of the KVI variable energy cyclotron, behind a 1 m thick concrete wall. It views the target through a 2 m long lead collimator equipped with a parallel opening for a Ge monitor detector. The diffracted radiation is detected with a 5.2 cm (diameter) × 1.2 cm (thick) HP-Ge detector placed in a lead housing. Details of the system are described in [8].

*On leave from University of Ioannina, Greece

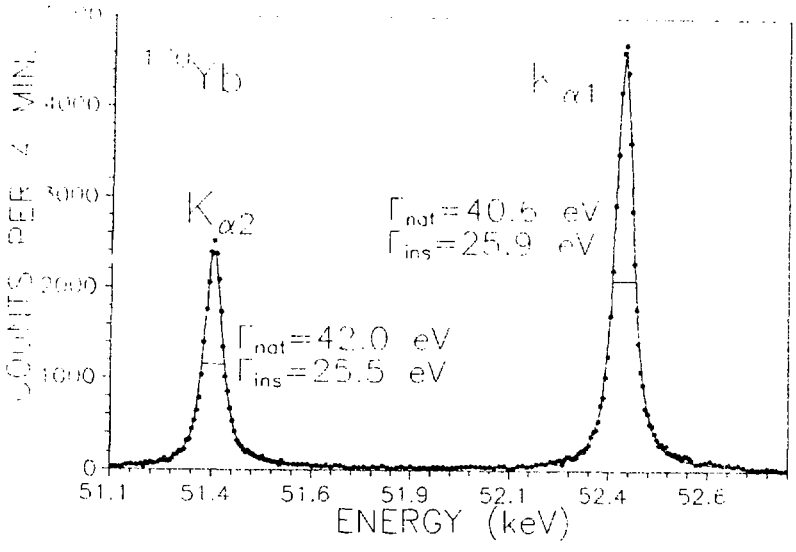

Figure 1: First order reflection of the $K\alpha_{1,2}$ ^{170}Yb line measured to test the focusing property of the spectrometer. Full curve represents the least square fit of Voigt profiles to the measured spectrum. Instrumental line width of Γ_{ins} =26 eV corresponds to 5 arcsec of angular resolution.

The spectrometer has been tested and optimized for the measurements of the satellite spectra using radioactive ^{170}Tm source. The Kα X-ray spectrum of ^{170}Yb accompanying the decay of ^{170}Tm was measured at negative and positive Bragg angles in first order of reflection. To demonstrate the focusing quality of the spectrometer an example of the $K\alpha_{1,2}$ spectrum is shown in fig. 1.

The natural widths of Yb lines are equal to 40 6 eV ($K\alpha_1$), and 42.0 eV ($K\alpha_2$), [9] and are of the order of the instrumental line width. Thus, the line shape should be well described by the Voigt function obtained by the convolution of the Lorentzian line shape with the Gaussian instrumental response. Solid curves in fig. 1 represent the least square fit of Voigt profiles to the measured KX-ray spectra. The best fit instrumental line widths are equal to 25.9 eV ($K\alpha_1$) and 25.5 eV ($K\alpha_2$) which corresponds to 5 arcsec of angular resolution. The angular resolution of that order allows to resolve the KX-ray satellites for all elements in the allowed energy range. For very heavy elements, however, the interpretation of the satellite spectra is more difficult since the natural line width becomes comparable to the satellite energy splitting and the complex structure of a single satellite line due to angular momentum coupling of the open shells is more pronounced [6].

In the first on-line measurement we have studied the $K\alpha_1$ profile of terbium bombarded with a 15 MeV/amu, 400 nA alpha beam. The $K\alpha_1$ line was measured at positive and negative Bragg angles. This provided an additional check that the instrumental asymmetries could be neglected. An example of the He induced Tb $K\alpha_1$ spectrum is shown in fig. 2.

Next, the Tb target was exposed to a 15 MeV/amu Ne beam with an intensity of about 30 nA. In order to survey the instrumental reproductibility, the spectra were collected in at least two successive step by step scannings for both sides of reflection. Good reproductibility has been achieved. The rich $K\alpha_1$ satellite spectrum obtained in this run is shown in the lower part in fig. 2.

Several interesting features can be noted from the comparison of the He and Ne induced spectra.

- Strong satellite peaks dominate the high energy side of Ne induced $K\alpha_1$ transition. (Peaks labelled $K\alpha_1 L^l$ originate from the $K\alpha_1$ transitions with additional l L-shell vacancies present at the moment of deexcitation). In the ^{4}He induced spectrum, the satellite peak is observed only as a weak shoulder of the diagram $K\alpha_1$ line.

- The linewidth of the $K\alpha_1 L^0$ line in the Ne-induced spectrum is larger than in the helium-induced transition, and the widths of the $K\alpha_1 L^l$ are substantially larger than those of the $K\alpha_1 L^0$ one.

- The main component line is shifted toward higher energies in the neon-induced spectrum.

The broadening and the net energy shift of the $K\alpha_1 L^0$ line in the case of Ne-induced spectrum indicates the effect of multiple M-shell ionization. The average M-shell ionization probability for the Ne projectiles could in principle be deduced from the relative energy differences between the $K\alpha_1 L^0$ lines in He and Ne induced spectra if one assumes the M-shell ionization for He to be negligible [4]. (The Doppler effect does not contribute any sizeable broadening and energy shift [5]).The analysis, however, is model dependent and will be not presented here. An additional clearly observable broadening of the $K\alpha_1 L^l$ lines results from different energy splitting for various L-subshell spectator hole configurations and angular momentum coupling of the open shells. In order to investigate the influence of the complex structure of single satellite line on the total shape of satellite spectrum we have performed the theoretical simulation of $K\alpha_1 L^1$ line profile of Tb. The energies and intensities of the $K\alpha_1 L^1$ components have been calculated with the use of Desclaux program package [10] with the inclusion of transverse (Breit) interaction and quantum electrodynamics (self energy and vacuum polarization) corrections. Only the L-shell spectator hole configurations has been taken into account. In this model, the satellite line with the single spectator hole in L-shell splits into 9 lines with average energy of 103 eV above the diagram line and spreads over the energy range from 42 eV to 160 eV. The theoretical shape of $K\alpha_1 L^{0.1}$ complex is shown in fig. 3.

The positions of the $K\alpha_1 L^1$ components originating from different initial and final state configurations are also shown. The shape of each particular component has been calculated as a convolution of natural line shape (the width taken from [9]) with the instrumental (gaussian) response function with the width corresponding to 5 arc sec of angular resolution.

In a standard analysis of the satellite spectra, the splitting of the atomic levels due to angular momentum coupling of the open shells is usually neglected and the average position of a single satellite line is used instead. Following this procedure we have fitted the set of two Voigt profiles of adjustable width to the diagram and satellite line complex. We find that the total shape of the satellite spectrum is relatively well described by this simple model (see fig. 3) but the reproduced satellite to diagram intensity ratio differ of about 5% in comparison with the value used in the model construction. The observed difference might suggests that the analysis of $K\alpha$ x-ray satellite spectra by the decomposition of the spectrum into the Voigt profiles leads to systematic deviation from the real value of satellite line yields.

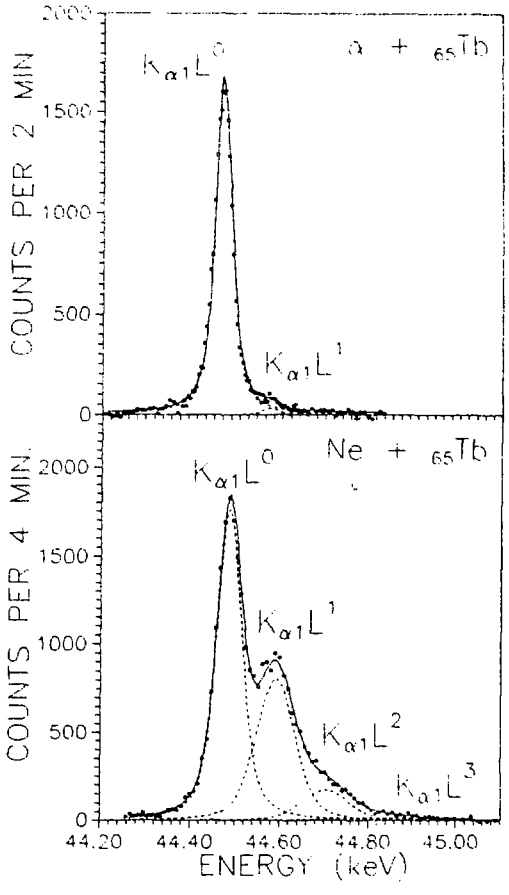

Figure 2: High resolution spectrum of the terbium $K\alpha_1$ X-line induced by ^4He and ^{20}Ne ions. The satellite lines labelled $K\alpha_1 L^l$ correspond to the transition with l "spectator" holes in L-shell. Results of the fitting procedure are also shown.

To confirm this conclusion, however, it is necessary to include into the theoretical model of the satellite spectra the possibility of M-shell ionization process which accompanies the L-shell ionization in H.I.–atom collision. The inclusion of the angular momentum coupling between open L and M shell leads to a large number of possible initial and final state configurations and can smooth to a large extent the shape of $K\alpha_1 L^1$ band [11].

The preliminary analysis of satellite spectra was carried out by fitting a set of Voigt functions resulting from the convolution of a Lorentzian line shape (with a fixed width taken from tables [9]) with a Gaussian instrumental response function. To take into account the multiplet structure of single satel-

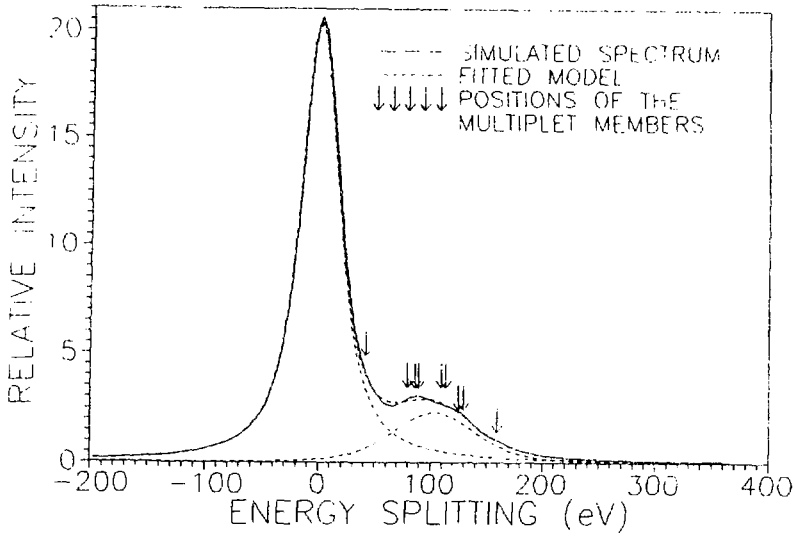

Figure 3: Simulated spectrum of Tb $K\alpha_1 L^1$ line profile. Positions of different contributions are marked by ↓ . (Only the L-shell angular momentum coupling mechanism has been included.)

lite line, the Gaussian parts of Voigt profiles were fitted with adjustable width. The results of the fitting procedure are also depicted in fig.2. The yield distribution of the Ne-induced satellite spectra is presented in table 1. The satellite yield distribution corresponds to the spectator vacancy distribution at the time of the KX-ray emission. The initial vacancy distribution can be deduced after correcting for the radiative and Auger processes, as a result of which the L-shell vacancies are filled prior to the KX-ray emission. In addition, the L and M - shell vacancies substantially change the fluorescence yields of $K\alpha_{1,2}$ and $K\beta$ transitions. The correction procedure for rearrangement transitions is presented in papers [4,12]. In table 1 the yield distribution of the Ne induced satellite spectrum and the corresponding primary vacancy distribution are shown for the Ne induced spectrum.

Satellite	Experimental satellite yield $X_{K\alpha}(KL^n)$	Primary distribution $I_{K\alpha}(KL^n)$
$K\alpha L^0$	530(15)	504(30)
$K\alpha L^1$	355(12)	356(19)
$K\alpha L^2$	103(11)	122(20)
$K\alpha L^3$	12(12)	18(18)

Table 1: Observed and primary vacancy distribution for $_{65}$Tb bombarded with 15 MeV/amu ^{20}Ne ions. Errors are due to experimental errors, and the uncertainties of rearrangement probabilities. The sum of intensities is normalized to 1000.

From the population of vacancies created at the moment of collision the L-shell ionization probabilities can be deduced. In the framework of the independent electron approximation, the distribution of the primary vacancies could be described as a binomial one. Neglecting in a first approach the differences in ionization probabilities for various L subshells, and assuming that the L-shell ionization probability is constant in the range of impact parameters where K-shell ionization takes place, the probability of direct ionization of l out of eight L-shell electrons depends on a single parameter P_L and is given by:

$$p(l) = \binom{8}{l} P_L^8 (1 - P_L)^{(8-l)},$$

where P_L - is the probability of ejecting one electron from the L-shell for an "effective" (close to zero in the L-shell scale) impact parameter. Using the presented model we have fitted the experimental satellite distribution obtaining P_L=0.083±0.005. The semiclassical calculations performed with relativistic hydrogenic wave functions and including the recoil effect yield the value P_L=0.060 [13].

There are several possible reasons of the observed difference between theoretical and experimental values of the ionization probability. First,

it may be caused by the use of hydrogenic wave functions in the SCA calculations which are too rough an approximation of the realistic wave functions especially in the energetic H.I.-atom collisions [16,15,12]. Second, it may originate from the approximate method of the analysis. Finally, L-subshell coupling [6,7], electron capture [4,6] as well as core relaxation mechanism can contribute to the total ionization probability in H.I.-atom collision. Detailed discussion of the observed difference between theoretical and experimental ionization probability is beyond the scope of the present note (see, however [17]) and will be published in a forthcoming paper.

It is worth noting that good agreement is generally found between the experimental and theoretical total K- and L-shell ionization cross section. A more demanding test of the theory is the comparison of ionization probabilities as a function of the impact parameter. Until now, however, only few such experiments have been carried out for the L-shell. These experiments require measuring the X-ray or Auger yields in coincidence with the scattered projectile and are particularly difficult for high bombarding energies. The "satellite" method allows the determination of L-shell ionization probabilities for close to zero impact parameters for any energy of the ionizing particle. Such data appear to give a more crucial test of the theory than the total cross sections. In comparison with impact parameter dependent measurements of L-shell ionization probabilities, the "satellite" method has an advantage that the rearrangement corrections are small due to the short lifetime of the K-shell hole. In the case of LX-ray–particle coincidence method the rearrangement corrections are large and greatly influenced by uncertainties of Auger and Coster-Kronig transition rates in multiply ionized atoms.

The results of theoretical simulation of the $K\alpha_1 L^1$ line profile of Tb show that the correct analysis of experimental spectra requires the detailed theoretical knowledge of $K\alpha$ satellite line structure.

References

[1] R.L.Kauffman, J.H. McGuire, P.Richard, Phys. Rev. A8, (1973) 1233

[2] A.R.Knudson, D.J.Negel, P.G.Bulkhalter, K.L.Dunning, Phys. Rev. Lett. 26, (1971) 1149

[3] C.R.Vane, E.Källne, J.Källne, G.Morford, S.Raman, M.S.Smith, Nucl. Instr. Meth. B10/11, (1985) 190

[4] P.Rymuza, Z.Sujkowski, M.Carlen, J.-Cl.Dousse, M.Gasser. J.Kern, B.Perny, Ch.Rhême, Z. Phys. D14, (1989) 37

[5] B.Perny, J.-Cl.Dousse, M.Gasser, J.Kern, Ch.Rhême, P.Rymuza, Z.Sujkowski, Phys. Rev. A36 (1987) 2120

[6] D.Anagnostopoulos, G.L.Borchert, D.Gotta, K.Rashid, Z.Phys. D18, (1991) 139

[7] R.Salziger, G.L.Borchert, D.Gotta, O.W.B. Schult, D.H.Jakubassa-Amundsen, P.A. Amundsen, K.Rashid, J. Phys. B22 (1989) 821

[8] G.Borchert, J.Bojowald, A.Ercan, M.Labus, Th.Rose, O.W.B.Schult, Nucl. Instr. Meth. A245 (1986) 393

[9] S.I.Salem, P.L.Lee, At. Data Nucl. Data Tables 18, (1976) 233

[10] J.P.Desclaux, Comp. Phys. Commun. 9, (1975) 31

[11] M.Polasik, Phys.Rev. A41, (1990) 3689

[12] D.Anagnostopoulos,G.L.Borchert, D.Gotta, to be published in J. Phys.B

[13] D.Trautmann, F.Rosel, Nucl.Instrum. Methods 169, (1980) 259

[14] C.K. Aashamar, P.A. Amundsen, J. Phys. B14, (1981) 483

[15] P.Rymuza, T.Ludziejewski, Z.Sujkowski, M.Carlen, J.-Cl.Dousse, M.Gasser, J.Kern, Ch.Rhême, to be published in Z. Phys. D

[16] C.K. Aashamar, P.A. Amundsen, J. Phys. B14, (1981) 483

[17] Z.Sujkowski Proc. XXIX Int. Winter Meeting on Nucl. Phys, ed. I. Iori, Universita de Milano, Supplemento n.83 p.390

Wydaje Instytut Energii Atomowej - OINTEA
Nakład 190 egz. Data złożenia maszynopisu - XI.1991r.
Zezwolenie GP.II/441/967/83 z dnia 19 lipca 1983 r.

OINTEA-5/92